



The Jurassic-Early Cretaceous Basalt-Chert association in the Ophiolites of the Ankara Mélange east of Ankara, Turkey: Age and Geochemistry

Journal:	<i>Geological Magazine</i>
Manuscript ID	GEO-16-1659.R1
Manuscript Type:	Article
Date Submitted by the Author:	n/a
Complete List of Authors:	Bortolotti, Valerio; Università degli Studi di Firenze, Dipartimento di Scienze della Terra Chiari, Marco; CNR Istituto di Geoscienze e Georisorse, Göncüoğlu, M. Cemal ; Middle East Technical University, Geological Engineering Department Principi, Gianfranco; Università degli Studi di Firenze, Dipartimento di Scienze della Terra Saccani, Emilio; Università degli studi di Ferrara, Dipartimento di Fisica e Scienze della Terra Tekin, U. Kagan ; Hacettepe University, Geological Engineering Department Tassinari, Renzo; Università degli Studi di Ferrara, Dipartimento di Fisica e Scienze della Terra
Keywords:	Ophiolites, geochemistry, radiolarian biostratigraphy, Jurassic, Early Cretaceous, Ankara Mélange, Turkey

1
2
3 **In blue new text**

4 **In green text removed**
5
6
7

8 **The Jurassic-Early Cretaceous Basalt-Chert association in the Ophiolites of the** 9 **Ankara Mélange east of Ankara, Turkey: Age and Geochemistry**

10
11 **Valerio Bortolotti***, **Marco Chiari****, **M. Cemal Göncüoğlu*****, **Gianfranco Principi***, **Emilio**
12 **Saccani^o ✉**, **U. Kagan Tekin^{oo}** & **Renzo Tassinari^o**
13
14

15 * *Dipartimento di Scienze della Terra, Università degli Studi di Firenze, Via G. La Pira 4,*
16 *50121 Firenze, Italy.*

17 ** *CNR, Istituto di Geoscienze e Georisorse, Via G. La Pira 4, 50121 Firenze, Italy.*

18 *** *Middle East Technical University, Geological Engineering Department, 06531, Ankara,*
19 *Turkey.*

20 ^o *Dipartimento di Fisica e Scienze della Terra, Università degli Studi di Ferrara, Via Saragat 1,*
21 *44122 Ferrara, Italy.*

22 ^{oo} *Hacettepe University, Geological Engineering Department, 06532, Beytepe, Ankara, Turkey.*
23
24

25 ✉ *Corresponding author, email: sac@unife.it*
26
27

28 **Keywords:** Ophiolites, geochemistry, radiolarian biostratigraphy, Jurassic, Early Cretaceous,
29 Ankara Mélange. Turkey.
30
31

32
33
34 **Abstract** This study is focused on slide blocks including oceanic lavas associated with pelagic
35 sediments within the eastern part of the Ankara Mélange. A detailed petrological characterization of
36 the volcanic rocks and a detailed biochronological investigation of the associated radiolarian cherts
37 **in eight sections (east of Ankara)** was carried out.
38
39
40

41
42
43 The volcanic rocks are largely represented by basalts and minor ferro-basalts and trachytes. They
44 show different geochemical affinities and overlapping ages including:
45

46
47 a) Late Jurassic-Early Cretaceous garnet-influenced MORB (Section 5, middle late Oxfordian to
48 late Kimmeridgian-early Tithonian and early-early late Tithonian; Section 8, late Valanginian-early
49 Barremian);
50
51

52
53 b) Early Cretaceous enriched-MORB (Section 4, middle late Barremian-early early Aptian; Section
54
55 7, Valanginian to middle Aptian-early Albian);
56
57
58
59
60

1
2
3 c) Middle Jurassic plume-type MORB (section 2, early-middle Bajocian to late Bathonian-early
4 Callovian);

5
6
7 d) Late Jurassic-Early Cretaceous alkaline basalts (Section 3, middle-late Oxfordian to late
8 Kimmeridgian-early Tithonian; Section 1, late Valanginian to late Hauterivian).

9
10 All rock types show a clear garnet signature, as testified by their high MREE/HREE ratios.

11
12 The coexistence of chemically different rock-types from Middle Jurassic to Early Cretaceous
13 suggests that they were formed at a mid-ocean ridge setting from partial melting of a highly
14 heterogeneous mantle characterized by the extensive occurrence of OIB-metasomatized portions,
15 which were likely inherited from a Triassic mantle plume activity associated with the continental
16 rift and opening of the Neotethys branch.
17
18
19
20
21
22
23
24
25
26
27

28 **1. Introduction**

29
30
31
32 Despite numerous studies since 1960's in Turkey, the locations, ages and geological evolution
33 of the branches of the Eastern Mesozoic Tethys Ocean or Eastern Neotethys are disputed (see
34 Sengör & Yilmaz, 1981;–Dercourt *et al.*, 1986; Robertson *et al.*, 1996; Dilek *et al.*, 1999;
35 Göncüoğlu *et al.*, 1997, 2000; 2006; 2010; Stampfli & Borel, 2002; Bortolotti & Principi, 2005;
36 Schmid *et al.*, 2008; Moix *et al.*, 2008). This is mainly due to two deficiencies. One of them is the
37 fact that next to definite ophiolitic suture belts separating continental blocks with distinct geological
38 history there are also suture-like alignments or pseudo-belts of allochthonous ophiolitic bodies. The
39 second shortcoming regards the method of the ophiolite research yet realized, as it was rarely based
40 upon a multidisciplinary approach. Several detailed petrological studies on different units from
41 different ophiolitic bodies lack age data and vice versa. A considerable number of studies were
42 concentrated on the larger and more or less complete ophiolitic bodies and neglected the remarkable
43 amount of basalt-radiolarian chert associations within the mélangé complexes. To overcome these
44 problems we applied a multi-disciplinary approach combining petrology and biostratigraphy on
45
46
47
48
49
50
51
52
53
54
55
56
57
58
59
60

1
2
3 crustal remnants of the Neotethys incorporated in the mélange complexes of the Izmir-Ankara-
4
5 Erzincan Suture Belt (IAESB).
6

7 As previously referred, the location, age and geological evolution of the branche(s) of the
8
9 Eastern Neotethys are disputed. In fact, most authors favour the hypothesis (presented herein) that
10
11 implies the existence of two parallel and contemporaneous oceans namely: the Izmir-Ankara Ocean,
12
13 to the south and the Intra-Pontide Ocean, to the north (see Göncüoğlu *et al.*, 2012, for an exhaustive
14
15 review). In contrast, other authors favour the hypothesis, which implies the existence of a single
16
17 oceanic basin represented by the Intra-Pontide Ocean (e.g., Bortolotti & Principi, 2005). In this case
18
19 the Intra Pontide Suture (IPS, see later) would be the eastward continuation of the Vardar Ocean
20
21 suture whereas the IAESB would represent fragments of the oceanic lithosphere pushed southwards
22
23 on the continent by orogenic movements (as happened more westwards, in the Hellenides) (see
24
25 Bortolotti *et al.*, 2013a).
26
27
28

29 The IAESB separates two completely different units of continental crust with different origin: a)
30
31 the Tauride-Anatolide terrane representing the rifted northern margin of NW Gondwana, in the
32
33 south and b) the Sakarya Composite Terrane comprising amalgamated oceanic and continental
34
35 bodies of Variscan and Cimmerian origin and their alpine platform, in the north. To the N of the
36
37 Sakarya Composite Terrane another suture, the Intra-Pontide Suture, represents the boundary
38
39 towards the Eurasian Istanbul-Zonguldak terrane (Fig.1).
40
41
42

43 The IAESB represents remnants of the Vardar-Izmir-Ankara-Erzincan-Lesser Caucasus Ocean in
44
45 Turkey. This ocean is considered as the main northern branch of Neotethys, whereas the Intra-
46
47 Pontide oceanic basin to the north of it is a matter of debate (see before and, for a brief discussion,
48
49 Göncüoğlu *et al.* 2012 and Tekin *et al.*, 2012a). In NW Turkey, IPS is clearly delineated by the
50
51 presence of ophiolitic melanges between the Sakarya and the Istanbul-Zonguldak continental plates
52
53 (e.g., Robertson & Ustaömer, 2004; Göncüoğlu *et al.*, 2008; Akbayram *et al.*, 2012). By wedging
54
55 out of the Sakarya Composite Terrane in northern Central Anatolia, however, the IPS belt
56
57 juxtaposes with the IAESB along splays of the North Anatolian Shear Zone (e.g., Ellero *et al.*,
58
59
60

1
2
3 2015a) and the Neotectonic strike-slip system generated due to the Tertiary indentation and
4 anticlockwise rotation of the Kırşehir Block (e.g., Cemen *et al.*, 1993; Kaymakci *et al.*, 2003).
5
6
7 Towards the east and in NE Anatolia, the IAESB is again in its accustomed position between the
8
9 Anatolides and the units of the Sakarya Composite Terrane (Topuz *et al.*, 2013a, 2013b; Parlak *et*
10
11 *al.*, 2013; Robertson *et al.*, 2013). The vanishing of the IPS belt in the Central Pontides by the North
12
13 Anatolian Shear Zone during the Neotectonic Period led some authors to completely ignore the IPS
14
15 and hence the presence of an oceanic basin (e.g., Elmas & Yiğitbaş, 2001, 2005).
16
17

18
19 The IAESB is composed of a number south-verging tectonic slices or giant slide blocks
20
21 representing 1) incomplete sequences of various portions of the Izmir-Ankara-Erzincan oceanic
22
23 lithosphere (e.g., Floyd *et al.*, 2000; Göncüoğlu *et al.*, 2000; Göncüoğlu, 2011); 2) an accretionary
24
25 prism, known as the “Ankara Mélange” (Bailey & McCallien, 1953) including blocks derived from
26
27 different parts of the oceanic basin; 3) imbricated slices of successions formed in a foredeep basin
28
29 associated with the emplacement of the oceanic material onto the Tauride-Anatolide passive
30
31 margin.
32
33

34
35 This study is focused on slide blocks including oceanic lavas associated with pelagic sediments
36
37 within the accretionary prism and the foredeep basin successions in the eastern part of the Ankara
38
39 Mélange (for the preliminary data see Bortolotti *et al.*, 2013b). This paper aims to draw a more
40
41 comprehensive picture of the different basaltic rock-types, erupted in the Neotethys from Middle
42
43 Jurassic to Early Cretaceous. To this purpose, a detailed petrological and geochemical
44
45 characterization of the volcanic rocks and a detailed biochronological investigation of the associated
46
47 radiolarian cherts will be carried out. Similar multidisciplinary studies were applied to other parts of
48
49 the IAESB between the Aegean coast and the western part of the Ankara Mélange (e.g., Bragin &
50
51 Tekin., 1996; Yaliniz *et al.*, 2000a; Göncüoğlu *et al.*, 2001, 2008, 2010, 2015; Rojay *et al.*, 2001;
52
53 Tekin *et al.*, 2002; Gökten & Floyd, 2007; Tekin & Göncüoğlu, 2007, 2009; Tekin *et al.* 2012a;
54
55 Moix & Goriçan, 2013; Soyacan *et al.*, 2015). These studies reported Middle Triassic to Cretaceous
56
57 ages for radiolarian cherts stratigraphically associated to basalts showing, in turn, different tectono-
58
59
60

1
2
3 magmatic settings of formation, such as mid-ocean ridge, seamount, forearc and backarc were
4 reported. Our new data from the eastern Ankara Mélange aims to interpret the tectono-magmatic
5 processes and their timing, which will be useful for improving the reconstruction of the geodynamic
6 history of the Neotethys Ocean mainly from the Jurassic to the Early Cretaceous time interval.
7
8
9
10
11
12
13

14 **2. Geological background**

15
16
17
18 The studied portion of the Izmir-Ankara-Erzincan Suture Belt (IAESB) was characterized by the
19 pre-Eocene development of a huge accretionary prism (for details see Rojay, 2013), which formed
20 between the Sakarya Composite Terrane to the North, and the southerly Kütahya-Bolkardag Belt of
21 the Anatolides, in the western part, and the Central Anatolian Crystalline Complex (CACC), in the
22 eastern part. The first juxtaposition of these oceanic and continental units occurred in the latest
23 Cretaceous-Paleocene. However, compression and related thrusting lasted until the Miocene
24 (Kocyigit *et al.*, 1995).
25
26
27
28
29
30
31
32

33
34 We sampled some ophiolitic outcrops from the IAESB east of Ankara (Fig. 1), where the concave
35 E-W trend of the belt between Izmir and Ankara makes a sharp turn towards NNW, caused by the
36 Tertiary indentation (e.g., Cemen *et al.*, 1993; Kaymakci *et al.*, 2003) and anticlockwise rotation of
37 the Kırşehir Block.
38
39
40
41
42

43 The Sakarya Unit marks the active margin of the Izmir-Ankara-Erzincan Ocean, and was thrust over
44 the IAESB both to the NNE of Ankara and to the SE of Çorum (Fig. 2). It consists of a composite
45 terrane comprising a Variscan arc complex and its Permian platform, as well as the Paleotethyan
46 subduction-accretion prism (the Triassic Karakaya Complex, Göncüoğlu *et al.*, 2000; Okay &
47 Göncüoğlu, 2004). It has a Jurassic to ?Late Cretaceous cover that belonged to a north-facing
48 passive continental margin but was transformed into an active margin by the northward subduction
49 of the Izmir-Ankara-Erzincan oceanic lithosphere.
50
51
52
53
54
55
56
57
58
59
60

1
2
3 The Karakaya Complex NNW of Ankara comprises low-grade metamorphic greywackes associated
4 with Permian and Carboniferous limestone blocks and ocean-island-type volcanic rocks with
5 Carnian radiolarian cherts (e.g., Sayit *et al.*, 2011). Unconformably overlying there is a Mesozoic
6 cover that comprises, from bottom to top: late Early Jurassic-Mid Jurassic neritic limestones, Late
7 Jurassic - Early Cretaceous (e.g., Altiner *et al.*, 1991) pelagic limestones and Late Cretaceous
8 turbidites. The oldest common overstep sequence on the Izmir-Ankara-Erzincan Suture Belt (and
9 the Sakarya Composite Terrane) comprises Late Paleocene lagoonal sediments, which occur as
10 discontinuous outcrops within the thrust zone between these two units (Göncüoğlu *et al.*, 2000).

11
12 The northern-central part of the sampled area has been recently evaluated as the North Anatolian
13 Shear Zone (Ellero *et al.*, 2015a, b). The North Anatolian Shear Zone corresponds to a complex
14 deformation zone where the strain is partitioned in a system of faults, folds and thrusts leading to
15 high-angle faults bounding E-W elongated blocks and pull-apart basins. The zone is more than 100
16 km wide and comprises several km long, lens-shaped tectonic inlayers belonging to the mélanges of
17 the IPS belt (e.g. Göncüoğlu *et al.*, 2014) the Sakarya Composite Terrane (mainly the Late Jurassic
18 - Early Cretaceous Sogukcam Limestone, e.g. Catanzariti *et al.* 2013), a Late Cretaceous island arc
19 (Berber *et al.*, 2014) belonging to the IPS Belt, a Late Cretaceous continental arc (Ellero *et al.*,
20 2015b) and the ophiolitic mélanges of the IAESB. The active main strand of the right-lateral North
21 Anatolian Transform Fault is located in the center of this mega-shear zone, where lateral
22 displacements ranging from 30 to 120 km, have been proposed in the literature (e.g. Hubert-Ferrari
23 *et al.*, 2002 and references therein).

24
25 The metamorphic rocks of the Sakarya Composite Terrane (the “Tokat Massif”, Yilmaz *et al.*,
26 1997), around Çorum, East of the sampled area (Fig. 2), are tectonically overlying the ophiolitic
27 mélange of the IAESB. In this area, both units are in turn unconformably overlain by Middle
28 Eocene rocks. Unfortunately, the primary relations between the Sakarya and IAESB rocks are
29 obscured by intensive Oligocene strike-slip faulting (Fig. 2).

30
31
32
33
34
35
36
37
38
39
40
41
42
43
44
45
46
47
48
49
50
51
52
53
54
55
56
57
58
59
60

1
2
3 Structurally underlying the IAESB units, the continental crust that was palinspastically located to
4 the south, and west of Ankara, represents the northern rim of the Tauride-Anatolide Platform. It
5 mainly includes high pressure-low temperature metamorphosed tectonic slices (e.g., Okay &
6 Tüysüz, 1999) which lithostratigraphic sequences are similar to the Paleozoic-Mesozoic slope-type
7 successions of the Anatolides (Göncüoğlu, 2011). In particular, in the sampled area (Fig. 2), the
8 IAESB units were thrust onto the Central Anatolian Crystalline Complex (Yaliniz *et al.*, 1996;
9 2000b), which comprises high temperature-medium pressure metamorphic successions similar to
10 the Paleozoic-Mesozoic Tauride-Anatolide Platform. In turn, they were overthrust by Turonian
11 supra-subduction ophiolite - the Central Anatolian Ophiolites (Yaliniz *et al.*, 2000a), which
12 represent remnants of the Izmir-Ankara-Erzican Ocean. Late Campanian granitoids intrude both the
13 basement rocks and the overlying ophiolite units (Köksal & Göncüoğlu, 2008), indicating a Late
14 Cretaceous age of the obduction inception. The oldest overstep sequences in this area are again
15 post-Maastrichtian pre- Early Eocene (Gülyüz *et al.*, 2013) red conglomerates, testifying a
16 Paleocene age for the main juxtaposition of the CACC and IAESB mélanges.

17
18 In the central part of the sampled area, the IAESB rocks are covered by the Paleocene-Eocene post-
19 orogenic marine clastic-volcanoclastics, carbonates and volcanics of the Çankırı Basin which, in his
20 turn, is partly covered by Neogene sediments (e.g., Göncüoğlu, 1992). Within the basin the
21 anticlockwise rotation of the CACC induced the formation of several NE-SW trending right-lateral
22 faults and, at its western margin, important left-lateral faults (Fig. 2). When restored, the IAESB
23 palinspastically follows also roughly an E-W trend and the present distortion of the main tectonic
24 units is re-established.

25
26 To attempt a reconstruction of the thickness of the IAESB rocks that comprise the subducted and
27 accreted remnants of the Izmir-Ankara-Erzican oceanic lithosphere, together with island arc and
28 sedimentary rocks of several Late Cretaceous-Paleocene piggy-back basins (e.g., Cater *et al.*, 1991;
29 Erdogan *et al.*, 1996) geophysical data would be necessary, but at present these data are not
30 available.

3. Description of the sampled sections

All the sampled sequences pertain to the radiolarites-basalts blocks included in the Ankara Mélange. For the numbers of the sections we referred to Bortolotti *et al.* (2013a). It is worth of note that in the present paper we don't report the samples of Section 6 of Late Triassic age Bortolotti *et al.* (2013a).

Section 1

In a massif of pillow basalts along the road Elmadag - Kırıkkale several metric intercalations of siliceous shales with scattered radiolarian cherts crop out.

We sampled one of these intercalations and the associated basalts (Fig. 3b, N 39°55.023, E 33°21.989). Samples:

TU10.4, radiolarian chert.

TU10.6, TU10.10, basalts below the radiolarian cherts intercalation.

TU 10.9, basalt about 20 metres above the radiolarian cherts intercalation.

Section 2

In a massif of mainly pillowed basalts along the road Sorgun - Çekerek thin layers of radiolarian cherts crop out.

We sampled one of these layers and the associated basalts (N 39°54.889, E 35°18.063), one radiolarian chert sample was collected along the road in uncertain stratigraphic position.

Samples:

TU10.11, radiolarian chert with uncertain stratigraphic position.

TU10.12, radiolarian chert.

TU10.14 basalt at the contact with the radiolarites.

1
2
3 TU10.15, TU10.16, TU10.17, basalts collected several metres from the radiolarites.
4
5
6

7 ***Section 3***

8
9 In a basalt block immediately north of Gökdere village, along the road, a sequence with radiolarian
10
11 cherts crops out.
12

13
14 Samples:

15
16 TU10.19, basalt at the contact with the radiolarian cherts (N 39°59.924, E. 35°24.272).
17

18 TU10.22, TU10.23, basalts collected some metres southward (N 39°59.921, E 35°24.274)
19
20 respectively 3,5 and 2 metres from the contact with the radiolarites.
21

22
23 TU10.28, radiolarian chert collected about 22 metres from the basalts (this sequence is intensely
24
25 folded)
26

27 28 29 ***Section 4***

30
31 An overturned sequence of basalts and radiolarian cherts with a sheared contact, along the road
32
33 about 3 km southeast of Bogazkale (N 40°00.377, E 34°38.762).
34

35
36 Samples:

37
38 TU10.29, TU10.30, TU10.31 radiolarian cherts collected in about 20 cm above the sheared level.
39

40
41 60 cm of sheared argillites and cherts separates the basalts from the above samples.
42

43
44 TU10.32, basalt at the contact with the sheared level.

45
46 TU10.33, basalt collected some metres upstairs.
47
48

49 ***Section 5***

50
51 Big quarry cut by small faults which pull up and down the contact basalts-cherts. The sequence
52
53 could be overturned: the cherts lie under the basalts the contact is very fine with pockets of argillites
54
55 and cherts in the mainly massif basalts.
56
57
58
59
60

1
2
3 The sampled quarry is along the road Çorum to Alaca, south of Küre village (Fig. 3c, N 40°15.861,
4
5 E 34°48.187).
6

7 Samples:

8
9 TU10.34, basalt, sample collected about 6 metres for the cherts.

10
11 TU10.35, TU10.36, TU10.37, samples collected in a radiolarian cherts-argillites sequence from the
12
13 base to 40 cm.
14

15
16 Small normal fault shifts of some metres the sequence.
17

18 TU10.38, radiolarian chert, collected beyond the fault, about 30 cm from the basalt sample
19
20 TU10.40.
21

22
23 TU10.40, basalt at the contact with the radiolarian cherts.
24

25 TU10.39, basalt nearby the sample TU10.40.
26
27

28 29 **Section 7**

30
31 Small outcrop of basalts and cherts along the road Iskilip - Tosya, 1,2 km before the junction to
32
33 Hacıhalil village (Fig. 3d, N 40°53.378, E 34°20.756).
34

35
36 Samples:

37
38 TU10.45, radiolarian chert nodule in the basalts.
39

40
41 TU10.46, basalt.
42
43
44

45 **Section 8**

46
47 Large body of breccia(?) with basalts, microgabbros, serpentinites, crystallized limestones in a
48
49 cherty matrix. We sampled the breccia in two near localities northeast of Yukariöz village. Samples:

50
51 First locality (N 40°51.097, E 33°50.723).
52

53
54 TU10.47, TU10.48, radiolarian cherts.
55

56
57 TU10.49a, TU10.49b, basalts.
58

59
60 Second locality (N 40°51.527, E 33°49.577).

1
2
3 TU10.51, M10 radiolarian cherts
4
5
6

7 **Section 9**

8
9 Pillow basalts enveloped in reddish limestones, road Eldivan - Sabanozu (N 40°31.488, E
10 33°28.106).
11

12
13 Samples:

14
15 TU10.52, TU10.53, basalts.

16
17 TU10.54, TU10.55, limestones.
18
19
20
21
22

23 **4. Biostratigraphy**

24
25 The radiolarian samples were etched with hydrochloric and hydrofluoric acid following the method
26 proposed by Dumitrica (1970), Pessagno & Newport (1972), Baumgartner *et al.* (1981), De Wever
27 (1982). The examined samples yielded radiolarians with moderate preservation and the principal
28 markers are illustrated in Figure 4 and Figure 5.
29

30
31 For the taxonomy and ranges of the Late Jurassic-Early Cretaceous principal markers we refer to
32 Aliev (1967), Kozur (1985), Kawabata (1988) Aita & Okada (1986), Goričan (1994), O'Dogherty
33 (1994), Baumgartner *et al.* (1995a, 1995b), Dumitrica & Dumitrica-Jud (1995), Dumitrica *et al.*
34 (1997), Bak (1996, 1999), Chiari *et al.* (2004), Danelian *et al.* (2004), Smuc & Goričan (2005),
35
36 Filippov & Kemkin (2005), Chiari *et al.* (2007), Danelian (2008), Dumitrica & Zügel (2008),
37
38 O'Dogherty *et al.* (2009), Robin *et al.* (2010), Bandini *et al.* (2011), Goričan *et al.* (2012), Chiari *et*
39
40 *al.* (2012).
41
42
43
44
45
46
47
48

49 From the analyzed cherts the following radiolarian assemblages and ages were obtained:
50
51
52
53

54 **Section 1 TU10.4:** *Angulobracchia portmanni* Baumgartner, *Archaeodictyomitra mitra* Dumitrica,
55
56 *Archaeodictyomitra* sp. cf. *A. lacrimula* (Foreman) (Fig. 4a), *Archaeodictyomitra* sp. cf. *A. mitra*
57
58 *Dumitrica*, *Archaeodictyomitra* sp., *Archaeodictyomitra* (?) sp., *Aurisaturnalis variabilis variabilis*
59
60

(Squinabol) (Fig. 4b), *Hemicryptocapsa* sp. cf. *H. capita* Tan (Fig. 4c), *Neorelumbra* (?) sp., *Pseudodictyomitra* sp., *Pseudodictyomitra* (?) sp., *Pyramispongia* (?) sp., *Tethysetta* (?) sp., *Thanarla brouweri* (Tan) (Fig. 4d), *Thanarla* sp., *Torculum* (?) sp., *Xitus* sp. cf. *X. robustus* Wu, *Xitus* sp.

AGE: late Valanginian to late Hauterivian (UAZ. 17- 20; UAZones after Baumgartner *et al.*, 1995b) for the presence of *Aurisaturnalis variabilis variabilis* (Squinabol). with *Hemicryptocapsa capita* Tan. Ranges after Baumgartner *et al.* (1995a). and Robin *et al.* (2010).

Section 2

TU10.11: *Eoxitus* (?) sp. (Fig. 4e), *Praewilliriedellum* sp. cf. *P. japonicum* (Yao), *Stichomitra* (?) *takanoensis* Aita (Fig. 4f), *Striatojaponocapsa* (?) sp.

AGE: early-middle Bajocian to late Bathonian-early Callovian (UAZ. 3-7; UAZones after Baumgartner *et al.*, 1995b) for the presence of *Stichomitra* (?) *takanoensis* Aita. Range after Baumgartner *et al.* (1995a).

TU10.12: *Hiscocaspsa* sp. (Fig. 4g), *Mirifusus* sp. cf. *M. guadalupensis* Pessagno (Fig. 4h), *Parahsuum* sp., *Parahsuum* (?) sp., *Praewilliriedellum* sp. cf. *P. japonicum* (Yao), *Praewilliriedellum* sp. cf. *P. convexum* (Yao), *Praewilliriedellum* (?) sp., *Pseudodictyomitra* (?) sp., *Stichomitra* (?) *takanoensis* Aita (Fig. 4i), *Transhsuum* sp., *Transhsuum* (?) sp., *Tritrabs* (?) sp.

AGE: early-middle Bajocian to late Bathonian-early Callovian (UAZ. 3-7; UAZones after Baumgartner *et al.*, 1995b) for the presence of *Stichomitra* (?) *takanoensis* Aita. Range after Baumgartner *et al.* (1995a).

Section 3

TU.10.28: *Acaeniotylopsis* sp., *Crolanium* (?) sp., *Emiluvia* sp. cf. *E. ordinaria* Ozvoldova (Fig. 4j), *Eoxitus* (?) sp., *Fultacapsa sphaerica* (Ozvoldova) (Fig. 4k), *Mirifusus* sp. cf. *M. guadalupensis*

1
2
3 Pessagno, *Mirifusus* sp., *Podocapsa amphitreptera* Foreman (Fig. 4l), *Spinosicapsa* sp. cf. *S.*
4 *triacantha* (Fischli), *Spinosicapsa* (?) sp. (Fig. 4m), *Spongocapsula* sp., *Svinitzium* sp., *Svinitzium*
5 (?) sp., *Triactoma* (?) sp.

6
7
8
9 AGE: middle-late Oxfordian to late Kimmeridgian-early Tithonian (UAZ. 9-11; UAZones after
10 Baumgartner *et al.*, 1995b) for the occurrence of *Podocapsa amphitreptera* Foreman with
11 *Fultacapsa sphaerica* (Ozoldova). Ranges after Baumgartner *et al.* (1995a).
12
13
14
15

16 17 18 **Section 4**

19
20 TU10.29: *Archaeodictyomitra lacrimula* (Foreman) (Fig. 4n), *Archaeodictyomitra mitra* Dumitrica
21 (Fig. 4o), *Archaeodictyomitra* sp., *Dicerosaturnalis trizonalis* (Rüst) (Fig. 4p), *Holocryptocanium*
22 sp. cf. *H. barbui* Dumitrica, *Orbiculiformella* (?) sp., *Pantanellium* sp. cf. *P. squinaboli* (Tan) (Fig.
23 4q), *Praeconosphaera* (?) sp. cf. *P. (?) multiconus* Yang, *Praeconosphaera* (?) sp.,
24 *Praewilliriedellum* sp. cf. *P. japonicum* (Yao), *Pseudoeucyrtis* sp., *Thanarla brouweri* (Tan) sensu
25 O'Dogherty (1994), *Thanarla* sp. cf. *T. gutta* Jud (Fig. 4r), *Thanarla* sp.
26
27
28
29
30
31
32

33
34 AGE: early-early late Berriasian to middle Aptian-early Albian (UAZ. 14 - Costata subzone of
35 Turbocapsula Zone, Zone after O'Dogherty, 1994; UAZone after Baumgartner *et al.*, 1995b) for the
36 occurrence of *Archaeodictyomitra lacrimula* (Foreman) and *Archaeodictyomitra mitra* Dumitrica.
37 Ranges after Baumgartner *et al.* (1995a), O'Dogherty (1994), Dumitrica *et al.* (1997) and Bandini *et*
38 *al.* (2011).
39
40
41
42
43
44
45

46
47 TU10.30: *Archaeodictyomitra* sp. cf. *A. communis* (Squinabol), *Archaeodictyomitra* sp. cf. *A.*
48 *lacrimula* (Foreman), *Archaeodictyomitra* sp. (Fig. 4s), *Archaeodictyomitra* (?) sp., *Emiluvia* (?)
49 sp., *Eoxitus* sp., *Hiscocapsa* (?) sp., *Holocryptocanium barbui* Dumitrica (Fig. 4t),
50 *Holocryptocanium* sp. cf. *H. barbui* Dumitrica, *Pantanellium* sp., *Praeconosphaera* (?) sp.,
51 *Pseudodictyomitra lanceoloti* Schaaf (Fig. 4u), *Pseudodictyomitra* sp. cf. *P. lanceoloti* Schaaf,
52 *Thanarla pulchra* (Squinabol), *Thanarla* sp. aff. *T. brouweri* (Tan), *Thanarla* sp. cf. *T. pacifica*
53
54
55
56
57
58
59
60

1
2
3 Nakaseko & Nishimura (Fig. 4v), *Thanarla* sp. cf. *T. praeveneta* Pessagno, ~~*Thanarla* sp. cf. *T.*~~
4
5 ~~*pulchra* (Squinabol)~~, *Thanarla* sp., *Thanarla* (?) sp.

6
7 AGE: late Hauterivian to middle Aptian-early Albian (UAZ. 20 - Costata subzone of Turbocapsula
8
9 Zone, Zone after O'Dogherty, 1994; UAZone after Baumgartner *et al.*, 1995b) for the presence of
10
11 *Pseudodictyomitra lanceoloti* Schaaf. Range after Baumgartner *et al.* (1995a) and Bandini *et al.*
12
13 (2011).
14

15
16
17
18 TU10.31: *Angulobracchia* (?) sp., *Archaeodictyomitra lacrimula* (Foreman) (Fig. 5a),
19
20 *Archaeodictyomitra mitra* Dumitrica, *Archaeodictyomitra* sp. cf. *A. lacrimula* (Foreman),
21
22 *Archaeodictyomitra* sp., *Aurisaturnalis carinatus perforatus* Dumitrica & Dumitrica Jud (Fig. 5b),
23
24 *Dicerosaturnalis trizonalis* (Rüst), *Halesium* (?) sp., *Pantanellium* sp., *Praeconosphaera* (?) sp. cf.
25
26 *P. (?) multiconus* Yang, *Praeconosphaera* (?) sp., *Praexitus* sp., *Pseudodictyomitra lanceoloti*
27
28 Schaaf, *Pseudodictyomitra* sp. cf. *P. lanceoloti* Schaaf, *Pseudodictyomitra* sp., *Pseudodictyomitra* (?)
29
30 sp., *Spinosicapsa* (?) sp., *Thanarla brouweri* (Tan) (Fig. 5c), *Thanarla* sp. cf. *T. brouweri* (Tan),
31
32 *Thanarla* sp. cf. *T. pacifica* Nakaseko & Nishimura, *Thanarla* sp. cf. *T. pulchra* (Squinabol),
33
34 *Thanarla* sp., *Xitus* sp., *Xitus* (?) sp.
35
36
37

38 AGE: middle late Barremian-early early Aptian for the occurrence of *Aurisaturnalis carinatus*
39
40 *perforatus* Dumitrica & Dumitrica Jud. Range after Dumitrica and Dumitrica-Jud (1995).
41
42
43
44

45 Section 5

46
47 TU10.35: *Archaeodictyomitra* (?) sp., *Dicerosaturnalis trizonalis* (Rüst), ~~*Dicerosaturnalis* sp. cf. *D.*~~
48
49 ~~*trizonalis* (Rüst)~~, *Dicerosaturnalis* sp. cf. *D. trizonalis* (Rüst), *Emiluvia* sp. cf. *E. ultima*
50
51 Baumgartner, *Emiluvia* sp., *Eucyrtidiellum pyramis* (Aita) (Fig. 5d), *Mirifusus* sp. cf. *M. dianae*
52
53 (Karrer) s.l., *Mirifusus* sp., *Napora* sp., *Podocapsa amphitreptera* Foreman (Fig. 5e), ~~*Podocapsa*~~
54
55 ~~*amphitreptera* Foreman~~, *Praeconosphaera* (?) sp., *Pseudodictyomitra* (?) sp., *Spinosicapsa* (?) sp.,
56
57
58
59
60

1
2
3 *Svinitzium* (?) sp., *Syringocapsa* (?) sp., *Triactoma* sp. cf. *T. jonesi* (Pessagno), *Triactoma* (?) sp.,
4
5 *Zhamoidellum* (?) sp.

7 AGE: early-early late Tithonian to latest Tithonian-earliest Berriasian (UAZ. 12-13; UAZones after
8
9 Baumgartner *et al.*, 1995b) for the presence of *Eucyrtidiellum pyramis* (Aita). Range after
10
11 Baumgartner *et al.* (1995a).

16 TU10.36: *Archaeodictyomitra apiarium* (Rüst), *Archaeodictyomitra* sp. aff. *A. excellens* (Tan),
17
18 *Archaeodictyomitra* sp. aff. *A. rigida* Pessagno, *Archaeodictyomitra* sp. cf. *A. apiarium* (Rüst),
19
20 *Archaeodictyomitra* sp. 1, *Archaeodictyomitra* sp., *Cinguloturris cylindra* Kemkin & Rudenko (Fig.
21
22 5f), *Emiluvia* sp. cf. *E. ordinaria* Ozvoldova (Fig. 5g), *Emiluvia* sp. cf. *E. orea* Baumgartner,
23
24 *Emiluvia* (?) sp., *Eucyrtidiellum pyramis* (Aita) (Fig. 5h), *Eucyrtidiellum* (?) sp. cf. *E. (?) quinatum*
25
26 Takemura, *Loopus primitivus* (Matsuoka & Yao) (Fig. 5i), *Loopus* sp. cf. *L. doliolum* Dumitrica,
27
28 *Mirifusus diana* s.l. (Karrer), *Mirifusus* sp., *Olanda* sp., *Podocapsa amphitreptera* Foreman,
29
30 *Praeconosphaera* (?) *sphaeroconus* (Rüst), *Praeconosphaera* (?) sp. cf. *P. (?) sphaeroconus* (Rüst),
31
32 *Praeconosphaera* (?) sp., *Pseudodictyomitra* sp. cf. *P. carpatica* (Lozyniak), *Pseudodictyomitra* (?)
33
34 sp., *Ristola cretacea* (Baumgartner) (Fig. 5j), *Ristola* (?) sp., *Sethocapsa horokanaiensis* Kawabata,
35
36 *Syringocapsa* (?) sp., *Zhamoidellum* sp. cf. *Z. sp. A* sensu Goričan (1994), *Zhamoidellum* sp.

40 AGE: early-early late Tithonian (UAZ. 12; UAZone after Baumgartner *et al.*, 1995b) for the
41
42 occurrence of *Cinguloturris cylindra* Kemkin & Rudenko, *Eucyrtidiellum pyramis* (Aita), *Ristola*
43
44 *cretacea* (Baumgartner) with *Loopus primitivus* (Matsuoka & Yao). Ranges after Baumgartner *et al.*
45
46 (1995a).

51 TU10.37: *Archaeodictyomitra* (?) sp., *Podocapsa amphitreptera* Foreman (Fig. 5k), *Podocapsa*
52
53 *amphitreptera* Foreman, *Praeconosphaera* (?) *sphaeroconus* (Rüst) (Fig. 5l), *Pseudodictyomitra* (?)
54
55 sp., *Spinocapsa* (?) sp.

1
2
3 AGE: late Oxfordian-early Kimmeridgian to latest Valanginian-earliest Hauterivian (UAZ. 10-18;
4 UAZones after Baumgartner *et al.*, 1995b) for the occurrence of *Praeconosphaera* (?) *sphaeroconus*
5 (Rüst) with *Podocapsa amphitreptera* Foreman. Ranges after Baumgartner *et al.* (1995a), Chiari *et*
6 *al.* (2007) and Bandini *et al.* (2011).
7
8
9
10

11
12
13
14 TU10.38: *Archaeodictyomitra* sp. aff. *A. chalilovi* (Aliev), *Archaeodictyomitra* sp. aff. *A. excellens*
15 (Tan), *Archaeodictyomitra* sp. aff. *A. ioniana* Danelian, *Archaeodictyomitra* sp. cf. *A. apiarium*
16 (Rüst), *Archaeodictyomitra* sp. cf. *A. excellens* (Tan) (Fig. 5m), *Archaeodictyomitra* sp. cf. *A.*
17 *minoensis* (Mizutani), *Archaeodictyomitra* sp., *Archaeodictyomitra* (?) sp., *Becus* (?) sp.,
18 *Cinguloturris* sp. cf. *C. carpatica* Dumitrica, *Dicerosaturnalis trizonalis* (Rüst), *Dicerosaturnalis*
19 sp. cf. *D. trizonalis* (Rüst), *Emiluvia* sp., *Pantanellium* sp., *Podocapsa amphitreptera* Foreman (Fig.
20 5n), *Praeconosphaera* (?) sp., *Pseudodictyomitra* sp. cf. *P. thurowi* Dumitrica, *Pseudodictyomitra*
21 sp., *Saitoum* sp. cf. *S. elegans* De Wever (Fig. 5o), *Saitoum* (?) sp., *Spinosicapsa* (?) sp.,
22 *Syringocapsa* (?) sp., *Zhamoidellum ovum* Dumitrica (Fig. 5p), *Zhamoidellum* sp.
23
24
25
26
27
28
29
30
31
32
33

34 AGE: middle-late Oxfordian to late Kimmeridgian-early Tithonian (UAZ. 9-11; UAZones after
35 Baumgartner *et al.*, 1995b) for the presence of *Podocapsa amphitreptera* Foreman and
36 *Zhamoidellum ovum* Dumitrica. Ranges after Baumgartner *et al.* (1995a) and Smuc and Goričan
37 (2005).
38
39
40
41
42
43
44

45 **Section 7**

46
47 TU10.45: *Archaeodictyomitra* sp. cf. *A. communis* (Squinabol), *Archaeodictyomitra* sp. cf. *A.*
48 *coniforma* Dumitrica (Fig. 5q), *Archaeodictyomitra* sp., *Archaeodictyomitra* (?) sp.,
49 *Cryptamphorella clivosa* (Aliev) (Fig. 5r), ~~*Dictyomitra* sp.~~ *Godia* sp. cf. *G. decora* (Li & Wu),
50 *Godia* (?) sp., *Holocryptocanium* sp. cf. *H. barbui* Dumitrica, *Praeconosphaera* (?) *sphaeroconus*
51 (Rüst) (Fig. 5s), *Praeconosphaera* (?) sp., ~~*Pseudodictyomitra* sp.~~ *Pseudodictyomitra* (?) sp.,
52
53
54
55
56
57
58
59
60

1
2
3 *Tethysetta* sp. cf. *T. usotanensis* (Tumanda), *Thanarla brouweri* (Tan), *Thanarla* sp. cf. *T. pulchra*
4
5 (Squinabol), *Thanarla* sp., *Thanarla* (?) sp.

7 AGE: Valanginian to middle Aptian-early Albian (Valanginian to Costata subzone of Turbocapsula
8
9 Zone; Zone after O'Dogherty, 1994) for the presence of *Cryptamphorella clivosa* (Aliev) with
10
11 *Praeconosphaera* (?) *sphaeroconus* (Rüst). Ranges after Aliev (1967), O'Dogherty (1994), Filippov
12
13 and Kemkin (2005), Chiari *et al.* (2007) and Bandini *et al.* (2011).

18 **Section 8**

20 TU10.47: *Archaeodictyomitra excellens* (Tan) (Fig. 5t), *Archaeodictyomitra lacrimula* (Foreman),
21
22 *Archaeodictyomitra* sp. cf. *A. communis* (Squinabol), *Archaeodictyomitra* sp. cf. *A. ioniana*
23
24 Danelian, *Archaeodictyomitra* sp. cf. *A. vulgaris* Pessagno, *Archaeodictyomitra* sp.,
25
26 *Archaeodictyomitra* (?) sp., *Cecrops Cana septemporatus* (Parona) (Fig. 5u), *Dictyomitra* sp.,
27
28 *Halesium* sp. cf. *H. palmatum* Dumitrica (Fig. 5v), *Hiscocapsa* sp. cf. *H. grutterinki* (Tan),
29
30 *Hiscocapsa* sp., *Holocryptocanium barbui* Dumitrica, *Holocryptocanium* sp. cf. *H. barbui*
31
32 Dumitrica, *Mictyoditra* sp. cf. *M. thiensis* (Tan), *Pantanellium* sp., *Praeconosphaera* (?) sp. cf. *P.*
33
34 (?) *sphaeroconus* (Rüst), *Praeconosphaera* (?) sp., *Pseudodictyomitra* sp. cf. *P. sp. 5* in Dumitrica
35
36 *et al.* (1997), *Pseudodictyomitra* sp., *Pseudodictyomitra* (?) sp., *Pseudoxitus* (?) sp., *Syringocapsa*
37
38 (?) sp., *Thanarla* sp. cf. *T. brouweri* (Tan), *Thanarla* sp., *Thanarla* (?) sp., *Williriedellum* (?) sp.,
39
40
41 *Xitus* sp. cf. *X. normalis* (Wu & Li), *Xitus* sp., *Xitus* (?) sp.

44
45 AGE: late Valanginian-early Barremian (UAZ. 17-21; UAZones after Baumgartner *et al.*, 1995b)
46
47 for the presence of *Cecrops Cana septemporatus* (Parona). Ranges after Baumgartner *et al.* (1995a).

51
52 TU10.48: Age not determinable for the very low preservation of radiolarians.

55
56 TU10.51: *Acaeniotyle* sp. cf. *A. umbilicata* (Rüst), *Archaeodictyomitra lacrimula* (Foreman) (Fig.
57
58 5w), *Archaeodictyomitra* sp. cf. *A. communis* (Squinabol), *Archaeodictyomitra* sp.,
59
60

1
2
3 *Archaeodictyomitra* (?) sp., *Crucella* (?) sp., *Praeconosphaera* (?) sp., *Pseudodictyomitra* (?) sp.,
4
5 *Pseudoeuycyrtis* sp. cf. *P. hanni* (Tan) sensu O'Dogherty (1994) (Fig. 5x), *Spinocapsa* (?) sp.,
6
7 *Thanarla* sp. cf. *T. pulchra* (Squinabol), *Thanarla* sp.

8
9
10 AGE: early-early late Berriasian to middle Aptian-early Albian (UAZ. 14 - Costata subzone of
11
12 Turbocapsula Zone, Zone after O'Dogherty, 1994; UAZone after Baumgartner *et al.*, 1995b) for the
13
14 presence of *Archaeodictyomitra lacrimula* (Foreman). Range after Baumgartner *et al.* (1995a) and
15
16 O'Dogherty (1994).

17
18
19
20
21 TU10.MIO: *Archaeodictyomitra* sp., *Archaeodictyomitra* (?) sp., *Kilinora* (?) sp., *Triversus* (?) sp.

22
23 AGE: Age not determinable for the low preservation of radiolarians.
24
25
26

27 **5. Petrography and Geochemistry of the basaltic rocks**

28 29 30 31 **5.a Petrography**

32
33
34 All the studied rocks are affected by low-temperature, ocean-floor alteration, which resulted in
35
36 the replacement of primary minerals, though primary igneous textures are well preserved.
37
38 Plagioclase is usually replaced by albite or calcite and rarely by clay mineral assemblages.
39
40 Clinopyroxene is normally pseudomorphosed either by chlorite or actinolitic amphibole. In samples
41
42 TU10-22 and TU10-23 (Section 3) clinopyroxene is replaced by brown hornblende, though fresh
43
44 clinopyroxene relics are locally observed. The groundmass secondary phases mainly consist of
45
46 chlorite, and clay minerals. Regardless of the secondary mineralogical transformation, the following
47
48 petrographic description of the various rock-types has been made on the bases of the primary
49
50 igneous phases. Moreover, for a better understanding, it has been made according to the
51
52 geochemical groups described in the next section.
53
54
55
56
57
58
59
60

1
2
3 *Group 1.* Pillow and massive lavas have aphyric, micro-crystalline sub-ophitic textures in which
4 only small laths of plagioclase can be recognized. Pillow breccias are generally monogenetic and
5 show coarse-grained, intergranular texture with euhedral plagioclase and interstitial clinopyroxene.
6
7

8
9 *Group 2.* Massive lavas show both aphyric and porphyritic (PI = ~40) textures. In both varieties,
10 the groundmass texture is hyalopilitic. Phenocrysts are represented by large crystals of plagioclase.
11
12

13
14 *Groups 3 and 4.* Pillow and massive lavas most commonly display aphyric, ophitic or sub-
15 ophitic textures with crystal size ranging from micro-crystalline to coarse-grained. Nonetheless, a
16 few samples display slightly porphyritic textures with plagioclase microphenocrysts. In addition,
17 hyalopilitic texture is locally observed. The groundmass mineral assemblage includes plagioclase,
18 clinopyroxene, and variable amount of opaque phases. Pillow breccias are generally monogenetic
19 and the individual fragments are texturally and compositionally similar to the pillow lavas. Most of
20 these rocks are characterized by variable abundance of varioles filled by calcite. In all the studied
21 rock groups, the crystallization order is: plagioclase + clinopyroxene ± Fe-Ti-oxides.
22
23
24
25
26
27
28
29
30
31
32
33

34 **5.b Analytical methods**

35
36 Whole-rock major and some trace element analyses were obtained by X-ray fluorescence (XRF)
37 on pressed-powder pellets, using an ARL Advant-XP automated X-ray spectrometer. The matrix
38 correction methods proposed by Lachance & Trail (1966) were applied. Volatile contents were
39 determined as loss on ignition (L.O.I.) at 1000°C. In addition, Rb, Sr, Nb, Hf, Ta, Th, U, and the
40 rare earth elements (REE) were determined on twelve representative samples by inductively
41 coupled plasma-mass spectrometry (ICP-MS) using a Thermo Series X-I spectrometer.
42
43
44
45
46
47
48

49 The CO₂ content was determined by simple volumetric technique (Jackson, 1958) only on the
50 samples affected by calcite veins and amygdales. This technique was calibrated using standard
51 amounts of reagent grade CaCO₃. In addition, for the discussion of the geochemical characteristics
52 and for a better comparison of chemical data, the major element composition of these samples was
53 recalculated on calcite-free bases. In detail, CaO content in secondary calcite has been calculated
54
55
56
57
58
59
60

1
2
3 according to stoichiometric proportions with CO₂ contents, given that the secondary carbonates are
4 exclusively composed of calcite. Major element composition has then been re-calculated to 100
5 wt% without considering L.O.I. and CaO in calcite.
6
7

8
9 The accuracy of the data for XRF and ICP-MS analyses were evaluated using results for
10 international standard rocks run as unknown. The detection limits for XRF and ICP-MS analyses
11 were evaluated using results from several runs of about twenty-nine international standards.
12 Accuracy and detection limits for the CO₂ analyses were determined using different amounts of
13 reagent grade CaCO₃ run as unknown. Results are given in Appendix A. All whole-rock analyses
14 were performed at the Dipartimento di Science della Terra, Università di Ferrara. The results are
15 shown in Table 1.
16
17
18
19
20
21
22
23
24
25
26

27 **5.c Geochemistry**

28
29 The following geochemical description is made mainly using those major and trace elements that
30 are virtually immobile during low-temperature alteration and metamorphism (e.g., Pearce & Norry,
31 1979). These elements include many incompatible element, such as: Ti, P, Zr, Y, Sc, Nb, Ta, Hf, Th,
32 middle (M-) and heavy (H-) REE, as well as some transition metals (e.g., Ni, Co, Cr, V). Light REE
33 (LREE) may be affected by some mobilization during alteration. However, the good correlations
34 between these elements and many immobile elements (not shown) indicate that LREE have not been
35 mobilized by the alteration. For example, the correlation coefficients (r^2) for the linear correlation Zr
36 – La and Zr – Ce are 0.96 and 0.90, respectively. Rb, Ba, K, and Sr are commonly mobilized during
37 alteration. In fact, these elements plotted against Zr generally show low or very low r^2 . However, the
38 fairly good correlation with Zr and Rb in Group 4 samples ($r^2 = 0.91$), as well as Ba in Group 4 ($r^2 =$
39 0.87) and in Group 2 samples ($r^2 = 0.85$), suggest that these elements were only slightly mobilized
40 during alteration in these rock-types.
41
42
43
44
45
46
47
48
49
50
51
52
53
54

55
56 According to Bortolotti *et al.* (2013b), four groups of volcanic rocks can be recognised in the
57 studied sections. Group 1 is represented by basalts cropping out in the Sections 5 and 8. These rocks
58
59
60

1
2
3 have a clear sub-alkaline nature with low Nb/Y ratios (Fig. 6) and show relatively high TiO₂, P₂O₅,
4 Zr, and Y contents. Ni is generally low, whereas Cr is relatively high, with the only exception of
5 sample TU10-49b. V content is also generally high (Table 1). The values of these elements are
6 similar to those of Group 2 basalts (see below). By contrast, Hf, Ta, Th, and U contents are low.
7 These rocks show a sharp increase of FO_t and Y and a sharp decrease of Mg# and Ni with increasing
8 Zr, as well as very low Th/Tb ratios (Fig. 7). *Group 1* basalts are characterized by flat normalized
9 incompatible element patterns (Fig. 8a). The REE abundance (Fig. 8b) varies from ~10 to ~20 times
10 that of chondrite and displays LREE/MREE smoothly depleted patterns with (La/Sm)_N ratios ranging
11 from 0.78 to 0.82. The overall geochemical features of these rocks, as well as both incompatible
12 elements and REE patterns resemble those of typical N-MORB (Sun & McDonough, 1989).
13 Nonetheless, HREE are slightly depleted with respect to both LREE and MREE (Fig. 8b) with
14 (La/Yb)_N ratios = 1.06 – 1.30 and (Sm/Yb)_N ratios = 1.31 – 1.58. In particular, the (Sm/Yb)_N ratios
15 are higher than that of typical N-MORB (Sm_N/Yb_N = 0.96, Sun & McDonough, 1989). These values
16 are comparable to those of garnet-influenced MORBs (G-MORB) from the External Ligurides of
17 Northern Apennine (Sm_N/Yb_N = 1.25-1.50, Montanini *et al.*, 2008), Corsica (Sm_N/Yb_N = 1.30-1.81,
18 Saccani *et al.*, 2008), and Elba Island (Sm_N/Yb_N = 1.49-2.10, Saccani & Principi, 2016), as well as to
19 those of the Paleozoic Misho mafic complex in north Iran (Saccani *et al.*, 2013a) and the Mesozoic
20 Kermanshah ophiolites in south Iran (Saccani *et al.*, 2013b). The G-MORB affinity of Group 1 rocks
21 is also suggested by Th-Nb co-variation and by their (Ce/Yb)_N and (Dy/Yb)_N ratios (Fig. 9), although
22 in the most common tectonic discrimination diagrams these basalts plot in the field for N-MORBs
23 (e.g., Fig. 10).

24
25
26
27
28
29
30
31
32
33
34
35
36
37
38
39
40
41
42
43
44
45
46
47
48
49
50
51
52
53
54
55
56
57
58
59
60
Group 2 is represented by basalts cropping out in the Sections 4 and 7. These rocks have a sub-alkaline nature with low Nb/Y ratios ranging from 0.27 to 0.40 (Fig. 6) and show relatively high TiO₂, P₂O₅, Zr, and Y contents (Table 1). Ni, though variable, is generally low, whereas Cr and V are rather high. As exemplified in the variation diagrams in Figure 7, these rocks have major element contents and compositions of many trace elements largely overlapping those of Group 1 basalts.

1
2
3 Nonetheless, as a distinctive feature, Group 2 basalts are characterized by LILE/HFSE smoothly
4 enriched patterns (Figs. 8c). Likewise, REE patterns show a slight enrichment in LREE compared to
5 HREE (Figs. 8d), with $(La/Sm)_N$ and $(La/Yb)_N$ ratios ranging from 1.12 to 1.51 and from 1.27 to
6 2.19, respectively. These patterns are similar to that of the typical enriched-type MORB (E-MORB)
7 of Sun & McDonough, 1989. The Th-Nb values are also similar to those of the typical E-MORB
8 (Fig. 9a). In the most common tectonic discrimination diagrams these basalts plot across the
9 boundary between the fields for N-MORB and E-MORB (e.g., Fig. 10).
10
11
12
13
14
15
16
17

18 *Group 3* is represented by pillow basalts and ferrobasalts from Section 2, as well as by massive
19 lava basalts from Section 9. These rocks have a transitional nature, as testified by their high Nb/Y
20 ratios (Fig. 6). Basalt TU10-15 (Section 2) displays a rather primitive composition with relatively
21 high Mg# and low TiO₂ and P₂O₅ contents (Table 1). In contrast, ferrobasalts from Section 2 and
22 basalts from Section 9 have rather evolved compositions with relatively low Mg# and very high
23 TiO₂ and P₂O₅ contents (Table 1). Accordingly, Ni and Cr contents are generally high in basalts,
24 whereas they are relatively low in the differentiated rocks. Except for Mg#, the variation of many
25 elements with respect to Zr display roughly common evolutionary trends towards high contents of
26 the incompatible elements and FeO_t and low contents of the compatible elements for all Group 3
27 samples (Fig. 7). In contrast, Mg# for samples from Sections 2 and 9 show distinct evolutionary
28 trends with respect to Zr. All these trends are compatible with a magmatic evolution by fractional
29 crystallization. The Th/Tb ratios of these rocks are significantly higher than those of Groups 1 and 2
30 rocks and significantly lower than those of Group 4 rocks (Fig. 7). Group 3 rocks show high
31 abundance in LFSE with respect to N-MORB and display regularly decreasing N-MORB
32 normalized patterns from Rb to Y (Fig. 8e). The REE abundance (Fig. 8f) varies from ~30 to ~100
33 and from ~10 to ~12 times that of chondrite for LREE and HREE, respectively. These rocks
34 displays LREE/MREE and LREE/HREE enriched patterns, with $(La/Sm)_N$ ratios = 2.61 - 4.15 and
35 $(La/Yb)_N$ ratios = 4.65 - 9.17. These incompatible elements and REE patterns are comparable with
36 those of P-MORB (plume-type MORB). This conclusion is also supported by the co-variation of the
37
38
39
40
41
42
43
44
45
46
47
48
49
50
51
52
53
54
55
56
57
58
59
60

1
2
3 Th and Nb concentrations (Fig. 9a). In the most common tectonic discrimination diagrams (e.g.,
4
5 Fig. 10) these rocks generally plot in the fields for E-MORBs and alkaline ocean island basalts
6
7 (OIB).
8

9
10 *Group 4* is represented mainly by alkaline basalts and subordinate trachytes from Sections 1 and
11
12 3. These rocks have a clear alkaline nature, as testified by their very high Nb/Y ratios (Fig. 6).
13
14 Alkaline basalts from Section 3 mainly display relatively primitive compositions, whereas alkaline
15
16 basalts from Section 1 represent rather evolved compositions. Generally, all samples have high
17
18 contents of TiO₂, P₂O₅, Zr, Nb, Hf, Th and low contents of compatible elements (Table 1, Fig. 7). In
19
20 the variation diagrams in Figure 7, rocks from the different sections show different evolutionary
21
22 trends, most likely reflecting the distinct evolutions of magmas of different initial compositions.
23
24 This is particularly evident in the FeO_t, Mg#, Ni, and Y vs. Zr diagrams. Nonetheless, the well-
25
26 defined trends observed for samples from each single section suggest that each section consist of
27
28 rocks belonging to a comagmatic suite. Group 4 rocks show high abundance in LFSE with respect
29
30 to N-MORB and display regularly decreasing N-MORB normalized patterns from Rb to Y (Fig.
31
32 8g). The REE abundance (Fig. 8h) varies from ~60 to ~400 and from ~9 to ~10 times that of
33
34 chondrite for LREE and HREE, respectively. These rocks displays LREE/MREE and LREE/HREE
35
36 strongly enriched patterns, with (La/Sm)_N ratios = 4.15 - 5.25 and (La/Yb)_N ratios = 18.75 - 23.13.
37
38 Group 4 rocks can readily be distinguished from Group 3 rocks, as they show higher Zr,
39
40 incompatible element, and LREE concentrations, as well as Th/Tb ratios at comparable Mg# (Figs.
41
42 7, 7g, h). The overall geochemistry of these basalts resembles that of alkaline basalts generated at
43
44 within-plate ocean island settings (OIB), as also exemplified by the generally high Ti/V ratios
45
46 (Table 1). This conclusion is also supported by the co-variation of the Th and Nb values (Fig. 9), as
47
48 well as by the most common tectonic discrimination diagrams (e.g., Fig. 10).
49
50
51
52
53
54
55
56
57
58
59
60

6. Discussion

6.a Mantle melting processes and magma generation

One of the main goals of this study is to assess the nature and tectonic significance of the magmatic events that occurred in the Turkish sector of the Neotethys during the Middle Jurassic – Early Cretaceous time span. According to many authors (e.g., Pearce, 1982), the compositional differences between magma types are related to different source characteristics that are associated, in turn, to distinct tectono-magmatic settings of formation. We will therefore focus our petrogenetic discussion to the identification of the possible mantle sources and related tectonic setting of formation of the four distinct lava groups identified in the previous chapter, which are: (1) G-MORBs (Group 1); (2) E-MORBs (Group 2); (3) P-MORBs (Group 3); (4) OIB-type alkaline volcanic rocks (Group 4). Unfortunately, the chemical variation due to fractional crystallization cannot be defined in detail, as the mélange nature of the sampled rocks prevents us to establish definite genetic relationships between rocks within each single chemical group. Nonetheless, some trace element ratios (e.g., Zr/Nb, Ce/Y, Th/Ta, Th/Tb) are little affected by fractional crystallization of predominantly olivine + clinopyroxene + plagioclase. Therefore, even in presence of significant amounts of fractionation, they are believed to represent the elemental ratios in the source (e.g., Allègre & Minster, 1978; Beker *et al.*, 1997). Ratios of incompatible elements (Ce/Y, Nb/Yb), ratios of hygromagmatophile element ratios ((Th/Ta)/(Th/Tb)) (Table 1), as well as distinct normalized multi-element and REE patterns (Fig. 8) suggest that the different magmatic rocks from the Ankara Mélange units have been most likely originated from chemically distinct mantle sources. In order to constrain the possible mantle sources of the different rock series of the Ankara Mélange, non-modal, batch partial melting models are presented in Figure 11. A rigorous quantification of the melting processes is not possible as the composition of the mantle sources are difficult to constrain. However, a semi-quantitative modelling of the REE can place some solid constraints. The melt modelling uses plots of LREE/HREE (i.e., La/Yb) vs. MREE/HREE (i.e., Dy/Yb) ratios, which are particularly useful for distinguishing between melting in the spinel and garnet stability fields (Thirlwall *et al.*, 1994). Partial melting of a mantle source in the spinel-facies produces little change

1
2
3 in Dy/Yb ratios in melts with respect to melt fraction. In contrast, mantle partial melting in the
4
5 garnet-facies produces large changes in Dy/Yb ratios with melt fraction. In both cases, La/Yb ratios
6
7 are particularly responsive to melt fraction change (Fig. 11). Another important feature of these plots
8
9 is that mixing between different melt fractions will generate linear mixing arrays (e.g., Beker *et al.*,
10
11 1997).
12

13
14 *Group 1 basalts.* As observed in the previous chapter, the Group 1 rocks (G-MORBs) show
15
16 unusually high MREE/HREE ratios ($Dy_N/Yb_N = 1.20 - 1.34$) compared to the typical N-MORB
17
18 ($Dy_N/Yb_N = 1$, Sun & McDonough, 1989). REE modelling for Group 1 basalts (Fig. 11a) shows that
19
20 these rocks cannot have been simply derived from partial melting of a typical depleted MORB
21
22 mantle (DMM) source (Workman & Hart, 2005) in the spinel-facies. Rather, their significant
23
24 HREE/MREE fractionation can be interpreted as a garnet signature, which can be related either to a
25
26 deep initiation of melting in the garnet peridotite stability field, or to the melting of an
27
28 heterogeneous mantle source characterized by garnet-bearing mafic/ultramafic layers (e.g.,
29
30 Montanini *et al.*, 2008; Saccani *et al.*, 2008; Saccani, 2015). However, melting of a DMM source
31
32 bearing garnet mafic/ultramafic layers would generate primary melts characterized by high
33
34 MREE/HREE ratios coupled with low (<0.8) LREE/HREE ratios (not shown). By consequence, the
35
36 high (1.06 - 1.30) LREE/HREE ratios observed in the Group 1 basalts are inconsistent with this
37
38 hypothesis. Therefore, in Figure 11a the partial melting model of DMM source that starts in the
39
40 garnet-facies and continues to larger degrees in the spinel-facies (with various combinations of
41
42 melting fractions in the garnet- and spinel-facies) is shown. It can be observed that the REE
43
44 composition of the Group 1 basalts is compatible with the calculated compositions for 2.5% melting
45
46 in the garnet-facies and 10% melting in the spinel-facies, assuming mixing of ~70-80% of melt
47
48 derived from spinel-facies mantle with ~30-20% melt from garnet-facies mantle.
49
50
51
52

53
54 *Group 2 basalts.* Group 2 basalts (E-MORBs) show variable LREE/HREE enrichments (Fig.
55
56 8d), which can be considered as a result from variable mixing between depleted and enriched
57
58 asthenospheric sources or, alternatively, from lower degree of partial melting of a DMM source,
59
60

1
2
3 compared to N-MORBs. In fact, basalt TU10-32 is generally compatible with low degree (~2.5%)
4 of partial melting of a DMM source in the spinel-facies (Fig. 11b). However, basalt TU10-46 shows
5 HREE values lower than those of the N-MORBs of Group 1, which cannot be generated by lower
6 degrees of partial melting of a common mantle source (Figs. 8b, d). In addition, lower degrees of
7 partial melting of a DMM source in the spinel-facies cannot generate the $(La/Yb)_N$ and $(Dy/Yb)_N$
8 ratios of this sample. The most appropriate solution for the genesis of this E-MORB sample is not
9 straightforward. The LREE/HREE and MREE/HREE ratios are compatible with mixing of melt
10 derived from very low degree (~1%) partial melting of a DMM source in the garnet-facies with melt
11 derived from much larger degree (~10%) of partial melting in the spinel-facies mantle (Fig. 11a).
12 The REE composition of these basalts is compatible with mixing of <10% of melts generated in the
13 garnet-facies with >90% of melts generated in the spinel-facies. Nonetheless, a possible alternative
14 solution is to invoke a more enriched source than DMM. Figure 11b shows that the melting curve of
15 a hypothetical DMM source slightly enriched LREE with $(La/Yb)_N = 1.09$ and $(Dy/Yb)_N = 1.49$,
16 and has a Yb concentration equal to that of DMM ($Yb_N = 2.08$). The model shows that the REE
17 composition of E-MORB TU10-46 is compatible with the calculated composition for ~8% partial
18 melting of this theoretical source in the spinel facies.
19
20
21
22
23
24
25
26
27
28
29
30
31
32
33
34
35
36
37

38 *Group 3 and Group 4 rocks.* The high LREE/HREE ratios displayed by the transitional basalts of
39 Group 3 rocks (P-MORBs) and by the alkaline basalts of Group 4 (Figs. 8f, h) suggest an
40 involvement of a garnet peridotite source. Moreover, the high La/Yb ratio observed in these basalts
41 implies a source more enriched in LREE than DMM. In fact, variable degrees of partial melting of a
42 DMM source in the spinel-facies cannot generate the observed La/Yb ratios and variable degrees of
43 partial melting of a DMM source in the garnet-facies cannot generate the observed La/Yb and Dy/Yb
44 ratios (Fig. 11a). Therefore, the most appropriate solution is to invoke a more enriched source than
45 DMM, although it is impossible to assess the exact composition of this source. The model in Figure
46 11c illustrates melting curves for a hypothetical LREE-enriched source (Beker *et al.*, 1997) with
47 $(La/Yb)_N = 1.32$ and $(Dy/Yb)_N = 1.49$, and has a Yb concentration equal to that of DMM ($Yb_N =$
48
49
50
51
52
53
54
55
56
57
58
59
60

1
2
3 2.08). Higher Yb concentrations (e.g., PM values) in the source would generate concentrations of
4 HREE in the melts that are too high compared with the Group 3 and Group 4 volcanic rocks.
5

6
7 The co-variation in La/Yb-Dy/Yb systematics of Group 3 and Group 4 samples (Fig. 11c) cannot
8 however be explained by variable degrees of partial melting of this enriched source in either the
9 spinel- or garnet-facies. Melting in the garnet-facies produces melts with much higher Dy/Yb ratios
10 than those of both Group 3 and Group 4 samples at reasonable degrees of melting (i.e., <20%).
11
12 Alternatively, the mantle source would require an unusually low Dy/Yb ratio if the samples were to
13 be simply the product of garnet-facies mantle melting. By contrast, melting in the spinel-facies
14 produces melts with both La/Yb and Dy/Yb ratios lower than those of both Group 3 and Group 4
15 samples. Therefore, the simplest model to account for the REE systematics of these rocks involves
16 mixing of small melt fractions from garnet-facies enriched mantle with relatively larger melt
17 fractions from spinel-facies (Fig. 11c). This figure shows that the La/Yb-Dy/Yb systematics of
18 Group 3 basalts can be explained by mixing of small degree melts (~0.5-1%) and larger degree melts
19 (~5%) from garnet- and spinel-facies mantle, respectively. In contrast Likewise, the observed REE
20 data for Group 4 basalts can be accounted for by mixing of small degree melts (~0.5%) and larger
21 degree melts (~5%) from garnet- and spinel facies mantle, respectively melts from ~0.5% and ~5%
22 partial melting from garnet- and spinel-facies mantle, respectively. Alternatively, the La/Yb-Dy/Yb
23 systematics of Group 4 basalts can be explained by comparatively higher degree of melting (~1%) in
24 the garnet-facies mantle and comparatively lower degree of melting (~2.5%) in the spinel-facies
25 mantle. In any case, the different La/Yb-Dy/Yb ratios shown by Group 3 and Group 4 basalts can be
26 accounted for by mixing of different proportions of melts generated in the garnet- and spinel facies
27 mantle. In detail, Group 4 basalts may have resulted from mixing of ~60% of melt derived from
28 spinel-facies mantle with ~40% melt from garnet-facies mantle, whereas Group 3 basalts may have
29 resulted from mixing of ~90% of melt derived from spinel-facies mantle with ~10% melt from
30 garnet-facies mantle (Fig. 11c).
31
32
33
34
35
36
37
38
39
40
41
42
43
44
45
46
47
48
49
50
51
52
53
54
55
56
57
58
59
60

1
2
3 Figure 11b shows that the La/Yb and Dy/Yb ratios of Group 3 basalts can also be compatible with
4
5 very low degree (<0.8%) of partial melting in the spinel-facies of the slightly metasomatized mantle
6
7 source hypothesized for the genesis of Group 2 rocks. Such very low degree of partial melting is
8
9 however unreasonable. In fact, experimental studies on melt mobility in peridotites showed that very
10
11 small melt fractions are not readily mobile and therefore they remain within the host peridotite rather
12
13 than migrating to form volcanic rocks melt (see Warren, 2016 for a more detailed discussion).
14
15 Finally, it should be noted that variations in the degree of partial melting in the spinel field are
16
17 difficult to constrain due to the small range in La/Yb ratios generated by spinel-facies melting. Some
18
19 scatter in the La/Yb-Dy/Yb systematics (Fig. 11c) might be accounted for by small fluctuations in
20
21 the degree of melting of garnet-facies mantle. In any case, from a semi-quantitative point of view,
22
23 melt fractions in the garnet field are restricted to <1% whereas those in the spinel field are probably
24
25 several percent (~5%).
26
27
28

29
30 The possible influence of crustal contamination can be excluded as the Th-Nb compositions of all
31
32 rock-types plot within the MORB-OIB array (Fig. 9). Other geochemical indicators further support
33
34 this conclusion. For example, high Th/Ta and low Nb/U ratios are effective indicators of crustal
35
36 contamination. All Groups of Middle Jurassic–Early Cretaceous basalts from the Ankara mélange
37
38 show very low Th/Ta ratios (<1.74), as well as Nb/U ratios averaging 44 in N-MORBs, 50 in E-
39
40 MORBs, 40 in P-MORBs, and 43 in OIBs. These Nb/U ratios are comparable to those of the typical
41
42 N-MORB (49.6), E-MORB (46.1), and OIB (47.1) of Sun & McDonough (1989).
43
44

45 Bortolotti *et al.* (2013b) have noted that the association of depleted basalts (N-MORBs),
46
47 moderately enriched basalts (E-MORBs), and variably enriched rocks (P-MORBs and OIBs)
48
49 occurring in the Ankara Mélange is also observed in many peri-Mediterranean ophiolitic complexes
50
51 (e.g., Saccani & Photiades, 2005, Saccani *et al.*, 2011, and references therein), as well as from
52
53 several Middle East ophiolites (Allahyari *et al.*, 2010; Saccani *et al.*, 2010, 2013a, 2013b), where it
54
55 is interpreted as the result of partial melting of a MORB-type asthenospheric source enriched in
56
57 HFSE and LREE by an ocean island basalt (OIB) type [chemical](#) component (plume-type
58
59
60

1
2
3 component). Bortolotti *et al.* (2013b) have used the co-variation of Zr/Y and Zr/Nb to qualitatively
4
5 depict the influence of a plume-type component on MORB compositions in the Middle Jurassic –
6
7 Early Cretaceous basalts from the Ankara Mélange (Fig. 12). From Figure 12 it is evident that the
8
9 data conform extremely well to the mixing curve calculated using the OIB and N-MORB end-
10
11 members. Such mixing relationships are consistent with either magma mixing or source region
12
13 mixing (or eventually, a combination of these).
14
15

16 17 18 **6.b Tectono-magmatic significance** 19

20
21 The melting models carried out for the different groups of volcanic rocks, which are presented in
22
23 the previous section, allow to draw the following conclusions: 1) the geochemically distinct Groups
24
25 of Middle Jurassic – Early Cretaceous volcanic rocks in the Ankara Mélange are related to different
26
27 mantle source compositions and partial melting degrees; 2) regardless of their geochemical
28
29 affinities, all the studied volcanic rocks were generated by partial melting starting in the garnet-
30
31 facies mantle and continuing to larger degrees in the spinel-facies mantle. Perhaps, Group 2 basalts
32
33 from Section 7 may represent the only exception to this conclusion. In fact, their chemistry is
34
35 compatible either with partial melting starting in the garnet-facies mantle and continuing to larger
36
37 degrees in the spinel-facies mantle, or partial melting in the spinel facies from a slightly enriched
38
39 source. As shown before, the formation of enriched alkaline and P-MORB type rocks imply the
40
41 occurrence of mantle sources strongly metasomatized by OIB-type (i.e., plume-type) components.
42
43 Two alternative hypotheses can account for such OIB-type metasomatism of depleted mantle
44
45 sources: 1) the existence of plume activity in the region during Middle Jurassic – Early Cretaceous
46
47 times and 2) the existence of deep mantle heterogeneously modified by previous mantle plume
48
49 activity that occurred in the same area in association with the opening of the Neo-Tethys. However,
50
51 the extant geological evidence suggests that the first hypothesis can be disregarded. In fact, the lack
52
53 of magmatic evolution from more depleted to more enriched rocks that is commonly observed in
54
55 plume-related magmatism, the absence of basaltic plateaus, and a relatively small volume of plume-
56
57
58
59
60

1
2
3 related volcanic rocks collectively argue against the existence of a well established, long-lasting
4
5 mantle plume in the region. Therefore, we favour the hypothesis that the different Middle Jurassic –
6
7 Early Cretaceous volcanic rock types from the Ankara mélangé were formed from partial melting of
8
9 a strongly heterogeneous mantle, with OIB-type components inherited from a previous mantle
10
11 plume activity associated with the opening of the Neo-Tethys. In fact, the Anisian alkaline
12
13 volcanics intruding the Kütahya-Bolkardag have been interpreted as the early products of the rifting
14
15 of the Neotethys Ocean with the involvement of a plume (Göncüoğlu *et al.*, 2003; Göncüoğlu 2010;
16
17 Akal *et al.*, 2012). Recent studies on modern oceanic basins further support our favoured
18
19 hypothesis. In fact, these studies have demonstrated the upper mantle is much more heterogeneous
20
21 than previously thought (e.g., Brunelli *et al.*, 2006; Warren, 2016). The mantle heterogeneities can
22
23 be either the result of earlier tectonic events or ancient episodes of melting, melt extraction, and
24
25 melt entrapment and they can occur at local or at regional scale (e.g., Liu *et al.*, 2008; Warren *et al.*,
26
27 2009).

28
29
30
31 A possible tectono-magmatic model that can explain the formation of the different volcanic rock
32
33 from the Ankara mélangé during the Middle Jurassic – Early Cretaceous is shown in Figure 13. In
34
35 this model, the OIB-type metasomatized portions are likely to be prominent in the asthenospheric
36
37 mantle. The uprising asthenospheric mantle underwent polybaric partial melting, which started in
38
39 the garnet-facies and continued in the spinel-facies. The strongly enriched alkaline and P-MORB
40
41 rocks were generated from various, but limited degrees of polybaric partial melting of OIB-type
42
43 metasomatized portions. G-MORB and E-MORB were generated from various degrees of polybaric
44
45 partial melting of depleted asthenosphere portions. Alternatively, E-MORB (particularly, that of
46
47 Section 7) may have been generated from partial melting of a slightly enriched mantle source in the
48
49 spinel stability field. The tectono-magmatic model presented in Figure 13 implies that the different
50
51 rocks were formed by partial melting of chemically different portions of the sub-oceanic mantle in
52
53 different times. In consequence, this model does not necessarily imply the existence of genetic
54
55 relationship between different rock-groups or within a single rock-group.
56
57
58
59
60

6.c Geodynamic implications

The ages obtained for the studied radiolarian assemblages coupled with the geochemistry of the associated basalts indicate that a composite oceanic crust including G-MORB, E-MORB, P-MORB and alkaline basalts was forming during the Middle Jurassic- Early Cretaceous times. These ages are in agreement with the radiolarians (Bragin & Tekin, 1996; Tekin, 1999; Celik, 2010; Uner, 2010; Tekin *et al.*, 2012b; Göncüoğlu *et al.*, 2015) and foraminifera (Boccaletti *et al.*, 1966; Bortolotti & Sagri, 1968; Yaliniz *et al.*, 2000b; Rojay *et al.*, 2001) data obtained from different parts of the IAESB. The age ranges from the published biostratigraphical data indicate gaps in Early Jurassic and late Early Cretaceous (see Göncüoğlu *et al.* 2010). Moreover, Middle Jurassic findings were restricted to a limited number of samples. Our new findings partially fill the gap during late Early Cretaceous (see Göncüoğlu *et al.*, 2010). In fact, the radiolarian cherts associated to the G-MORB of Section 8 indicated a late Valanginian-early Barremian age.

The Middle Jurassic-Early Cretaceous rock assemblage found in the mélangé complexes of the IAESB, as well as the tectono-magmatic model presented in the previous section can be framed within the geodynamic model presented by Göncüoğlu (2010) (Fig. 14). According to this model, the rifting of the Neotethys Ocean started in Late Triassic with the involvement of a mantle plume (Fig. 14a). Anisian and Norian volcanic rocks showing alkaline affinity were erupted at this stage (Göncüoğlu *et al.*, 2003; Göncüoğlu 2010, Akal *et al.*, 2012; Bortolotti *et al.*, 2013b). The Early Jurassic history of this oceanic basin cannot be straightforwardly constrained due to the lack of data. In fact, Early Jurassic (Hettangian-Sinemurian) radiolarian chert blocks were found as single blocks in the Ankara Mélangé, but they are not associated with volcanic rocks (Çelik, 2010; Göncüoğlu *et al.*, 2015). Nonetheless, it is reasonable to postulate that during this time the Neotethys Ocean experienced an oceanic spreading phase. During the Middle Jurassic-Early Cretaceous time span the formation of a composite oceanic crust including G-MORB, E-MORB, P-

1
2
3 MORB and alkaline basalts suggest that the volcanic rocks of IAESB formed at a mid-ocean ridge
4 setting by tapping different portions of a deep, highly heterogeneous mantle (Fig. 14b). Mantle
5 heterogeneities consisted in portions variably enriched by OIB-type components, which were
6 inherited from the Triassic mantle plume activity associated with the opening of this Neotethys
7 oceanic branch (Fig. 14a). Our findings show that P-MORBs have Middle Jurassic age, G-MORBs
8 have Late Jurassic age, E-MORBs were erupted during the Early Cretaceous, and alkaline basalts
9 were erupted from Late Jurassic to Early Cretaceous. Partial melting of different portions of a
10 heterogeneous sub-oceanic mantle (Figs. 13, 14b) can explain the formation of different and
11 genetically unrelated magmatic rocks in the same time span.
12
13
14
15
16
17
18
19
20
21
22

23 The intra-oceanic subduction likely started from late Early Cretaceous on the northern side of
24 the Neotethys branch, leading to the production of SSZ-type rocks during the late Early Cretaceous
25 (Fig. 14c). Previous data on the earliest ages related to supra-subduction type volcanism and
26 formation of metamorphic sole indicated early Late Cretaceous (e.g., Ünner, 2010), therefore the
27 intra-oceanic decoupling within the ocean was considered as pre-Late Cretaceous. This age could
28 not be verified in this study, since in contrast to the western part of the IAESB, none of the basalt
29 samples collected from the eastern part yielded supra-subduction characteristics. The different rock-
30 types formed in the ocean were then incorporated into the accretionary prism during the Late
31 Cretaceous closure.
32
33
34
35
36
37
38
39
40
41
42
43
44
45
46
47
48
49
50
51
52
53
54
55
56
57
58
59
60

7. Conclusion

This study is focused on slide blocks including oceanic lavas associated with pelagic sediments within the eastern part of the Ankara Mélange. A detailed petrological characterization of the volcanic rocks and a detailed biochronological investigation of the associated radiolarites was carried out. The main conclusions can be summarized as follows.

1
2
3 1) The radiolarian cherts associated with volcanic rocks show the following ages: late
4 Valanginian to late Hauterivian (Section 1, OIB); early-middle Bajocian to late Bathonian-early
5 Callovian (Section 2, P-MORB); middle-late Oxfordian to late Kimmeridgian-early Tithonian
6 (Section 3, OIB); middle late Barremian-early early Aptian (Section 4, E-MORB); middle late
7 Oxfordian to late Kimmeridgian-early Tithonian and early-early late Tithonian (Section 5, G-
8 MORB); Valanginian to middle Aptian-early Albian (Section 7, E-MORB); late Valanginian-early
9 Barremian (Section 8, G-MORB).
10
11
12
13
14
15
16
17

18 2) Volcanic rocks are largely represented by basalts and minor ferro-basalts and trachytes. They
19 show different geochemical affinities and overlapping ages including: a) Late Jurassic-Early
20 Cretaceous garnet-influenced MORB; b) Early Cretaceous enriched-MORB; c) Middle Jurassic
21 plume-type MORB; d) Late Jurassic-Early Cretaceous alkaline basalts. All rock types show a clear
22 garnet signature, as testified by their high MREE/HREE ratios.
23
24
25
26
27
28

29 3) REE modelling shows that their garnet signature is related to polybaric partial melting starting
30 in the garnet peridotite stability field and continuing to larger degrees in the spinel-facies mantle.
31 However, the different geochemical affinities displayed by the studied rocks are related to different
32 mantle source compositions. G-MORBs were generated from 2.5% melting in the garnet-facies and
33 10% melting in the spinel-facies of a depleted MORB mantle source. E-MORBs composition is
34 compatible with mixing of melts derived from very low degree (~1%) partial melting of a DMM
35 source in the garnet-facies with melts derived from much larger degree (~10%) of partial melting in
36 the spinel-facies mantle. Alternatively, these rocks may have derived from for ~8% partial melting of
37 a theoretical slightly enriched source in the spinel facies. P-MORBs and alkaline basalts have REE
38 composition that can accounted for by mixing of different proportions of melts generated in the
39 garnet- and spinel facies from an enriched mantle source metasomatized by OIB-type (plume-type)
40 components.
41
42
43
44
45
46
47
48
49
50
51
52
53
54

55 4) The coexistence of chemically different rock-types from Middle Jurassic to Early Cretaceous
56 suggests that they were formed at a mid-ocean ridge setting from partial melting of a highly
57
58
59
60

1
2
3 heterogeneous mantle characterized by the extensive occurrence of OIB-metasomatized portions,
4
5 which were likely inherited from a Triassic mantle plume activity associated with the continental
6
7 rift and opening of the Neotethys branch.
8
9

10 11 **Aknowledgments**

12
13
14
15
16 The Italian Ministry of Education, University and Research (MIUR) is acknowledged for the
17
18 financial support (Prin 2010-2011). [This research has also been funded by the Ferrara University](#)
19
20 [\(FIR-2016 Project\)](#). Many thanks go to Mirella Bonora (Ferrara University) for her support with
21
22 analytical techniques. Radiolarian micrographs were taken with a Philips XL20 of the Ivalsa
23
24 Institute (CNR) by Simona Lazzeri [and with a Zeiss EVO MA15 of the MEMA \(University of](#)
25
26 [Florence\) by Maurizio Ulivi](#). Special thanks go to [Špela Goričan and anonymous reviewer](#) for their
27
28 constructive reviews of this paper.
29
30
31
32
33
34

35 **References**

- 36
37 AKAL, C., CANDAN, O., KORALAY, E., OBERHÄNSLI, R., CHEN, F. & PRELEVIC, D. 2012. Early
38
39 Triassic potassic volcanism in the Afyon Zone of the Anatolides/Turkey: implications for the rifting
40
41 of the Neo-Tethys. *International Journal of Earth Sciences* **101**, 177–194.
42
43
44 AKBAYRAM, K., OKAY, A. I. & SATIR, M. 2012. Early Cretaceous closure of the Intra-Pontide
45
46 Ocean in western Pontides (northwestern Turkey). *Journal of Geodynamics* **65**, 38–55.
47
48
49 AITA, Y. & OKADA, H. 1986. Radiolarians and calcaerous nannofossils from the Uppermost
50
51 Jurassic-Lower Cretaceous strata of Japan and Tethyan Regions. *Micropaleontology* **32**, 97–128.
52
53
54 ALIEV, K. 1967. New Radiolarian Species of the Valanginian and Albian Stages of Northeastern
55
56 Azerbaidzhan. In: *Cretaceous Deposits of the Eastern Caucasus and Adjacent Areas*
57
58 *(Biostratigraphy and Paleogeography)*. Academy of Sciences USSR, Ministry of Oil Industry USSR,
59
60

1
2
3 *Institute of Geology and of the Processing of Fuel Minerals, Laboratory of the Biostratigraphy of*
4
5 *Oil- and Gas-bearing areas, 23–30.*

6
7 ALLAHYARI, K., SACCANI, E., POURMOAFI, M., BECCALUVA, L. & MASOUDI, F. 2010. Petrology of
8
9 mantle peridotites and intrusive mafic rocks from the Kermanshah ophiolitic complex (Zagros belt,
10
11 Iran): Implications for the geodynamic evolution of the Neo-Tethyan oceanic branch between
12
13 Arabia and Iran. *Ofioliti* **35**, 71–90.

14
15
16 ALLÈGRE, C. J. & MINSTER, J. F. 1978. Quantitative models of trace element behaviour in magmatic
17
18 processes. *Earth and Planetary Science Letters* **38**, 1–25.

19
20
21 ALTINER, D., KOÇYIĞIT, A., FARINACCI, A., NICOSIA, U. & CONTI, M. A. 1991. Jurassic-Lower
22
23 Cretaceous stratigraphy and paleogeographic evolution of the southern part of north-western
24
25 Anatolia (Turkey). *Geologica Romana* **27**, 13–80.

26
27 BAILEY, E. B. & MCCALLIEN, W. J. 1953. Serpentinite lavas, the Ankara Mélange, and the
28
29 Anatolian Thrust. *Transactions of the Royal Society of Edinburgh* **57**, 403–442.

30
31
32 BAK, M. 1996. Cretaceous radiolaria from Niedzica Succession of the Pieniny Klippen Belt in
33
34 Polish Carpathians. *Acta Palaeontologica Polonica* **41**, 91–110.

35
36 BAK, M. 1999. Cretaceous radiolarian zonation in the Polish part of the Pieniny Klippen Belt
37
38 (Western Carpathians). *Geologica Carpathica* **50**, 21–31.

39
40
41 BANDINI, A. N., BAUMGARTNER, P. O., FLORES, K., DUMITRICA, P. & JACKETT, S. J. 2011. Early
42
43 Jurassic to early Late Cretaceous radiolarians from the Santa Rosa accretionary complex
44
45 (northwestern Costa Rica). *Ofioliti* **31**, 1–35.

46
47 BAUMGARTNER, P. O., O'DOHERTY, L., GORIČAN, Š., DUMITRICA-JUD, R., DUMITRICA, P.,
48
49 PILLEVUIT, A., URQUHART, E., MATSUOKA, A., DANELIAN, T., BARTOLINI, A. C., CARTER, E. S., DE
50
51 WEVER, P., KITO, N., MARCUCCI, M. & STEIGER, T. A. 1995a. Radiolarian catalogue and
52
53 systematics of Middle Jurassic to Early Cretaceous Tethyan genera and species. In *Middle Jurassic*
54
55 *to Lower Cretaceous Radiolaria of Tethys: occurrences, systematics, biochronology* (eds P.O.
56
57 Baumgartner et al.), Mémoires de Géologie, Lausanne, **23**, 37–685.
58
59
60

- 1
2
3 BAUMGARTNER, P. O., BARTOLINI, A. C., CARTER, E. S., CONTI, M., CORTESE, G., DANELIAN, T.,
4
5 DE WEVER, P., DUMITRICA, P., DUMITRICA-JUD, R., GORIČAN, Š., GUEX, J., HULL, D. M., KITO, N.,
6
7 MARCUCCI, M., MATSUOKA, A., MURCHEY, B., O'DOHERTY, L., SAVARY, J., VISHNEVSKAYA, V.,
8
9 WIDZ, D. & YAO, A. 1995b. Middle Jurassic to Early Cretaceous Radiolarian biochronology of
10
11 Tethys based on Unitary Associations. In *Middle Jurassic to Lower Cretaceous Radiolaria of*
12
13 *Tethys: occurrences, systematics, biochronology* (eds P.O. Baumgartner et al.), Mémoires de
14
15 *Géologie, Lausanne*, **23**, 1013–1048.
16
17
18 BAUMGARTNER, P. O., BJØRKLUND, K. R., CAULET, J. P., DE WEVER, P., KELLOGG, D.,
19
20 LABRACHERIE, M., NAKASEKO, K., NISHIMURA, A., SCHAAF, A., SCHIMDT-EFFING, R. & YAO A.
21
22 1981. Eurorad II, 1980. Second European meeting of radiolarian paleontologists: current research
23
24 on Cenozoic and Mesozoic radiolarians. *Eclogae Geologicae Helvetiae* **74**, 1027–1061.
25
26
27 BEKER, J. A., MENZIES, M. A., THIRLWALL, M. F. & MACPHERSON, C. G. 1997. Petrogenesis of
28
29 Quaternary intraplate volcanism, Sana'a, Yemen: Implications for plume-lithosphere interaction and
30
31 polybaric melt hybridization. *Journal of Petrology* **38**, 1359–1390.
32
33
34 BERBER, F., GÖNCÜOĞLU, M. C. & SAYIT, K. 2014. Geochemistry and tectonic significance of the
35
36 Kösedag metavolcanic rocks from the Sakarya Zone, Northern Turkey. Bulletin. In *Proceedings of*
37
38 *the 20th CBGA Congress 24-26 Sept 2014, Tirana* (eds A. Begiraj et al.). *Shkencave Gjeologjike*
39
40 *Special Issue* **2**, 161–163.
41
42
43 BOCCALETTI, M., BORTOLOTTI, V. & SAGRI, M. 1966. Ricerche sulle ofioliti delle catene alpine: I.
44
45 Osservazioni sull'Ankara Mélange nella zona di Ankara. *Bollettino della Società Geologica*
46
47 *Italiana* **85**, 485–508.
48
49
50 BORTOLOTTI, V. & PRINCIPI, G. 2005. Tethyan ophiolites and Pangea break-up. *The Island Arc* **14**,
51
52 442–470.
53
54
55 BORTOLOTTI, V. & SAGRI, M. 1968. Ricerche sulle ofioliti delle catene alpine. 4- Osservazioni
56
57 sull'età e la giacitura delle ofioliti tra Smirne ed Erzurum (Turchia). *Bollettino della Società*
58
59 *Geologica Italiana* **87**, 661–666.
60

1
2
3 BORTOLOTTI, V., CHIARI, M., GÖNCÜOĞLU, M. C., MARCUCCI, M., PRINCIPI, G., TEKIN, U. K.,
4
5 SACCANI, E. & TASSINARI, R. 2013a. Age and geochemistry of basalt-chert associations in the
6
7 ophiolitic complexes of the Izmir-Ankara Mélange East of Ankara, Turkey: preliminary data.
8

9
10 *Ofioliti* **38**, 157–173.

11
12 BORTOLOTTI, V., CHIARI, M., MARRONI, M., PANDOLFI, L., PRINCIPI, G. & SACCANI, E. 2013b.
13
14 Geodynamic evolution of the ophiolites from Albania and Greece (Dinaric-Hellenic belt): One, two
15
16 or more oceanic basins? *International Journal of Earth Sciences* **102**, 783–811.

17
18 BRAGIN, N. YU. & TEKIN, U. K. 1996. Age of radiolarian-chert blocks from the Senonian ophiolitic
19
20 mélange (Ankara, Turkey). *The Island Arc* **5**, 114–122.

21
22 BRUNELLI, D., SEYLER, M., CIPRIANI, A., OTTOLINI, L., BONATTI, E., 2006. Discontinuous melt
23
24 extraction and weak refertilization of mantle peridotites at the Vema Lithospheric Section (Mid-
25
26 Atlantic Ridge). *Journal of Petrology* **47**, 745–771.

27
28 CATANZARITI, R., ELLERO, A., GÖNCÜOĞLU, M. C., MARRONI, M., OTTRIA, G. & PANDOLFI, L. 2013.
29
30 The Taraklı Flysch in the Boyalı area (Sakarya Terrane, northern Turkey): Implications for the
31
32 tectonic history of the IntraPontide suture zone. *Comptes Rendus de Geoscience*, **345**, 454–461.

33
34 CATER, J. M. L., HANNA, S. S., RIES, A. C. & TURNER, P. 1991. Tertiary evolution of the Sivas
35
36 Basin, central Turkey. *Tectonophysics* **195**, 29–46

37
38 CELIK, S. 2010. Taxonomy and biostratigraphy of Jurassic-Early Cretaceous radiolarian fauna of the
39
40 pelagic deposits in Izmir-Ankara-Erzincan suture complex, NE and SW Çankırı, northern Turkey.
41
42 Master of Sciences Thesis, Hacettepe University, Ankara, Turkey. Unpublished thesis (in Turkish
43
44 with English abstract).

45
46 CEMEN, I., GÖNCÜOĞLU, M. C., ERLER, A., KOZLU, H. & PERİNÇEK, D. 1993. Indentation tectonics
47
48 and associated lateral extrusion in East, Southeast and Central Anatolia. *Geological Society of*
49
50 *America, Programs and Abstracts*, A116–117.
51
52
53
54
55
56
57
58
59
60

1
2
3 CHIARI, M., BORTOLOTTI, V., MARCUCCI, M., PHOTIADES, A., PRINCIPI, G. & SACCANI E. 2012.
4 Radiolarian biostratigraphy and geochemistry of the Koziakas Massif ophiolites (Greece). *Bulletin*
5 *de la Société Géologique de France* **183**, 289–309.

6
7
8
9 CHIARI, M., COBIANCHI, M. & PICOTTI, V. 2007. Integrated stratigraphy (radiolarians and calcareous
10 nanofossils) of the Middle to Upper Jurassic Alpine radiolarites (Lombard Basin, Italy):
11 Constraints to their genetic interpretation. *Palaeogeography, Palaeoclimatology, Palaeoecology* **249**,
12 233–270.

13
14
15
16
17
18 CHIARI, M., MARCUCCI, M. & PRELA, M. 2004. Radiolarian assemblages from the Jurassic cherts of
19 Albania: new data. *Ofioliti* **29**, 95–105.

20
21
22 DANELIAN, T. 2008. Diversity and biotic changes of Archaeodictyomitrid Radiolaria from the
23 Aptian/Albian transition (OAE1b) of southern Albania. *Micropaleontology* **54**, 3–13.

24
25
26 DANELIAN, T., TSIKOS, H., GARDIN, S., BAUDIN, F., BELLIER, J. P. & EMMANUEL, L. 2004. Global
27 and regional palaeoceanographic changes as recorded in the Mid-Cretaceous (Aptian–Albian)
28 sequence of the Ionian zone (NW Greece). *Journal of the Geological Society, London*, **161**, 703–
29 709.

30
31
32
33
34
35
36 DERCOURT, J., ZONENSHAIN, L. P., RICOU, L. E., KAZMIN, V. G., LE PICHON, X., KNIPPER, A. L.,
37 GRANDJACQUET, C., SBORTSHIKOV, I. M., GEYSSANT, J., LEPVRIER, C., PECHERSKY, D. H.,
38 BOULIN, J., SIBUET, J. C., SAVOSTIN, L. A., SOROKHTIN, O., WESTPHAL, M., BAZHENOV, M. L.,
39 LAUER, J. P. & BIJU-DUVAL, M. B. 1986. Geological evolution of the Tethys belt from the Atlantic
40 to the Pamirs since the Lias. In *Evolution of the Tethys* (eds J. Aubouin, X. Le Pichon & A. S.
41 Monin), *Tectonophysics* **123**, 241–315.

42
43
44
45
46
47 DE WEVER, P. 1982. Radiolaires du Trias et du Lias de la Téthys (systématique, stratigraphie).
48 *Société Géologique du Nord* **7**, 1–600.

49
50
51
52
53
54
55
56
57
58
59
60 DILEK, Y., THY, P., HACKER, B. & GRUNDTVIG, S. 1999. Structure and petrology of Tauride
ophiolites and mafic dike intrusions (Turkey): Implications for the Neo-Tethyan Ocean. *Geological*
Society of America Bulletin **111**, 1192–1216.

1
2
3 DUMITRICA, P. 1970. Cryptocephalic and cryptothoracic Nassellaria in some Mesozoic deposits of
4 Romania. *Revue Roumaine de Géologie, Géophysique et Géographie (série Géologie)* **14**, 45–124.

5
6
7 DUMITRICA, P. & DUMITRICA-JUD, R. 1995. *Aurisaturnalis carinatus* (Foreman), an example of
8 phyletic gradualism among Saturnalid-type radiolarians. *Revue de Micropaléontologie* **38**,
9 195–216.

10
11
12 DUMITRICA, P. & ZÜGEL, P. 2008. Early Tithonian Saturnalidae (Radiolaria) from the Solnhofen
13 area (Southern Franconian Alb, southern Germany). *Paläontologische Zeitschrift* **82**, 55–84.

14
15
16 DUMITRICA, P., IMMENHAUSER, A. & DUMITRICA-JUD, R. 1997. Mesozoic radiolarian
17 biostratigraphy from Masirah Ophiolite, Sultanate of Oman Part I: Middle Triassic, uppermost
18 Jurassic and Lower Cretaceous Spumellarians and multisegmented Nassellarians. *Bulletin of the*
19 *National Museum of Natural Sciences, Taiwan* **9**, 1–106.

20
21
22 ELLERO, A., OTTRIA, G., MARRONI, M., PANDOLFI, L. & GÖNCÜOĞLU, M. C. 2015a. Analysis of the
23 North Anatolian Shear Zone in Central Pontides (northern Turkey): Insight for geometries and
24 kinematics of deformation structures in a transpressional zone. *Journal of Structural Geology* **72**,
25 124–141.

26
27
28 ELLERO, A., OTTRIA, G., SAYIT, K., CATANZARITI, R., FRASSI, C., GÖNCÜOĞLU, M. C., MARRONI, M.
29 & PANDOLFI, L. 2015b. Geological and geochemical evidence for a Late Cretaceous continental arc
30 in the central Pontides, northern Turkey. *Ophioliti* **40**, 73–90

31
32
33 ELMAŞ, A. & YİĞİTBAŞ, E. 2001. Ophiolite emplacement by strike-slip tectonics between the
34 Pontide Zone and the Sakarya Zone in northwestern Anatolia, Turkey. *International Journal of*
35 *Earth Sciences* **90**, 257–269.

36
37
38 ELMAŞ, A. & YİĞİTBAŞ, E. 2005. Comment on “Tectonic evolution of the Intra-Pontide suture zone
39 in the Armutlu Peninsula, NW Turkey” by Robertson & Ustaömer. *Tectonophysics* **405**, 213–221.

40
41
42 ERDOĞAN, B., AKAY, C & UĞUR, M. S. 1996. Geology of the Yozgat region and evolution of the
43 collisional Çankırı basin. *International Geological Revue* **38**, 788–806.

1
2
3 FILIPPOV, A.N. & KEMKIN, I.V. 2005. First finds of Middle Jurassic and Early Cretaceous
4 (Valanginian) radiolarian assemblages in the Western Sikhote-Alin: their paleogeographic and
5 tectonic significance. *Doklady Earth Sciences*, **405**, 1141–1144.
6
7

8
9 FLOYD, P. A., GÖNCÜOĞLU, M. C., WINCHESTER, J. A. & YALINIZ, M. K. 2000. Geochemical
10 character and tectonic environment of Neotethyan ophiolitic fragments and metabasites in the
11 Central Anatolian Crystalline Complex, Turkey. In *Tectonics and magmatism in Turkey and the*
12 *surrounding area* (eds E. Bozkurt, J. Winchester & J. A. Piper.), pp. 183–202. Geological Society
13 of London, Special Publication no. 173.
14
15

16
17 GÖKTEN, E. & FLOYD, P. A. 2007. Stratigraphy and geochemistry of pillow basalts within the
18 ophiolitic mélange of the Izmir-Ankara-Erzincan suture zone: implications for the geotectonic
19 character of the northern branch of Neotethys. *International Journal of Earth Sciences*
20 (*Geologische Rundschau*) **96**, 725–741.
21
22

23
24 GÖNCÜOĞLU, M. C. 1992. Structural and stratigraphical framework of the Central Anatolian
25 Tertiary basins. In *Introduction to the Early Paleogene of the Haymana-Polatlı Basin* (eds E. Sirel
26 & E. Yazgan), pp. 1–11. Field Trip Guidebook. General Direction of Mineral Resources
27 Exploration, Ankara.
28
29

30
31 GÖNCÜOĞLU, M. C. 2010. Introduction to the geology of Turkey: Geodynamic evolution of the pre-
32 Alpine and Alpine terranes. General Directorate of Mineral. *Resources Exploration Monography*
33 *Series*, 5, 1–66.
34
35

36
37 GÖNCÜOĞLU, M. C. 2011. Geology of the Kütahya-Bolkardağ Belt. *Mineral Resources Exploration*
38 *Bulletin* **142**, 223–277.
39
40

41
42 GÖNCÜOĞLU, M. C., DIRIK, K. & KOZLU, H. 1997. General characteristics of pre-Alpine and Alpine
43 Terranes in Turkey: Explanatory notes to the terrane map of Turkey. *Annales Géologiques des Pays*
44 *Helléniques* **37**, 515–536.
45
46
47
48
49
50
51
52
53
54
55
56
57
58
59
60

1
2
3 GÖNCÜOĞLU, M. C., TURHAN, N. & TEKIN, K. 2003. Evidence for the Triassic rifting and opening of
4 the Neotethyan Izmir-Ankara Ocean, northern edge of the Tauride-Anatolide platform, Turkey.
5 *Bollettino della Società Geologica Italiana, Special Volume 2*: 203–212.
6
7

8
9 GÖNCÜOĞLU, M. C., GÜRSU, S., TEKIN, U. K. & KÖKSAL S., 2008. New data on the evolution of the
10 Neotethyan oceanic branches in Turkey: Late Jurassic ridge spreading in the Intra-Pontide branch.
11 *Ofioliti* **33**, 153–164.
12
13

14
15 GÖNCÜOĞLU, M. C., MARRONI, M., SAYIT, K., TEKIN, U. K., PANDOLFI, L. & ELLERO, A. 2012. The
16 Ayli Dağ ophiolite sequence (Central-Northern Turkey): a fragment of Middle Jurassic oceanic
17 lithosphere within the Intra-Pontide Suture Zone. *Ofioliti* **37**, 77–92.
18
19

20
21 GÖNCÜOĞLU, M. C., MARRONI, M., PANDOLFI, L., ELLERO, A., OTTRIA, G., CATANZARITI, R., TEKIN,
22 U. K. & SAYIT, K. 2014. The Arkot Dağ Mélange in Araç area, central Turkey: Evidence of its
23 origin within the geodynamic evolution of the Intra-Pontide suture zone. *Journal of Asian Earth*
24 *Sciences* **85**, 117–139.
25
26

27
28 GÖNCÜOĞLU, M. C., SAYIT, K. & TEKIN, U. K. 2010. Oceanization of the northern Neotethys:
29 Geochemical evidence from ophiolitic mélange basalts within the İzmir-Ankara suture belt, NW
30 Turkey. *Lithos* **116**, 175–187.
31
32

33
34 GÖNCÜOĞLU, M. C., TEKIN, U. K. & TURHAN, N. 2001. Geological meaning of the Late Carnian
35 basalts blocks with radiolarites within the Late Cretaceous Central Sakarya ophiolitic complex (NW
36 Anatolia). *Jeo 2000 Proceedings CD-54-6*: 6.
37
38

39
40 GÖNCÜOĞLU, M. C., TEKIN, U. K., SAYIT, K., BEDI, Y. & UZUNÇİMEN, S. 2015. Opening, evolution
41 and closure of the Neotethyan oceanic branches in Anatolia as inferred by radiolarian research.
42 *Radiolaria* **35**, 88–90.
43
44

45
46 GÖNCÜOĞLU, M. C., TURHAN, N., SENTÜRK, K., ÖZCAN, A. & UYSAL, S. 2000. A geotraverse across
47 NW Turkey: tectonic units of the Central Sakarya region and their tectonic evolution. In *Tectonics*
48 *and magmatism in Turkey and the surrounding area* (eds E. Bozkurt, J Winchester & J.A. Piper),
49 pp. 139-161. Geological Society of London, Special Publication no. 173.
50
51
52
53
54
55
56
57
58
59
60

1
2
3 GÖNCÜOĞLU, M. C., YALINIZ, K. & TEKIN, U. K. 2006. Geochemistry, tectono-magmatic
4 discrimination and radiolarian ages of basic extrusives within the Izmir-Ankara Suture Belt (NW
5 Turkey): time constraints for the Neotethyan evolution. *Ofioliti* **31**, 25–38.

6
7
8
9 GORIČAN, Š. 1994. Jurassic and Cretaceous radiolarian biostratigraphy and sedimentary evolution of
10 the Budva Zone (Dinarides, Montenegro). *Mémoires de Géologie, Lausanne*, **18**, 1–120.

11
12
13 GORIČAN, Š., PAVSIC, J. & ROZIC, B. 2012. Bajocian to Tithonian age of radiolarian cherts in the
14 Tolmin basin (NW Slovenia). *Bulletin de la Société Géologique de France*, **183**, 369–382.

15
16
17
18 GÜLYÜZ, E., KAYMAKCI, N., MEIJERS, M. J. M., VAN HINSBERGEN, D. J. J., LEFEBVRE, C., VISSERS,
19 R. L. M., BART, W. H., HENDRIKS, B. W. H. & PEYNIRCIOĞLU, A. A. 2013. Late Eocene evolution of
20 the Çiçekdağı Basin (central Turkey): syn-sedimentary compression during microcontinent-
21 continent collision in central Anatolia. *Tectonophysics*. **602**: 286–299.

22
23
24
25 HANAN, B. B., BLICHERT-TOFT, J., KINGSLEY, R. & SCHILLING, J. G. 2000. Depleted Iceland mantle
26 plume geochemical signature: Artifact of multicomponent mixing? *Geochemistry, Geophysics,*
27 *Geosystems* **1**, 1–19.

28
29
30
31 HUBERT-FERRARI, A., ARMIJO, R., KING, G., MEYER, B. & BARKA, A. 2002. Morphology,
32 displacement, and slip rates along the North Anatolian Fault, Turkey. *Journal of Geophysical*
33 *Research* **107**: ETG 9-1–ETG 9-33.

34
35
36
37 IRVING, A. J. & FREY, F. A. 1984. Trace element abundances in megacrysts and their host basalts:
38 constraints on partition coefficients and megacryst genesis. *Geochimica et Cosmochimica Acta* **48**,
39 1201–1221.

40
41
42 JACKSON, M. L. 1958. Soil chemical analysis. Prentice-Hall, 498 pp.

43
44
45
46
47 KAYMAKCI, N., DUERMEIJER, C. E., LANGEREIS, C., WHITE, S. H. & VAN DIJK, P. M. 2003.
48 Paleomagnetic evolution of the Çankırı Basin (Central Anatolia, Turkey: Implication for oroclinal
49 bending due to indentation. *Geological Magazine* **140**, 343–355.

50
51
52
53
54
55
56 KAWABATA, K. 1988. New species of Latest Jurassic and Earliest Cretaceous radiolarians from the
57 Sorachi group in Hokkaido, Japan. *Bulletin of the Osaka Museum of Natural History*, **43**, 1–13.
58
59
60

1
2
3 KOCYIGIT, A., TÜRKMEENOGLU, A., BEYHAN, A., KAYMAKÇI, N. & AKYOL, E. 1995. Post-collisional
4 tectonics of Eskisehir-Ankara-Çankırı segment of Izmir-Ankara-Erzincan Suture Zone. *Turkish*
5 *Association of Petroleum Geologists Bulletin* **6**, 69–87.

6
7
8
9 KÖKSAL, S. & GÖNCÜOĞLU, C. M. 2008. Sr and Nd isotopic characteristics of some S-, I- and A-
10 type granitoids from Central Anatolia. *Turkish Journal of Earth Sciences* **17**: 111–127.

11
12
13 KOZUR, H. 1985. The radiolarian genus *Eoxitus* n. gen from the *Unuma echinatus* zone (Bajocian)
14 of Northern Hungary. *Proceed Koninklijke Nederoands Academie Van Wetenschappen*, **88**, 211–220.

15
16
17 LACHANCE, G. R. & TRAIL, R. J. 1966. Practical solution to the matrix problem in X-ray analysis.
18 *Canadian Spectroscopy* **11**, 43–48.

19
20
21
22 LIU, C.-Z., SNOW, J.E., HELLEBRAND, E., BRÜGMANN, G.E., VON DER HANDT, A.B., HOFMANN,
23 A.W., 2008. Ancient, highly heterogeneous mantle beneath Gakkel ridge, Arctic Ocean. *Nature*
24 **452**, 311–316.

25
26
27
28
29 MCKENZIE, D. & O'NIONS, R. K. 1991. Partial melt distributions from inversion of rare Earth
30 element concentrations. *Journal of Petrology* **32**, 1021-1091.

31
32
33
34 MOIX, P. & GORIČAN, Š. 2013. Jurassic and Cretaceous radiolarian assemblages from the Bornova
35 mélange in northern Karaburun Peninsula (western Turkey) and its connection to the İzmir-Ankara
36 mélanges. *Geodinamica Acta* **26**, 56–67.

37
38
39
40
41 MOIX, P., BECCALETTO, L., KOZUR, H. W., HOCHARD, C., ROSSELET, F. & STAMPFLI, G. M. 2008. A
42 new classification of the Turkish terranes and sutures and its implication for the paleotectonic
43 history of the region. *Tectonophysics* **451**, 7–39.

44
45
46
47 MONTANINI, A., TRIBUZIO, R. & VERNIA, L. 2008. Petrogenesis of basalts and gabbros from an
48 ancient continent-ocean transition (External Liguride ophiolites, Northern Italy). *Lithos* **101**, 453–
49 479.

50
51
52
53
54 O'DOGHERTY, L. 1994. Biochronology and paleontology of Mid-Cretaceous radiolarians from
55 Northern Apennines (Italy) and Betic Cordillera (Spain). *Mémoires de Géologie, Lausanne*, **21**,
56
57
58 1–415.
59
60

1
2
3 O'DOHERTY, L., CARTER, E. S., DUMITRICA, P., GORIČAN, Š., DE WEVER, P., BANDINI, A. N.,
4
5 BAUMGARTNER, P. O. & MATSUOKA, A. 2009. Catalogue of Mesozoic radiolarian genera. Part 2:
6
7 Jurassic-Cretaceous. *Geodiversitas* **31**, 271–356.

8
9
10 OKAY, A. I. & GÖNCÜOĞLU, M. C. 2004. The Karakaya Complex: A review of data and concepts.
11
12 *Turkish Journal of Earth Sciences* **13**, 75–95.

13
14 OKAY, A. I. & TÜYSÜZ, O. 1999. Tethyan sutures of northern Turkey. In *The Mediterranean Basin:
15
16 Tertiary extension within the Alpine orogen* (eds B. Durand, L. Jolivet, F Horváth & M. Séranne),
17
18 pp. 475-515. Geological Society of London, Special Publication no. 156.

19
20
21 PARLAK, O., ÇOLAKOĞLU, A., DÖNMEZ, C., SAYAK, H., YILDIRIM, N., TÜRKEL, A., & ODABAŞI, İ.
22
23 2013. Geochemistry and tectonic significance of ophiolites along the İzmir-Ankara-Erzincan Suture
24
25 Zone in northeastern Anatolia. In *Geological development of Anatolia and the easternmost
26
27 Mediterranean* (eds A. H. F. Robertson, O. Parlak & U. Unlugenc), pp. 75–105. Geological Society
28
29 of London, Special Publication no. 372.

30
31
32 PEARCE, J. A. 1982. Trace element characteristics of lavas from destructive plate boundaries. In
33
34 *Andesites* (ed R. S. Thorpe), pp. 525-548. John Wiley & Sons, New York.

35
36 PEARCE, J. A. & NORRY, M. J. 1979. Petrogenetic implications of Ti, Zr, Y, and Nb variations in
37
38 volcanic rocks. *Contributions to Mineralogy and Petrology* **6**, 33–47.

39
40
41 PESSAGNO, E. A. & NEWPORT, L. A., 1972. A technique for extracting Radiolaria from radiolarian
42
43 chert. *Micropaleontology* **18**, 231–234.

44
45 ROBERTSON, A. H. F. & USTAÖMER, T. 2004. Tectonic evolution of the Intra-Pontide suture zone IN
46
47 the Armutlu Peninsula, NW Turkey. *Tectonophysics* **381**, 175–209

48
49 ROBERTSON, A. H. F., DIXON, J. E., BROWN, S. COLLINS, A., MORRIS, A., PICKETT, E. A., SHARP, I. &
50
51 USTAÖMER, T. 1996. Alternative tectonic models for the Late Palaeozoic-Early Tertiary
52
53 development of Tethys in the Eastern Mediterranean region. In *Palaeomagnetism and tectonics of
54
55 the Mediterranean region* (eds A. Morris & D. H. Tarling), pp. 239–263. Geological Society of
56
57 London, Special Publication no. 105.
58
59
60

1
2
3 ROBERTSON, A., PARLAK, O., USTAÖMER, T., TASLI, K., İNAN, N., DUMITRICA, P., & KARAOĞLAN, F.
4
5 2013. Subduction, ophiolite genesis and collision history of Tethys adjacent to the Eurasian
6
7 continental margin: new evidence from the Eastern Pontides, Turkey. *Geodinamica Acta* **26**,
8
9 230–293.

10
11 ROBIN, C., GORIČAN, Š., GUILLOCHEAU, F., RAZIN, P., DROMART, G. & MOSAFFA, H. 2010.
12
13 Mesozoic deep-water carbonate deposits from the southern Tethyan passive margin in Iran
14
15 (Pichakun nappes, Neyriz area): biostratigraphy, facies sedimentology and sequence stratigraphy. In
16
17 *Tectonic and stratigraphic evolution of Zagros and Makran during the Mesozoic-Cenozoic* (eds P.
18
19 Leturmy & C. Robin), pp. 179–210. Geological Society of London, Special Publication no. 330.

20
21 ROJAY, B. 2013. Tectonic evolution of the Cretaceous Ankara Ophiolitic Mélange during the Late
22
23 Cretaceous to pre-Miocene interval in Central Anatolia, Turkey. *Journal of Geodynamics* **65**, 66-81.

24
25 ROJAY, B., YALINIZ, M. K. & ALTINER, D. 2001. Tectonic implications of some Cretaceous pillow
26
27 basalts from the North Anatolian Ophiolitic Mélange (Central Anatolia-Turkey) to the evolution of
28
29 Neotethys. *Turkish Journal of Earth Sciences* **10**, 93–102.

30
31 SACCANI, E. 2015. A new method of discriminating different types of post-Archean ophiolitic
32
33 basalts and their tectonic significance using Th-Nb and Ce-Dy-Yb systematics. *Geoscience*
34
35 *Frontiers* **6**, 481–501..

36
37 SACCANI, E. & PHOTIADES, A. 2005. Petrogenesis and tectono-magmatic significance of volcanic
38
39 and subvolcanic rocks in the Albanide-Hellenide ophiolitic mélanges. *The Island Arc* **14**, 494–516.

40
41 SACCANI, E. & PRINCIPI, G. 2016. Petrological and tectono-magmatic significance of ophiolitic
42
43 basalts from the Elba Island within the Alpine Corsica-Northern Apennine system. *Mineralogy and*
44
45 *Petrology*. doi: 10.1007/s00710-016-0445-3.

46
47 SACCANI, E., ALLAHYARI, K., BECCALUVA, L. & BIANCHINI, G. 2013a. Geochemistry and petrology
48
49 of the Kermanshah ophiolites (Iran): Implication for the interaction between passive rifting, oceanic
50
51 accretion, and plume-components in the Southern Neo-Tethys Ocean. *Gondwana Research* **24**,
52
53 392–411.
54
55
56
57
58
59
60

1
2
3 SACCANI, E., AZIMZADEH, Z., DILEK, Y. & JAHANGIRI, A. 2013b. Geochronology and petrology of
4 the Early Carboniferous Misho Mafic Complex (NW Iran), and implications for the melt evolution
5 of Paleo-Tethyan rifting in Western Cimmeria. *Lithos* **162-163**, 264–278.

6
7
8
9 SACCANI, E., BECCALUVA, L., PHOTIADES, A. & ZEDA, O. 2011. Petrogenesis and tectono-magmatic
10 significance of basalts and mantle peridotites from the Albanian-Greek ophiolites and sub-ophiolitic
11 mélanges. New constraints for the Triassic-Jurassic evolution of the Neo-Tethys in the Dinaride
12 sector. *Lithos* **124**, 227–242.

13
14
15
16 SACCANI, E., DELAVARI, M., BECCALUVA, L. & AMINI, S. A. 2010. Petrological and geochemical
17 constraints on the origin of the Nehbandan ophiolitic complex (eastern Iran): Implication for the
18 evolution of the Sistan Ocean. *Lithos* **117**, 209–228.

19
20
21
22 SACCANI, E., PHOTIADES, A., SANTATO, A. & ZEDA, O. 2008. New evidence for supra-subduction
23 zone ophiolites in the Vardar Zone from the Vermion Massif (northern Greece): Implication for the
24 tectono-magmatic evolution of the Vardar oceanic basin. *Ofioliti* **33**, 65–85.

25
26
27
28 SACCANI, E., PRINCIPI, G., GARFAGNOLI, F., MENNA, F. 2008. Corsica ophiolites: geochemistry and
29 petrogenesis of basaltic and metabasaltic rocks. *Ofioliti* **33**, 187–207.

30
31
32
33 SAYIT, K., TEKIN, U. K. & GÖNCÜOĞLU, M. C. 2011. Early-Middle Carnian radiolarian cherts within
34 the Eymir Unit, Central Turkey: Constraints for the age of the Palaeotethyan Karakaya Complex.
35
36
37
38
39
40
41
42 *Journal of Asian Earth Sciences* **42**, 398–407.

43
44
45
46 SCHMID, S. M., BERNOULLI, D., FÜGENSCHUH, B., MATENCO, L., SCHEFER, S., SCHUSTER, R.,
47 TISCHLER, M. & USTASZEWSKI, K. 2008. The Alpine-Carpathian-Dinaridic orogenic system:
48 correlation and evolution of tectonic units. *Swiss Journal of Geosciences* **101**, 139–183.

49
50
51
52 SENGÖR, A. M. C. & YILMAZ, Y. 1981. Tethyan evolution of Turkey: a plate tectonic approach.
53
54
55
56
57
58
59
60 *Tectonophysics*, **75**, 181–241.

SMUC, A. & GORIČAN, Š. 2005. Jurassic sedimentary evolution of a carbonate platform into a deep-
water basin, Mt. Mangart (Slovenian-Italian Border). *Rivista Italiana di Paleontologia e*
Stratigrafia **111**, 45–70.

1
2
3 SOYCAN, H., ERDOGAN, K. & KONAK, N. 2015. Aalenian-Early Bathonian (Middle Jurassic)
4 radiolarian assemblages in the Tavas nappe within Lycian nappes in the western Taurides (SW
5 Turkey): The first dating of carbonate platform drowning. *Journal of Asian Earth Sciences*, **104**,
6
7 3–21.
8
9

10
11 STAMPFLI, G. M. & BOREL, G. D. 2002. A plate tectonic model for the Palaeozoic and Mesozoic
12 constrained by dynamic plate boundaries and restored synthetic oceanic isochrones. *Earth and*
13
14 *Planetary Science Letters* **169**, 17–33.
15
16

17
18 SUN, S. S. & MCDONOUGH, W. F. 1989. Chemical and isotopic-systematics of oceanic basalts:
19 implications for mantle composition and processes. In *Magmatism in the ocean basins* (eds A .D.
20
21 Saunders & M. J. Norry), pp. 313-345. Geological Society of London, Special Publication no. 42.
22
23

24
25 TEKIN, U. K. 1999. Biostratigraphy and systematics of Late Middle to Late Triassic radiolarians
26 from the Taurus Mountains and Ankara region, Turkey. *Geologische und Paläontologische*
27
28 *Mitteilungen Innsbruck, Sonderband* **5**, 1–296.
29
30

31
32 TEKIN, U. K. & GÖNCÜOĞLU, M. C. 2007. Discovery of the oldest (Upper Ladinian to Middle
33 Carnian) radiolarian assemblages from the Bornova Flysch Zone in western Turkey: Implications
34 for the evolution of the Neotethyan Izmir-Ankara Ocean. *Ofioliti* **32**, 131–150.
35
36

37
38 TEKIN, U. K. & GÖNCÜOĞLU, M. C. 2009. Late Middle Jurassic (late Bathonian-early Callovian)
39 radiolarian cherts from the Neotethyan Bornova Flysch Zone, Spil Mountains, Western Turkey.
40
41 *Stratigraphical and Geological Correlation* **17**: 298–308.
42
43

44
45 TEKIN, U. K., GÖNCÜOĞLU, M. C. & TURHAN, N. 2002. First evidence of Late Carnian radiolarian
46 fauna from the Izmir-Ankara Suture Complex, Central Sakarya, Turkey: implications for the
47 opening age of the Izmir-Ankara branch of Neotethys. *Geobios* **35**, 127–135.
48
49

50
51 TEKIN, U. K., GÖNCÜOĞLU, M. C., PANDOLFI, L. & MARRONI, M. 2012a. Middle-Late Triassic
52 radiolarian cherts from the Arkotdağ mélange in northern Turkey: implications for the life span of
53
54 the northern Neotethyan branch *Geodinamica Acta* **25**, 305–319
55
56
57
58
59
60

1
2
3 TEKIN, U. K., GÖNCÜOĞLU, M. C & UZUNCIMEN, S. 2012b. Radiolarian assemblages of Middle and
4
5 Late Jurassic to early Late Cretaceous (Cenomanian) ages from an olistolith record pelagic
6
7 deposition within the Bornova Flysch Zone in western Turkey. *Bulletin de la Société Géologique de*
8
9 *France* **183**, 307–318.

10
11 THIRLWALL, M., UPTON, B. G. J. & JENKINS, C. 1994. Interaction between continental lithosphere
12
13 and the Iceland plume-Sr-Nd-Pb isotope geochemistry of tertiary basalts, NE Greenland. *Journal of*
14
15 *Petrology* **35**, 839–879.

16
17
18 TOPUZ, G., GÖÇMENGİL, G., ROLLAND, Y., ÇELİK, Ö. F., ZACK, T. & SCHMITT, A. K. 2013a. Jurassic
19
20 accretionary complex and ophiolite from northeast Turkey: No evidence for the Cimmerian
21
22 continental ribbon. *Geology* **45**, 255–258.

23
24
25 TOPUZ, G., ÇELİK, Ö. F., ŞENGÖR, A. M. C., ALTINTAŞ, İ. E., ZACK, T., ROLLAND, Y. & BARTH, M.
26
27 2013b. Jurassic ophiolite formation and emplacement as backstop to a subduction-accretion
28
29 complex in northeast Turkey, the Refahiye ophiolite, and relation to the Balkans ophiolites.
30
31 *American Journal of Science* **313**, 1054–1087.

32
33
34 ÜNER, T. 2010. Petrology of Eldivan and Ahlat (Çankırı) ophiolites. PhD thesis Hacettepe
35
36 University, Ankara, Turkey. Unpublished thesis (in Turkish with English abstract).

37
38
39 WARREN, J. M. 2016, Global variations in abyssal peridotite compositions. *Lithos* **248-251**,
40
41 193–219.

42
43 WARREN, J.M., SHIMIZU, N., SAKAGUCHI, C., DICK, H.J.B., NAKAMURA, E., 2009. An assessment of
44
45 upper mantle heterogeneity based on abyssal peridotite isotopic compositions. *Journal of*
46
47 *Geophysical Research* **114** (B12203).

48
49
50 WOOD, D. A. 1980. The application of a Th-Hf-Ta diagram to problems of tectonomagmatic
51
52 classification and to establishing the nature of crustal contamination of basaltic lavas of the British
53
54 Tertiary volcanic province. *Earth and Planetary Science Letters* **50**, 11-30.

55
56
57 WORKMAN, R. K. & HART, S. R. 2005. Major and trace element composition of the depleted MORB
58
59 mantle (DMM). *Earth and Planetary Science Letters* **2**, 53–72.
60

1
2
3 YALINIZ, M. K., FLOYD, P. A. & GÖNCÜOĞLU, M. C. 1996, Supra-subduction zone ophiolites of
4
5 Central Anatolia: geochemical evidence from the Sarıkaraman Ophiolite, Aksaray. *Turkish*
6
7 *Mineralogical Magazine* **60**, 697–710.

8
9
10 YALINIZ, K., GÖNCÜOĞLU, M. C. & FLOYD, P. A. 2000a. Geochemistry of volcanic rocks from the
11
12 Çicekdağ Ophiolite, Central Anatolia, Turkey, and their inferred tectonic setting within the northern
13
14 branch of the Neotethyan ocean. In *Tectonics and magmatism in Turkey and the surrounding area*
15
16 (eds E. Bozkurt, J. Winchester & J. A. Piper), pp. 203-218. Geological Society of London, Special
17
18 Publication no. 173.

19
20
21 YALINIZ, M. K., GÖNCÜOĞLU, M. C. & ÖZKAN-ALTINER, S. 2000b. Formation and emplacement
22
23 ages of the SSZ-type Neotethyan ophiolites in Central Anatolia, Turkey: paleotectonic implications.
24
25 *Geological Journal* **35**, 53–68.

26
27
28 YILMAZ, Y., SERDAR, H. S., GENÇ, C., YIGITBAS, E., GURER, F., ELMAS, A., YILDIRIM, M., BOZCU,
29
30 M. & GURPINAR, O. 1997. The geology and evolution of the Tokat Massif, south central Pontides,
31
32 Turkey. *International Geological Revue* **39**, 365–382.

33
34
35 YOLSAL-ÇEVİKBİLEN, S., BIRYOL, C. B., BECK, S., ZANDT, G., TAYMAZ, T., ADIYAMAN, H. E. &
36
37 ÖZACAR, A. A. 2012. 3-D crustal structure along the North Anatolian Fault Zone in north-central
38
39 Anatolia revealed by local earthquake tomography. *Geophysical Journal International*, **188**,
40
41 819–849.

42 43 44 45 46 47 48 49 **CAPTIONS**

50
51
52
53
54 **Figure 1.** The main tectonic zones of Turkey (modified after Sengör & Yılmaz, 1981; Göncüoğlu
55
56 *et al.* 2012, modified).
57
58
59
60

Figure 2. Sketch geological map of the study area, with the location of the sampled sections (after Bortolotti *et al.* 2013a, modified and Yolsal-Çevikbilen *et al.*, 2012) EFZ: Eldivan Fault Zone; ODFZ: Orta–Devrez Fault Zone, KFZ, Kızılırmak Fault Zone; ESFZ: Ezine Pazarı–Sungurlu Fault Zone, AFZ: Alaca Fault Zone, CF: Çekerek Fault.

Figure 3. a) Serpentinite mélangé near Beynam; b) Pillow basalts along the road from Elmadag to Kırıkkale (Section 1); c) Overtuned sequence of basalts and radiolarian cherts along the road from Çorum to Alaca (Section 5); d) Outcrop of basalts and radiolarian cherts along the road from Iskilip to Tosya (Section 7). Modified from Bortolotti *et al.* (2013a).

Figure 4. (scale bar = 50 µm), a) *Archaeodictyomitra* sp. cf. *A. lacrimula* (Foreman), Section 1, TU10.4; b) *Aurisaturnalis variabilis variabilis* (Squinabol), Section 1, TU10.4; c) *Hemicryptocapsa* sp. cf. *H. capita* Tan, Section 1, TU10.4; d) *Thanarla brouweri* (Tan), Section 1, TU10.4; e) *Eoxitus* (?) sp., Section 2, TU10.11; f) *Stichomitra* (?) *takanoensis* Aita, Section 2, TU10.11; g) *Hiscocapsa* sp. *Praewillriedellum* sp. cf. *P. convexum* (Yao), Section 2, TU10.12; h) *Mirifusus* sp. cf. *M. guadalupensis* Pessagno, Section 2, TU10.12; i) *Stichomitra* (?) *takanoensis* Aita, Section 2, TU10.12; j) *Emiluvia* sp. cf. *E. ordinaria* Ozvoldova, Section 3, TU10.28; k) *Fultacapsa sphaerica* (Ozvoldova), Section 3, TU10.28; l) *Podocapsa amphitrepta* Foreman, Section 3, TU10.28; m) *Spinocapsa* (?) sp., Section 3, TU10.28; n) *Archaeodictyomitra lacrimula* (Foreman), Section 4, TU10.29; o) *Archaeodictyomitra mitra* Dumitrica, Section 4, TU10.29; p) *Dicerosaturnalis trizonalis* (Rüst), Section 4, TU10.29; q) *Pantanellium* sp. cf. *P. squinaboli* (Tan), Section 4, TU10.29; r) *Thanarla* sp. cf. *T. gutta* Jud, Section 4, TU10.29; s) *Archaeodictyomitra* sp., Section 4, TU10.30; t) *Holocryptocanium barbui* Dumitrica, Section 4, TU10.30; u) *Pseudodictyomitra lanceoloti* Schaaf, Section 4, TU10.30; v) *Thanarla pulchra* (Squinabol) *Thanarla* sp. cf. *T. pacifica* Nakaseko & Nishimura, Section 4, TU10.30.

1
2
3 **Figure 5.** (scale bar = 50 μm), a) *Archaeodictyomitra lacrimula* (Foreman), Section 4, TU10.31; b)
4
5 *Aurisaturnalis carinatus perforatus* Dumitrica & Dumitrica Jud, Section 4, TU10.31; c) *Thanarla*
6
7 *brouweri* (Tan), Section 4, TU10.31; d) *Eucyrtidiellum pyramis* (Aita), Section 5, TU10.35; e)
8
9 *Podocapsa amphitreptera* Foreman, Section 5, TU10.35; f) *Cinguloturris cylindra* Kemkin &
10
11 Rudenko, Section 5, TU10.36; g) *Emiluvia* sp. cf. *E. ordinaria* Ozvoldova, Section 5, TU10.36; h)
12
13 *Eucyrtidiellum pyramis* (Aita), Section 5, TU10.36; i) *Loopus primitivus* (Matsuoka & Yao),
14
15 Section 5, TU10.36; j) *Ristola cretacea* (Baumgartner), Section 5, TU10.36; k) *Podocapsa*
16
17 *amphitreptera* Foreman, Section 5, TU10.37; l) *Praeconosphaera* (?) *sphaeroconus* (Rüst), Section
18
19 5, TU10.37; m) *Archaeodictyomitra* sp. cf. *A. excellens* (Tan), Section 5, TU10.38; n) *Podocapsa*
20
21 *amphitreptera* Foreman, Section 5, TU10.38; o) *Saitoum* sp. cf. *S. elegans* De Wever, Section 5,
22
23 TU10.38; p) *Zhamoidellum ovum* Dumitrica, Section 5, TU10.38; q) ~~*Pseudodictyomitra* sp.~~
24
25 *Archaeodictyomitra* sp. cf. *A. coniforma* Dumitrica, Section 7, TU10.45; r) *Cryptamphorella*
26
27 *clivosa* (Aliev), Section 7, TU10.45; s) *Praeconosphaera* (?) *sphaeroconus* (Rüst), Section 7,
28
29 TU10.45; t) *Archaeodictyomitra excellens* (Tan), Section 8, TU10.47; u) ~~*Ceeroops*~~—*Cana*
30
31 *septemporatus* (Parona), Section 8, TU10.47; v) *Halesium* sp. cf. *H. palmatum* Dumitrica, Section
32
33 8, TU10.47; w) *Archaeodictyomitra lacrimula* (Foreman), Section 8, TU10.51; x) *Pseudoeucyrtis*
34
35 sp. cf. *P. hanni* (Tan) sensu O'Dogherty (1994), Section 8, TU10.51.
36
37
38
39
40
41
42

43 **Figure 6.** Ti/Y vs. Nb/Y discrimination diagram (Pearce, 1982) for Middle Jurassic – Early
44
45 Cretaceous volcanic rocks from the Ankara Mélange. Modified from Bortolotti *et al.* (2013a).
46
47
48

49 **Figure 7.** Variation diagrams for some representative major and trace elements vs. Zr for Middle
50
51 Jurassic – Early Cretaceous volcanic rocks from the Ankara Mélange. Major elements are re-
52
53 calculated on volatiles-free and calcite-free bases. Abbreviations, pl: plagioclase; ol: olivine; cpx:
54
55 clinopyroxene; opx: orthopyroxene; mt: magnetite. $\text{Mg\#} = 100 \times \text{Mg} / (\text{Mg} + \text{Fe}^{2+})$. Lines represent
56
57 the inferred fractionation trends for the different rock-groups.
58
59
60

1
2
3
4
5 **Figure 8.** N-MORB normalized incompatible element patterns (a, c, e, g) and chondrite-normalized
6 REE patterns (b, d, f, h) for Middle Jurassic – Early Cretaceous volcanic rocks from the Ankara
7 Mélange. Normalizing values and the compositions of normal mid-ocean ridge basalt (N-MORB),
8 enriched mid-ocean ridge basalt (E-MORB), and ocean-island basalt (OIB) are from Sun &
9 McDonough (1989).
10
11
12
13
14
15
16
17

18 **Figure 9.** a) Th_N vs. Nb_N and b) $(Dy/Yb)_N$ vs. $(Ce/Yb)_N$ discrimination diagrams for Middle
19 Jurassic – Early Cretaceous volcanic rocks from the Ankara Mélange. Modified after Saccani
20 (2015). N-MORB and Chondrite normalization values for panels a) and b), respectively are from
21 Sun & McDonough (1989).
22
23
24
25
26
27
28

29 **Figure 10.** Th-Ta-Hf/3 (Wood, 1980) discrimination diagrams for Middle Jurassic – Early
30 Cretaceous volcanic rocks from the Ankara Mélange.
31
32
33
34
35

36 **Figure 11.** Melt curve models based on Dy/Yb vs. La/Yb. Melt curves are calculated using non-
37 modal, batch melts of garnet and spinel lherzolites. a) melt curves for DMM mantle (Workman &
38 Hart, 2005); b) melt curves for a theoretical DMM mantle (Workman & Hart, 2005) enriched in
39 LREE by OIB-type) components; c) melt curves for a theoretical enriched (OIB-type) mantle.
40
41
42
43
44
45 Garnet lherzolite mode is: 0.598 ol, 0.211 opx; 0.076 cpx, 0.115 gt that melts in the proportions
46 0.05 ol, 0.20 opx, 0.30 cpx, 0.45 gt. Spinel lherzolite mode is: 0.578 ol, 0.270 opx, 0.119 cpx, 0.033
47 spl that melts in the proportions 0.10 ol, 0.27 opx, 0.50 cpx, 0.13 spl. Mantle mode and melting
48 proportions are from Thirlwall *et al.* (1994). Arrays representing the mixing between various
49 proportions of melt fractions from the garnet-facies mantle and melt fractions from spinel-facies
50 mantle are also shown. Distribution coefficients are from Irving & Frey (1984) with the exception
51
52
53
54
55
56
57
58
59
60

1
2
3 of those for spinel, which are from McKenzie & O'Nions (1991). Normalizing values are from Sun
4
5 & McDonough (1989).
6
7
8

9
10 **Figure 12.** Zr/Y vs. Zr/Nb diagram for volcanic rocks from the Middle Jurassic – Early Cretaceous
11 volcanic rocks from the Izmir-Ankara Mélange (modified from Bortolotti *et al.*, 2013a). The
12 compositions of modern normal mid-ocean ridge basalt (N-MORB) and ocean-island basalt (OIB)
13 are from Sun & McDonough (1989). The compositional variation for ocean-floor basalts erupted in
14 the North Atlantic Ocean is shown for comparison (data from Hanan *et al.*, 2000). The dashed line
15 represents the mixing curve calculated using the OIB and N-MORB end members.
16
17
18
19
20
21
22
23
24

25 **Figure 13.** 2-D cartoon showing the tectono-magmatic mechanisms responsible for the formation of
26 garnet-influenced (G-) enriched (E-), and plume-type (P-) mid-ocean ridge basalts (MORB), as well
27 as alkaline ocean island-type (OIB) basalts from the Ankara Mélange during the Late Jurassic-Early
28 Cretaceous. Other abbreviations, sp: spinel; gt: garnet.
29
30
31
32
33
34
35

36 **Figure 14.** 2-D cartoon showing the geodynamic evolution the Izmir-Ankara Neotethys branch
37 from Late Triassic to late Early Cretaceous (modified from Göncüoğlu, 2010). Abbreviations,
38 MORB: mid-ocean ridge basalts; G-: garnet-influenced MORB; E-: enriched-MORB; P-: plume-
39 type MORB; alk: alkaline basalts; SSZ: supra-subduction zone.
40
41
42
43
44
45
46

47 **Table 1.** Representative major and trace element analyses of Middle Jurassic – Early Cretaceous
48 volcanic rocks from the Ankara Mélange. Abbreviations, bas: basalt; tra: trachyte; Fe-bas:
49 ferrobasalt; trans: transitional-type; sub-alk: sub-alkaline-type; OIB: ocean island basalt; P-MORB:
50 plume-type mid-ocean ridge basalt; E-MORB: enriched-type mid-ocean ridge basalt; G-MORB:
51 garnet-influenced mid-ocean ridge basalt; E: Early; M: Middle; L: Late; Jr: Jurassic; Cr: Cretaceous;
52
53
54
55
56
57
58
59
60

1
2
3 mlf: massive lava flow; n.d.: not detected. $Mg\# = 100 \times Mg / (Mg + Fe^{2+})$. $Fe_2O_3 = 0.15 \times FeO$.

4
5 Normalizing values for REE ratios are from Sun & McDonough (1989).
6
7
8
9
10
11
12
13
14
15
16
17
18
19
20
21
22
23
24
25
26
27
28
29
30
31
32
33
34
35
36
37
38
39
40
41
42
43
44
45
46
47
48
49
50
51
52
53
54
55
56
57
58
59
60

Proof For Review

Table 1.

Section	1			2				3		
	TU10-6	TU10-9	TU10-10	TU10-14	TU10-15	TU10-16	TU10-17	TU10-19	TU10-22	TU10-23
Sample	TU10-6	TU10-9	TU10-10	TU10-14	TU10-15	TU10-16	TU10-17	TU10-19	TU10-22	TU10-23
Rock	bas	tra	bas	bas	bas	Fe-bas	Fe-bas	bas	bas	bas
Group	4	4	4	3	3	3	3	4	4	4
Type	alkaline OIB	alkaline OIB	alkaline OIB	trans P-MORB	trans P-MORB	trans P-MORB	trans P-MORB	alkaline OIB	alkaline OIB	alkaline OIB
Age	E Cr			M Jr	M Jr	M Jr	M Jr		L Jr	L Jr
Note	pillow	breccia	pillow	pillow	pillow	pillow	pillow	mlf	pillow	pillow
	(XRF)	(XRF)	(XRF)	(XRF)	(XRF)	(XRF)	(XRF)	(XRF)	(XRF)	(XRF)
SiO ₂	41.40	56.12	39.61	44.12	40.20	42.40	44.87	44.36	46.03	44.81
TiO ₂	1.91	2.35	1.96	2.28	1.65	3.27	2.55	2.97	2.32	2.21
Al ₂ O ₃	11.76	15.96	11.81	14.48	11.92	13.81	13.82	13.41	17.06	16.49
Fe ₂ O ₃	0.93	1.33	1.00	1.74	1.00	2.08	1.96	1.45	1.42	1.40
FeO	6.18	8.90	6.67	11.60	6.66	13.89	13.06	9.63	9.47	9.31
MnO	0.15	0.11	0.12	0.23	0.22	0.19	0.19	0.40	0.20	0.20
MgO	4.24	1.68	3.86	9.25	6.32	7.42	9.98	9.14	7.31	9.05
CaO	16.69	3.61	17.84	8.16	18.02	8.04	6.23	6.96	6.48	7.45
Na ₂ O	3.73	7.37	2.93	2.39	2.11	3.07	1.74	3.24	2.07	1.84
K ₂ O	1.72	0.65	2.06	0.82	1.89	0.69	1.26	1.13	3.54	2.95
P ₂ O ₅	0.48	0.59	0.60	0.33	0.21	0.54	0.62	0.52	0.96	0.86
L.O.I.	10.94	1.16	11.56	4.65	9.89	4.65	3.73	6.94	3.15	3.50
Total	100.13	99.84	100.03	100.05	100.08	100.05	100.01	100.15	100.01	100.06
CO ₂	6.23		6.13		7.05					
Mg#	55.0	25.2	50.8	58.7	62.9	48.8	57.7	62.8	57.9	63.4
Zn	73	104	57	72	63	110	101	109	75	72
Cu	25	35	44	77	71	59	57	69	40	40
Sc	23	9	18	36	40	43	35	36	8	10
Ga	15	14	16	21	15	24	20	16	17	19
Ni	70	26	54	78	53	8	11	100	25	42
Co	27	16	23	37	33	37	30	36	23	25
Cr	227	56	115	135	81	26	21	271	16	29
V	204	180	206	334	275	403	329	474	188	210
Ba	289	186	340	246	717	199	177	193	1980	1380
Pb	4	7	5	7	4	7	6	16	8	7
Zr	217	320	225	165	128	239	196	265	330	287
	(ICP-MS)		(ICP-MS)	(ICP-MS)	(ICP-MS)			(ICP-MS)		(ICP-MS)
Rb	30.8	12	36.7	8.41	17.6	8	16	27.2	75	58.5
Sr	575	441	478	292	280	391	371	197	740	760
Y	28.5	40	29.3	22	27.6	58	48	29	39	36.1
La	40.3	64	39	20.7	24.6	50	45	49.7	65	58.9
Ce	70.3	192	70.9	43	46.7	129	82	85.3	160	109
Pr	8.01		8.14	4.91	5.35			9.25		11.3
Nd	27.2	45	28.1	18.1	19.1	33	30	30.4	60	39.7
Sm	5.84		6.07	4.63	4.54			6.11		9.08
Eu	1.77		1.84	1.53	1.53			1.69		2.77
Gd	4.50		4.69	4.6	4.45			4.62		7.11
Tb	0.702		0.722	0.718	0.657			0.697		1.03
Dy	3.71		3.76	4.28	3.82			3.67		5.33
Ho	0.704		0.711	0.896	0.793			0.707		0.992
Er	1.78		1.78	2.38	2.11			1.81		2.58
Tm	0.239		0.236	0.339	0.295			0.242		0.35
Yb	1.49		1.49	2.21	1.92			1.54		2.19
Lu	0.214		0.213	0.335	0.291			0.221		0.324
Nb	61.5	83	65.9	30.6	40.4	50	45	88	142	88
Hf	5.11	5	5.34	4.56	3.69	4	3	4.82	5	7
Ta	2.93		3.71	1.76	3.34			4.77		7.13
Th	5.09	9	5.49	2.77	3.48	7	5	7.49	9	11.6
U	1.48		1.34	0.793	1.04			1.75		2.99
(La/Sm) _N	4.46		4.15	2.88	3.49			5.25		4.19
(Sm/Yb) _N	4.36		4.52	2.33	2.63			4.40		4.62
(La/Yb) _N	19.43		18.75	6.72	9.17			23.13		19.33
Ti/V	69	79	71	43	44	51	48	40	76	65
Ce/Y	2.40	4.80	2.69	1.87	1.64	2.20	1.60	3.16	4.10	4.01
Nb/Yb	41.32		44.13	13.86	21.03			57.02		40.25
(Th/Ta)/(Th/Tb)	0.24		0.19	0.41	0.20			0.15		1.14

Table 1 (cont.)

Section	4		5			7	8		9	
Sample	TU10-32	TU10-33	TU10-34	TU10-39	TU10-40	TU10-46	TU10-49a	TU10-49b	TU10-52	TU10-53
Rock	bas	bas	bas	bas	bas	bas	bas	bas	bas	bas
Group	2	2	1	1	1	2	1	1	3	3
Type	sub-alk E-MORB	sub-alk E-MORB	sub-alk G-MORB	sub-alk G-MORB	sub-alk G-MORB	sub-alk E-MORB	sub-alk G-MORB	sub-alk G-MORB	trans P-MORB	trans P-MORB
Age	E Cr	E Cr	L Jr	L Jr	L Jr	E Cr	E Cr	E Cr		
Note	mlf	mlf	mlf	breccia	mlf	mlf	pillow	pillow	mlf	mlf
	<i>(XRF)</i>	<i>(XRF)</i>	<i>(XRF)</i>	<i>(XRF)</i>	<i>(XRF)</i>	<i>(XRF)</i>	<i>(XRF)</i>	<i>(XRF)</i>	<i>(XRF)</i>	<i>(XRF)</i>
SiO ₂	45.98	46.18	47.04	48.28	46.35	48.35	53.76	48.67	48.72	39.89
TiO ₂	1.51	1.46	1.48	1.46	1.74	1.20	1.51	1.46	1.89	1.37
Al ₂ O ₃	13.44	13.30	13.50	14.84	15.70	17.65	13.26	13.83	17.70	11.71
Fe ₂ O ₃	1.44	1.26	1.28	1.42	1.59	0.77	1.28	1.65	1.42	1.05
FeO	9.61	8.43	8.51	9.49	10.60	5.14	8.52	11.01	9.49	6.97
MnO	0.29	0.27	0.26	0.19	0.11	0.11	0.13	0.16	0.05	0.17
MgO	5.69	5.14	5.24	5.48	2.40	4.69	5.80	7.48	3.77	4.26
CaO	14.15	15.60	15.85	9.28	12.16	9.55	8.03	6.18	4.16	21.76
Na ₂ O	2.82	3.21	3.27	3.39	3.77	5.71	3.88	2.49	2.04	1.88
K ₂ O	0.46	0.40	0.41	1.49	1.31	0.29	0.36	0.88	4.64	0.53
P ₂ O ₅	0.14	0.13	0.14	0.17	0.28	0.12	0.17	0.11	0.32	0.14
L.O.I.	4.58	4.66	3.02	4.56	3.94	6.45	3.2	6.02	5.83	10.28
Total	100.11	100.06	100.00	100.05	99.95	100.03	99.89	99.94	100.04	100.01
CO ₂	1.80	2.27	0.95		0.93					7
Mg#	51.4	52.1	52.3	50.7	28.8	61.9	54.8	54.8	41.4	52.2
Zn	84	87	87	115	124	63	79	97	115	63
Cu	77	94	92	62	27	95	55	12	35	27
Sc	42	39	44	55	48	26	19	40	28	32
Ga	16	14	16	18	17	14	21	18	16	19
Ni	139	139	139	106	69	40	32	15	140	213
Co	39	41	41	33	32	33	26	24	35	36
Cr	389	371	372	197	273	266	67	18	392	305
V	390	377	370	300	368	194	176	380	317	333
Ba	83	75	73	69	130	132	116	173	274	85
Pb	4	3	3	5	n.d.	3	5	6	6	6
Zr	74	73	73	97	98	75	84	88	135	84
	<i>(ICP-MS)</i>		<i>(ICP-MS)</i>	<i>(ICP-MS)</i>		<i>(ICP-MS)</i>		<i>(ICP-MS)</i>	<i>(ICP-MS)</i>	
Rb	6.35	5	25.2	28.4	17	3.15	2	14.8	68.8	2
Sr	130	136	129	385	201	429	120	129	160	96
Y	31.8	27	14.8	19.9	40	12.5	29	26.3	28.1	26
La	5.63	5	2.76	3.15	3	5.16	3	3.77	14.5	13
Ce	14.0	12	7.84	9.59	n.d.	11.8	9	10.1	26.2	31
Pr	2.18		1.32	1.59		1.63		1.67	3.38	
Nd	10.1	9	6.49	7.88	13	7.59	10	8.91	14.0	10
Sm	3.24		2.16	2.61		2.20		2.99	3.59	
Eu	1.13		0.778	0.907		0.811		1.10	1.06	
Gd	4.21		2.68	3.21		2.72		3.99	4.13	
Tb	0.752		0.47	0.560		0.463		0.714	0.698	
Dy	5.04		3.03	3.63		2.95		4.70	4.42	
Ho	1.15		0.638	0.791		0.626		1.01	0.869	
Er	3.23		1.70	2.15		1.75		2.78	2.43	
Tm	0.478		0.247	0.32		0.258		0.401	0.354	
Yb	3.18		1.52	2.03		1.69		2.54	2.24	
Lu	0.492		0.224	0.304		0.258		0.362	0.322	
Nb	7.81	9	2.88	3.36	5	5.25	4	2.74	25.7	19
Hf	2.78	3	1.61	2.24	n.d.	2.45	3	1.81	3.51	n.d.
Ta	0.404		0.161	0.188		0.277		0.159	1.48	
Th	0.619	n.d.	0.112	0.211	1	0.342	n.d.	0.195	2.51	3
U	0.151		0.071	0.008		0.102		0.052	0.573	
(La/Sm) _N	1.12		0.82	0.78		1.51		0.81	2.61	
(Sm/Yb) _N	1.13		1.58	1.43		1.45		1.31	1.78	
(La/Yb) _N	1.27		1.30	1.12		2.19		1.06	4.65	
Ti/V	25	25	25	31	30	40	53	25	38	31
Nb/Y	0.27	0.30	0.14	0.12	0.20	0.25	0.20	0.09	0.86	0.70
Nb/Yb	2.46		1.90	1.66		3.12		1.08	11.46	
(Th/Ta)/(Th/Tb)	1.86		2.91	2.98		1.67	4.50	0.88		

1
2
3
4
5
6
7
8
9
10
11
12
13
14
15
16
17
18
19
20
21
22
23
24
25
26
27
28
29
30
31
32
33
34
35
36
37
38
39
40
41
42
43
44
45
46
47
48
49
50
51
52
53
54
55
56
57
58
59
60

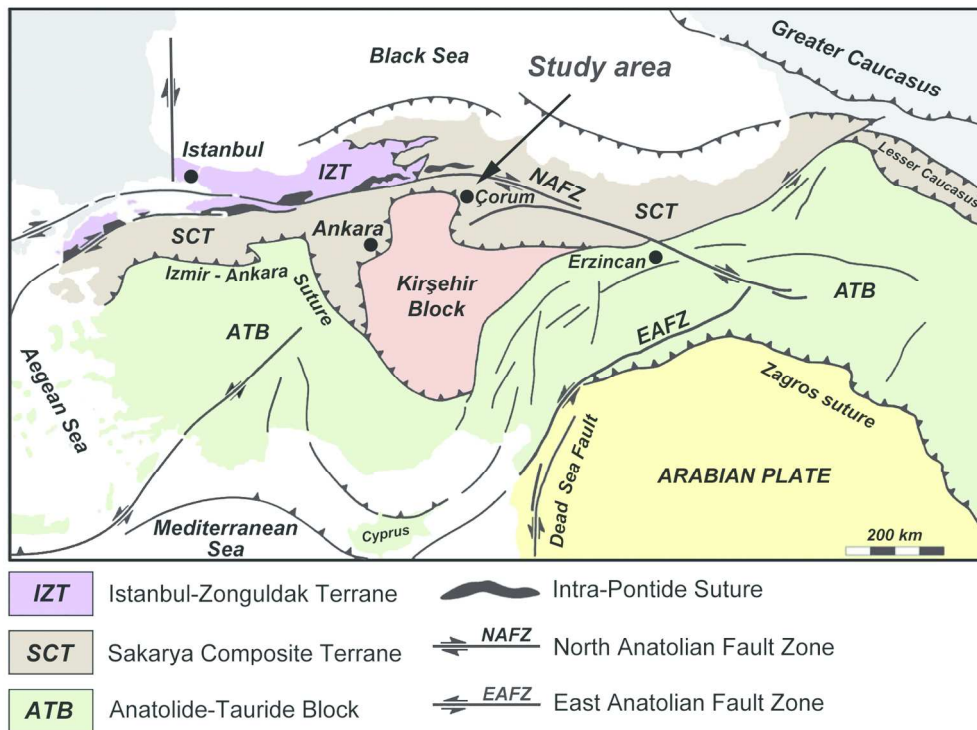


FIGURE 1

168x128mm (300 x 300 DPI)

review

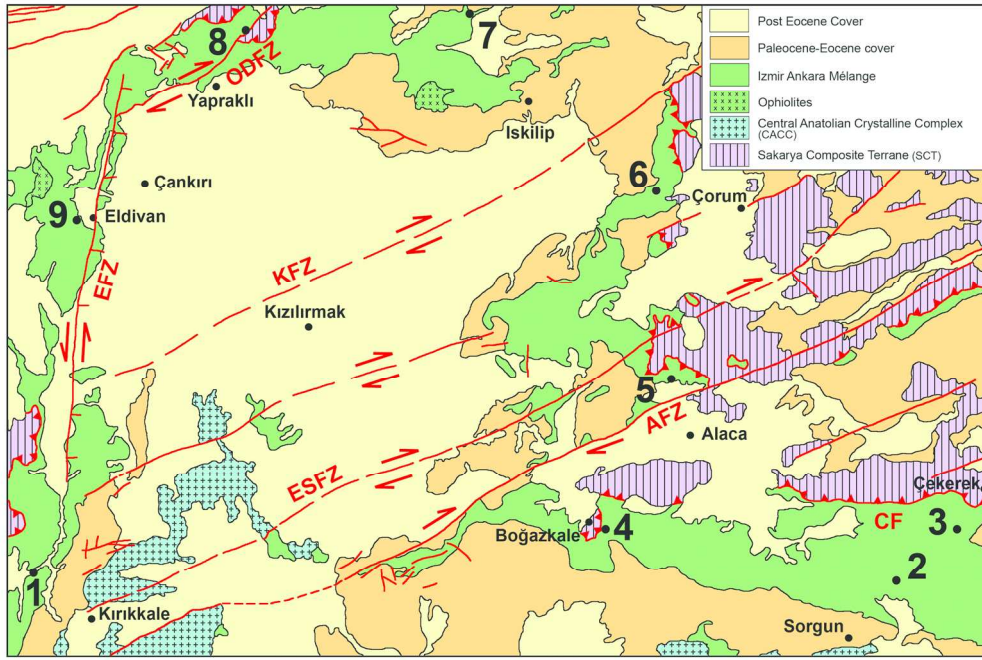


FIGURE 2

168x112mm (300 x 300 DPI)

Review

1
2
3
4
5
6
7
8
9
10
11
12
13
14
15
16
17
18
19
20
21
22
23
24
25
26
27
28
29
30
31
32
33
34
35
36
37
38
39
40
41
42
43
44
45
46
47
48
49
50
51
52
53
54
55
56
57
58
59
60

1
2
3
4
5
6
7
8
9
10
11
12
13
14
15
16
17
18
19
20
21
22
23
24
25
26
27
28
29
30
31
32
33
34
35
36
37
38
39
40
41
42
43
44
45
46
47
48
49
50
51
52
53
54
55
56
57
58
59
60

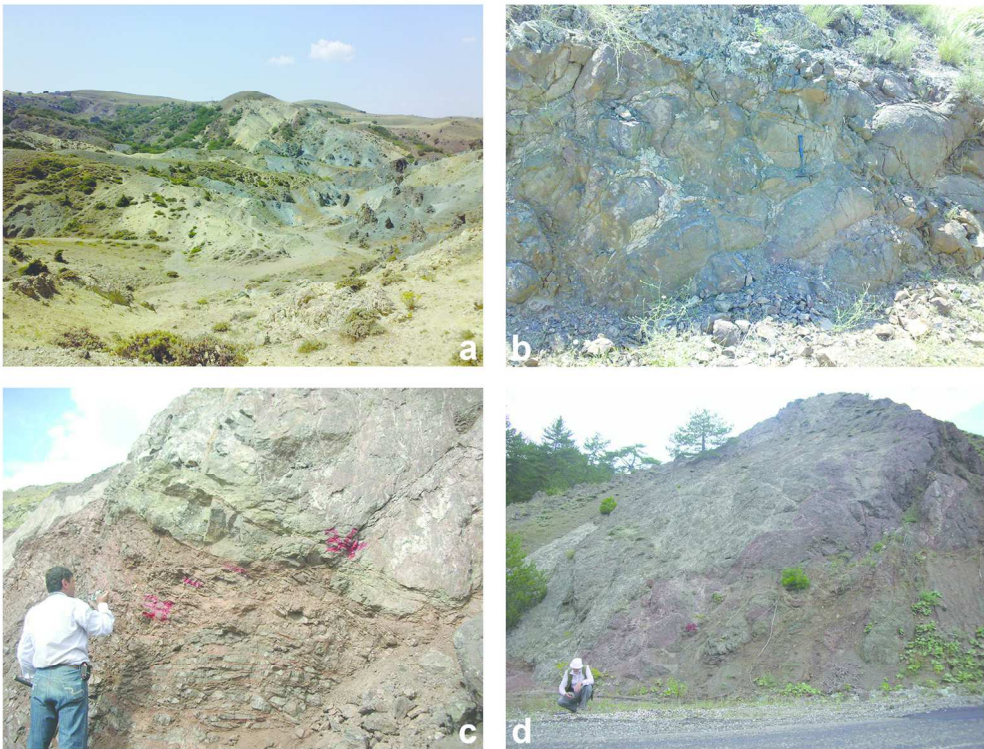


FIGURE 3

168x129mm (300 x 300 DPI)

review

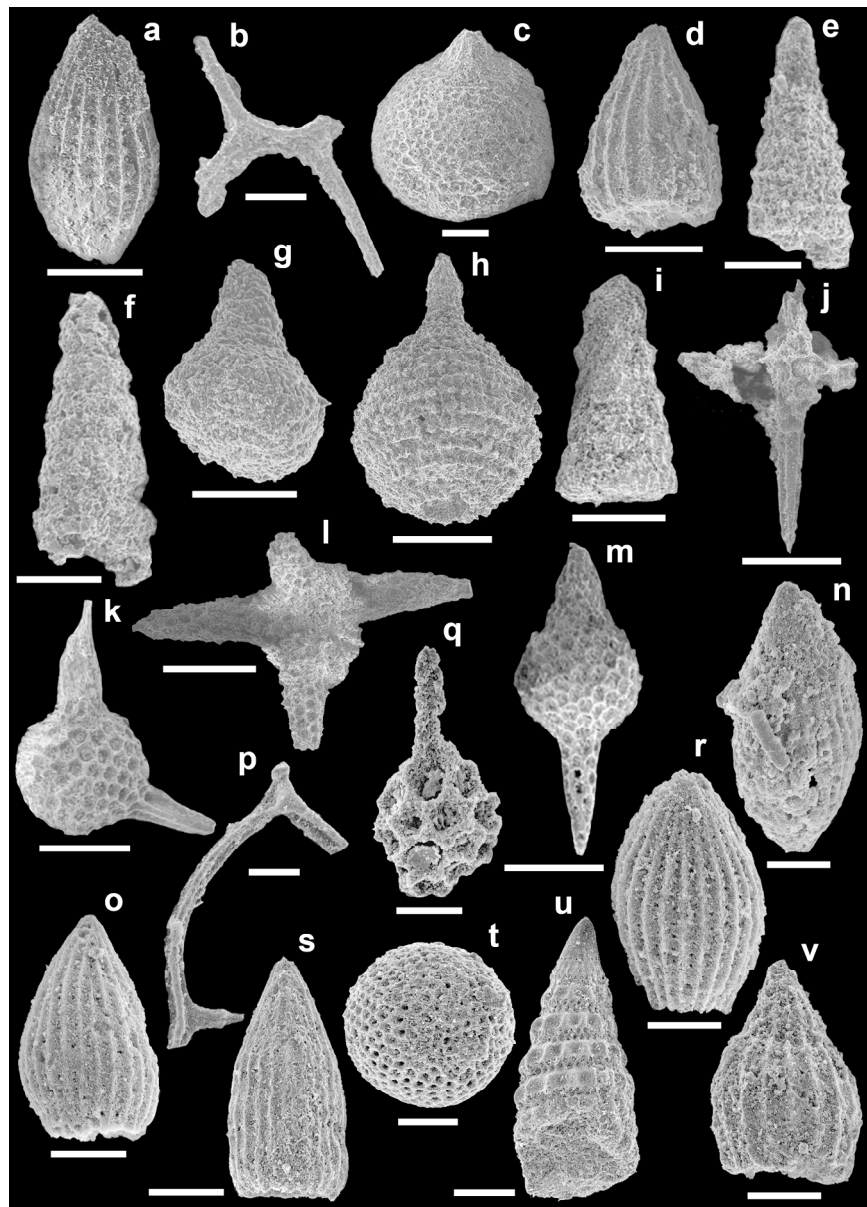


FIGURE 4

168x235mm (300 x 300 DPI)

1
2
3
4
5
6
7
8
9
10
11
12
13
14
15
16
17
18
19
20
21
22
23
24
25
26
27
28
29
30
31
32
33
34
35
36
37
38
39
40
41
42
43
44
45
46
47
48
49
50
51
52
53
54
55
56
57
58
59
60

1
2
3
4
5
6
7
8
9
10
11
12
13
14
15
16
17
18
19
20
21
22
23
24
25
26
27
28
29
30
31
32
33
34
35
36
37
38
39
40
41
42
43
44
45
46
47
48
49
50
51
52
53
54
55
56
57
58
59
60

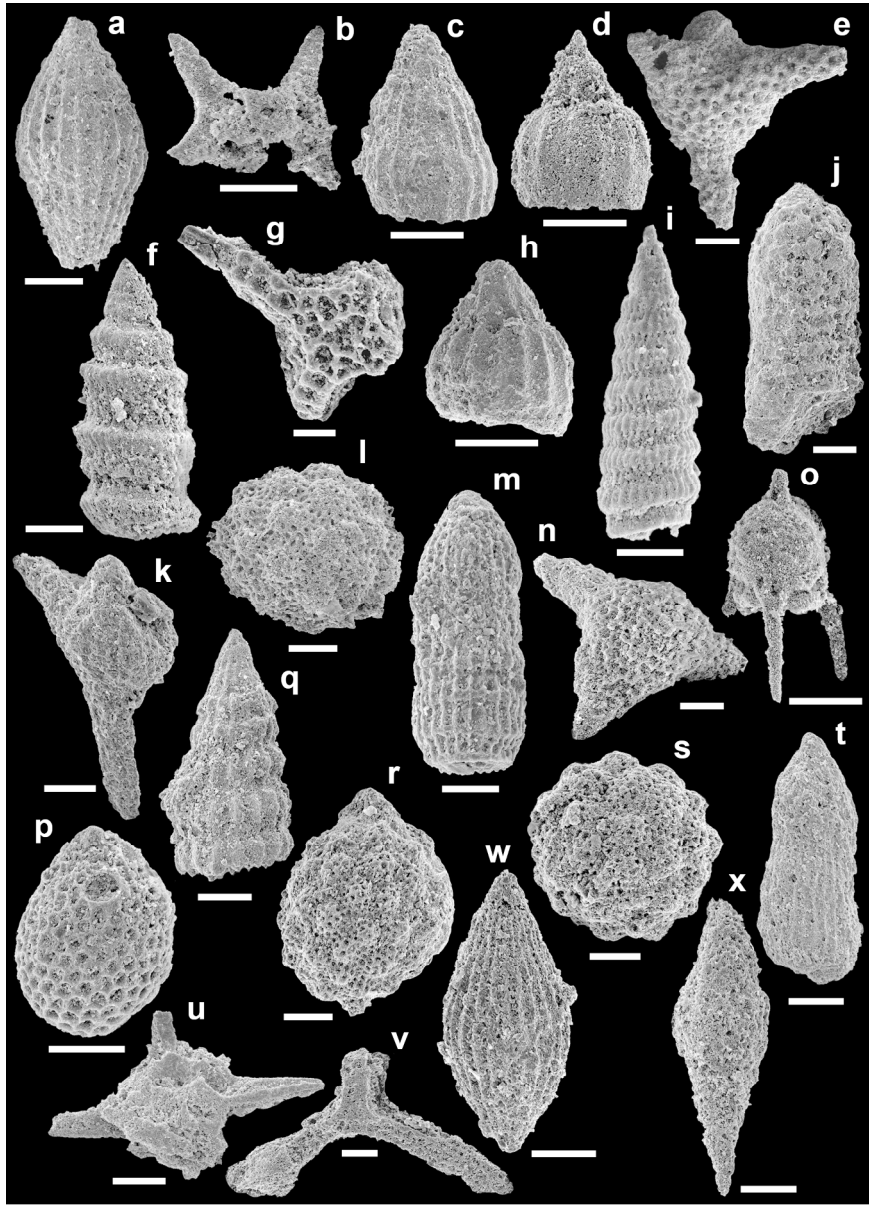


FIGURE 5

168x235mm (300 x 300 DPI)

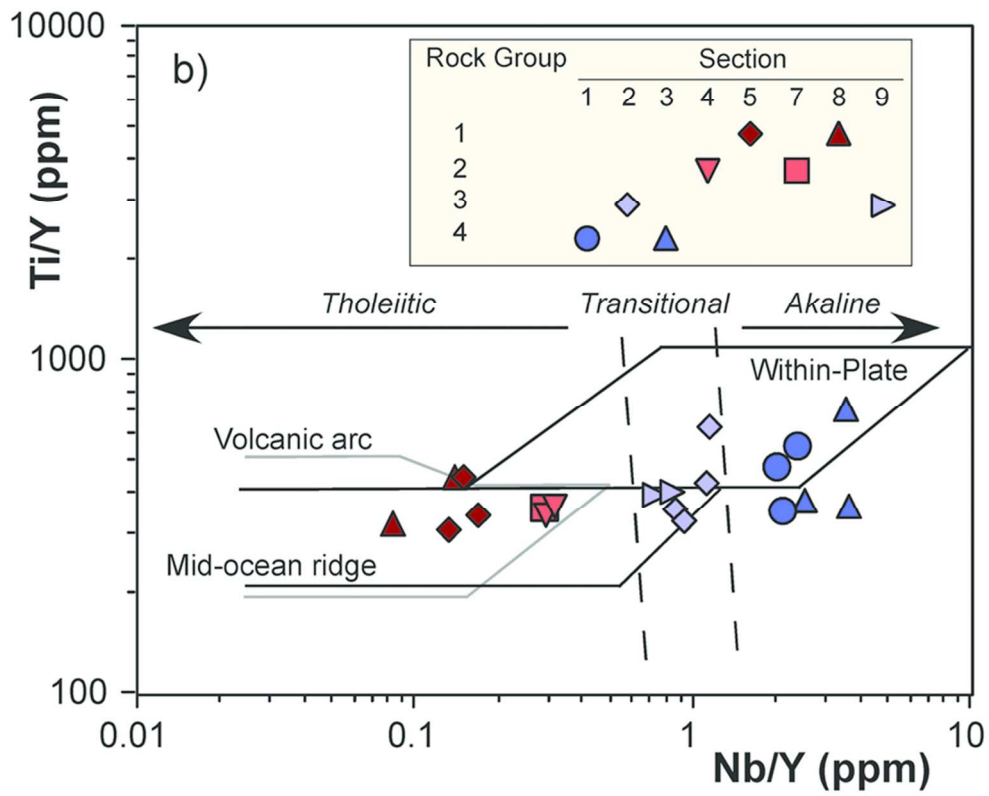


FIGURE 6

80x65mm (300 x 300 DPI)

view

1
2
3
4
5
6
7
8
9
10
11
12
13
14
15
16
17
18
19
20
21
22
23
24
25
26
27
28
29
30
31
32
33
34
35
36
37
38
39
40
41
42
43
44
45
46
47
48
49
50
51
52
53
54
55
56
57
58
59
60

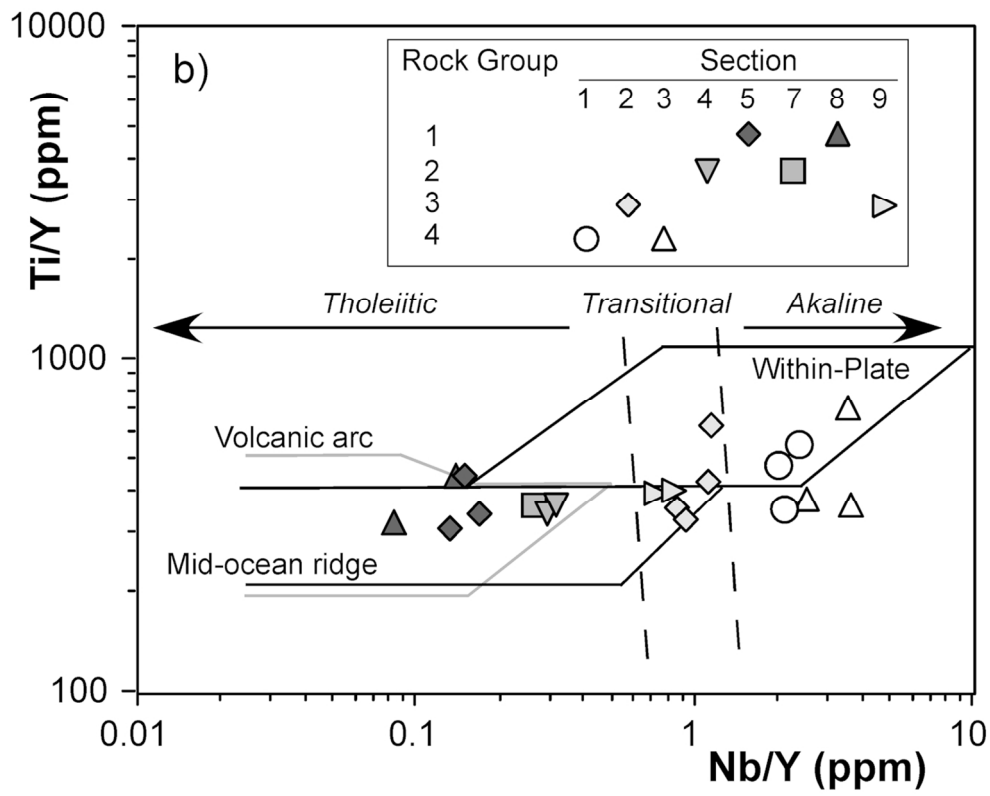


FIGURE 6 black and white

117x94mm (300 x 300 DPI)

Review

1
2
3
4
5
6
7
8
9
10
11
12
13
14
15
16
17
18
19
20
21
22
23
24
25
26
27
28
29
30
31
32
33
34
35
36
37
38
39
40
41
42
43
44
45
46
47
48
49
50
51
52
53
54
55
56
57
58
59
60

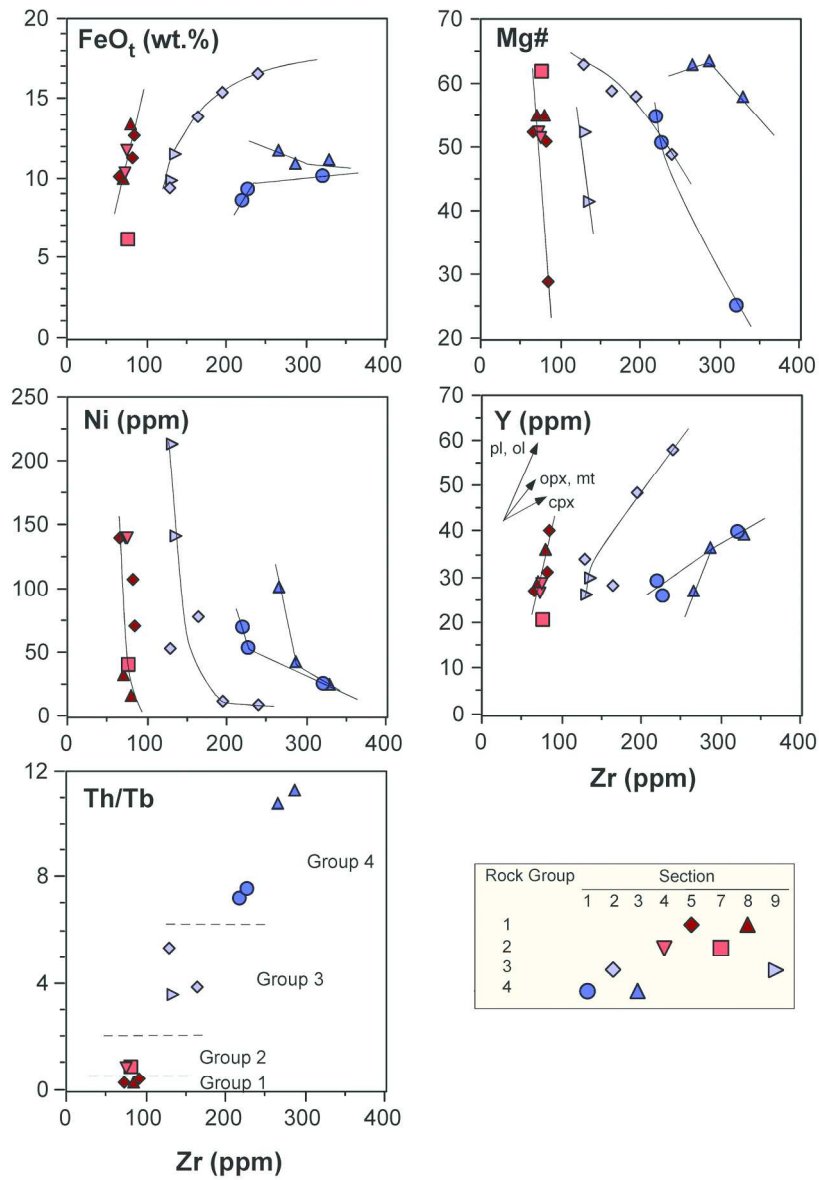


FIGURE 7

168x246mm (300 x 300 DPI)

1
2
3
4
5
6
7
8
9
10
11
12
13
14
15
16
17
18
19
20
21
22
23
24
25
26
27
28
29
30
31
32
33
34
35
36
37
38
39
40
41
42
43
44
45
46
47
48
49
50
51
52
53
54
55
56
57
58
59
60

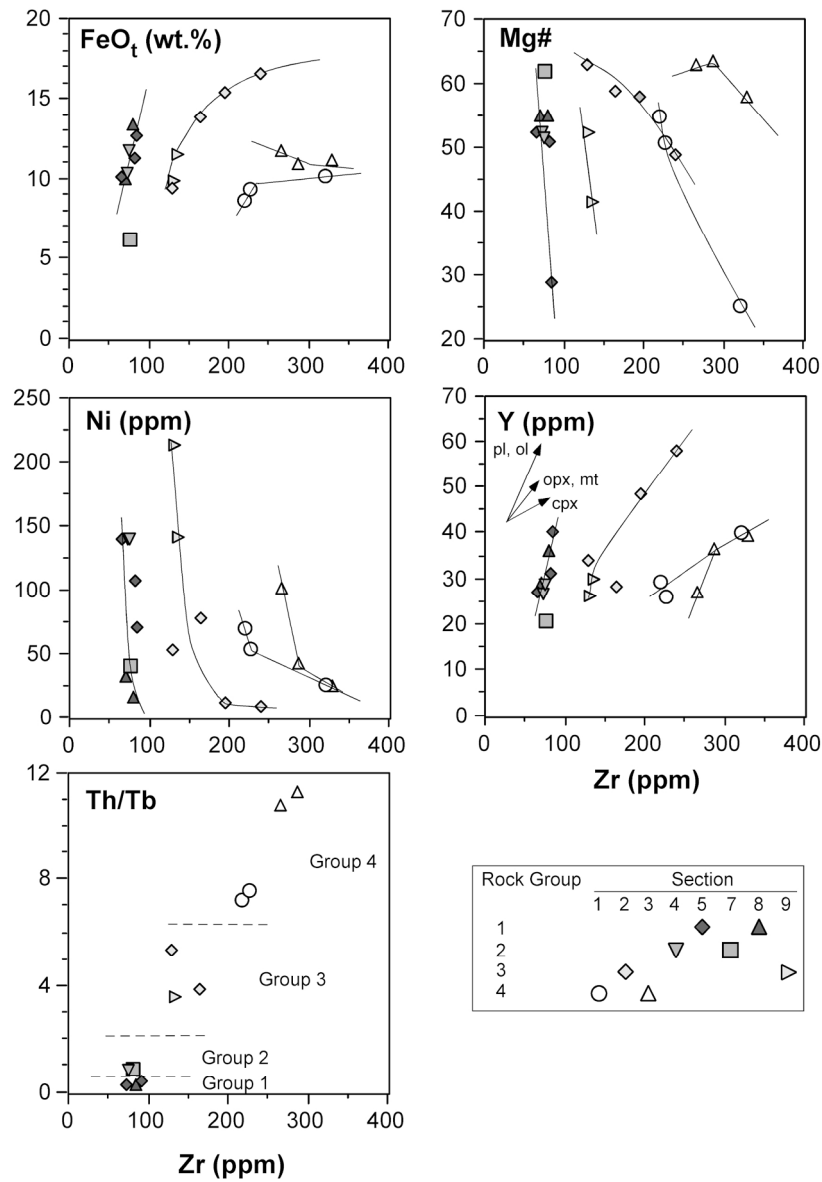


FIGURE 7 black and white

151x220mm (300 x 300 DPI)

1
2
3
4
5
6
7
8
9
10
11
12
13
14
15
16
17
18
19
20
21
22
23
24
25
26
27
28
29
30
31
32
33
34
35
36
37
38
39
40
41
42
43
44
45
46
47
48
49
50
51
52
53
54
55
56
57
58
59
60

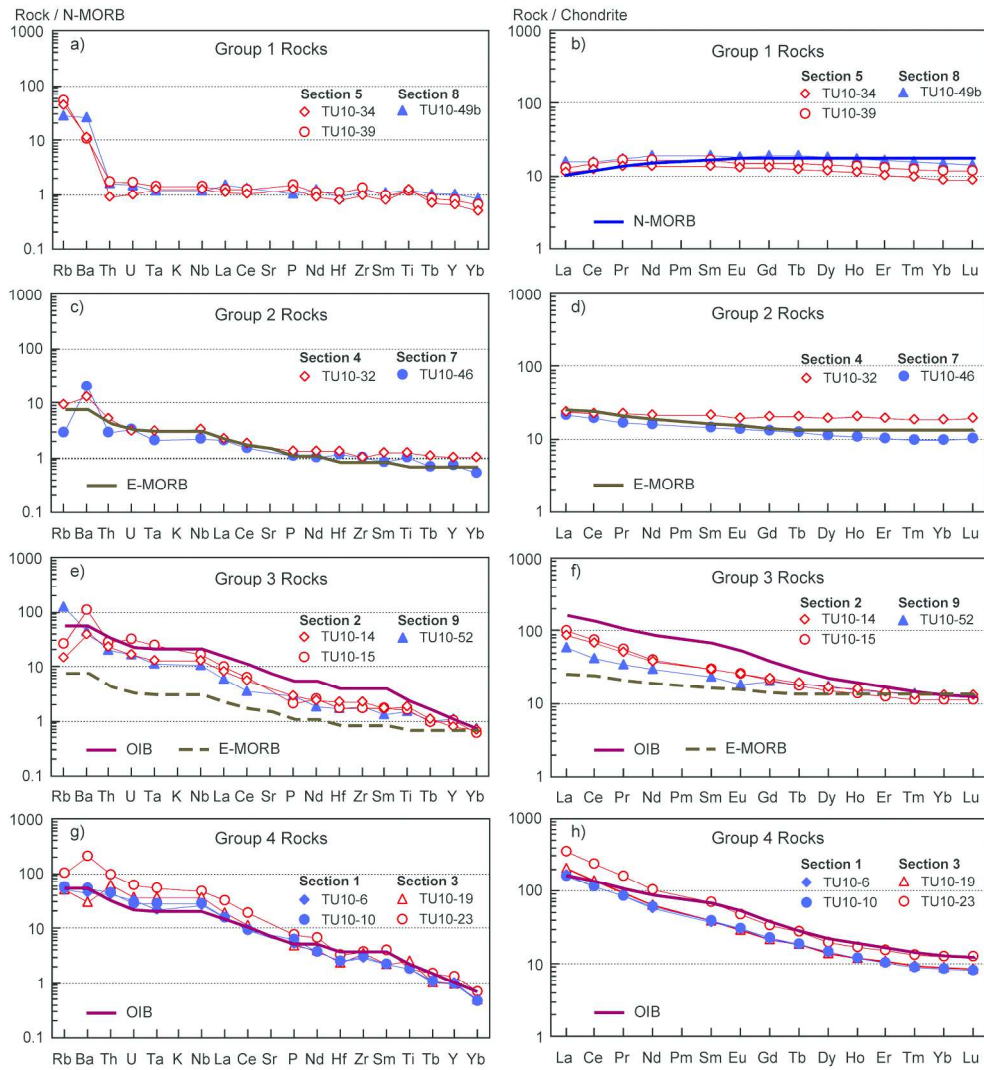


FIGURE 8

224x242mm (300 x 300 DPI)

1
2
3
4
5
6
7
8
9
10
11
12
13
14
15
16
17
18
19
20
21
22
23
24
25
26
27
28
29
30
31
32
33
34
35
36
37
38
39
40
41
42
43
44
45
46
47
48
49
50
51
52
53
54
55
56
57
58
59
60

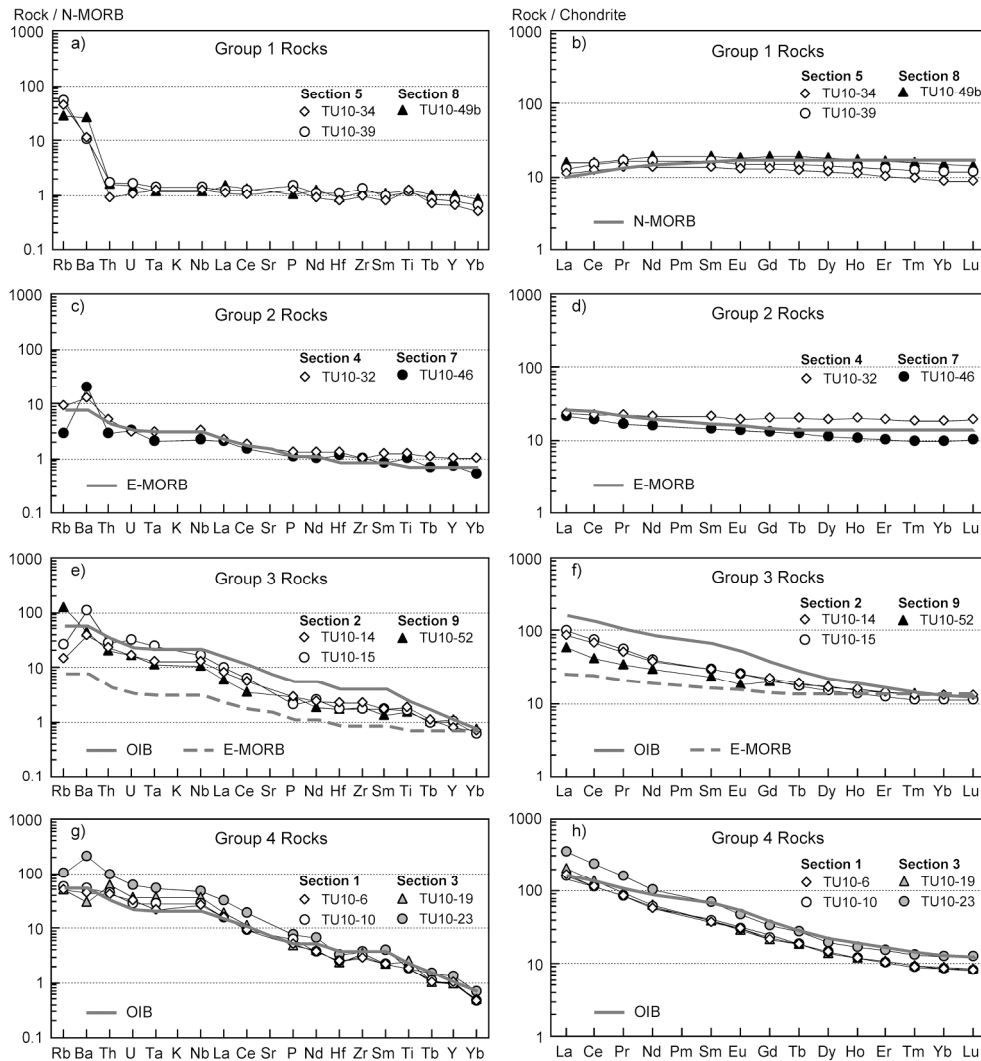


FIGURE 8 black and white

224x241mm (300 x 300 DPI)

1
2
3
4
5
6
7
8
9
10
11
12
13
14
15
16
17
18
19
20
21
22
23
24
25
26
27
28
29
30
31
32
33
34
35
36
37
38
39
40
41
42
43
44
45
46
47
48
49
50
51
52
53
54
55
56
57
58
59
60

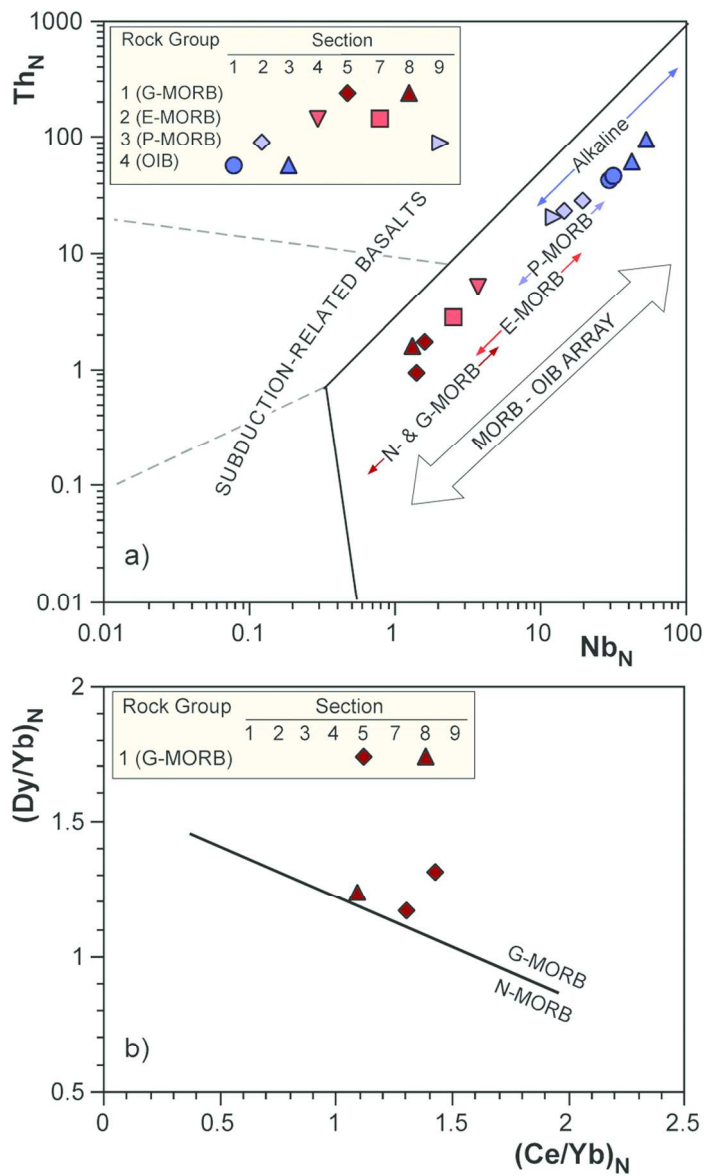


FIGURE 9

80x134mm (300 x 300 DPI)

1
2
3
4
5
6
7
8
9
10
11
12
13
14
15
16
17
18
19
20
21
22
23
24
25
26
27
28
29
30
31
32
33
34
35
36
37
38
39
40
41
42
43
44
45
46
47
48
49
50
51
52
53
54
55
56
57
58
59
60

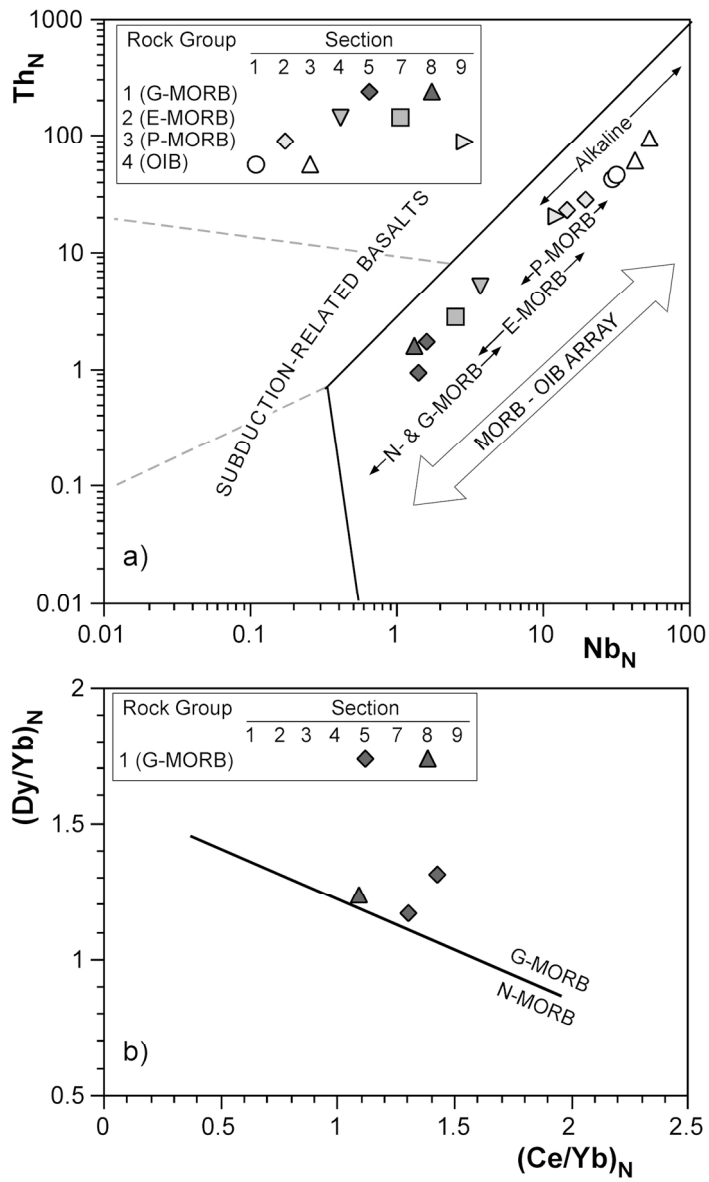


FIGURE 9 black and white

119x201mm (300 x 300 DPI)

1
2
3
4
5
6
7
8
9
10
11
12
13
14
15
16
17
18
19
20
21
22
23
24
25
26
27
28
29
30
31
32
33
34
35
36
37
38
39
40
41
42
43
44
45
46
47
48
49
50
51
52
53
54
55
56
57
58
59
60

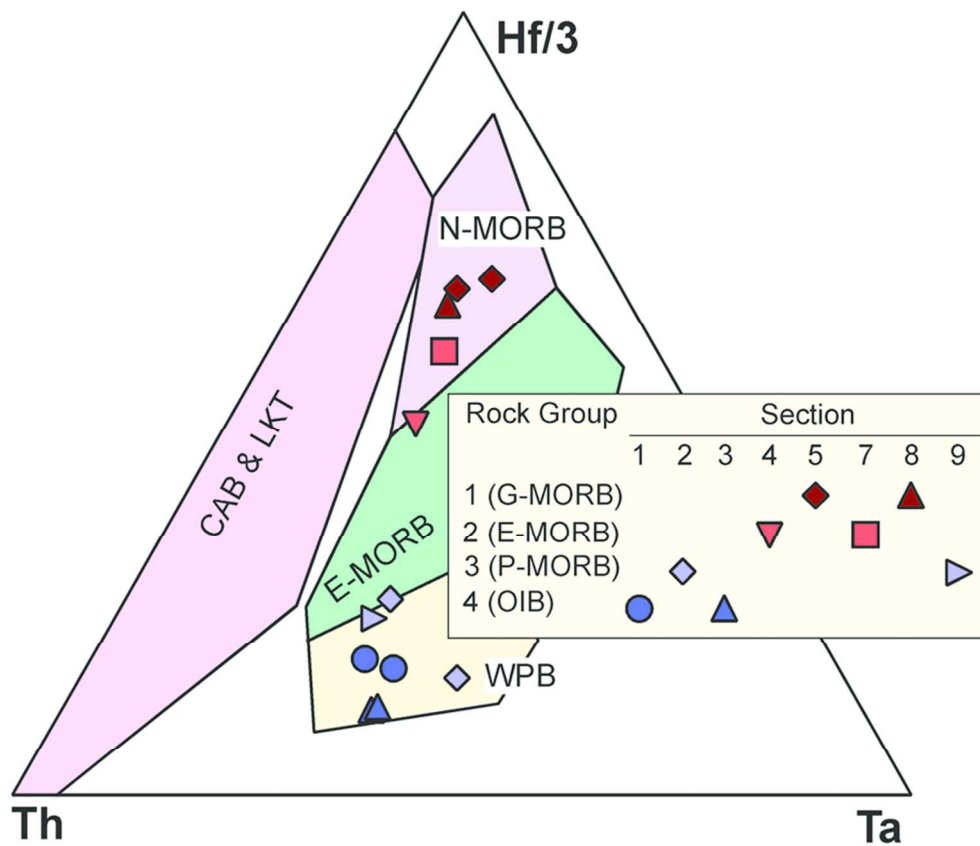


FIGURE 10

80x68mm (300 x 300 DPI)

view

1
2
3
4
5
6
7
8
9
10
11
12
13
14
15
16
17
18
19
20
21
22
23
24
25
26
27
28
29
30
31
32
33
34
35
36
37
38
39
40
41
42
43
44
45
46
47
48
49
50
51
52
53
54
55
56
57
58
59
60

1
2
3
4
5
6
7
8
9
10
11
12
13
14
15
16
17
18
19
20
21
22
23
24
25
26
27
28
29
30
31
32
33
34
35
36
37
38
39
40
41
42
43
44
45
46
47
48
49
50
51
52
53
54
55
56
57
58
59
60

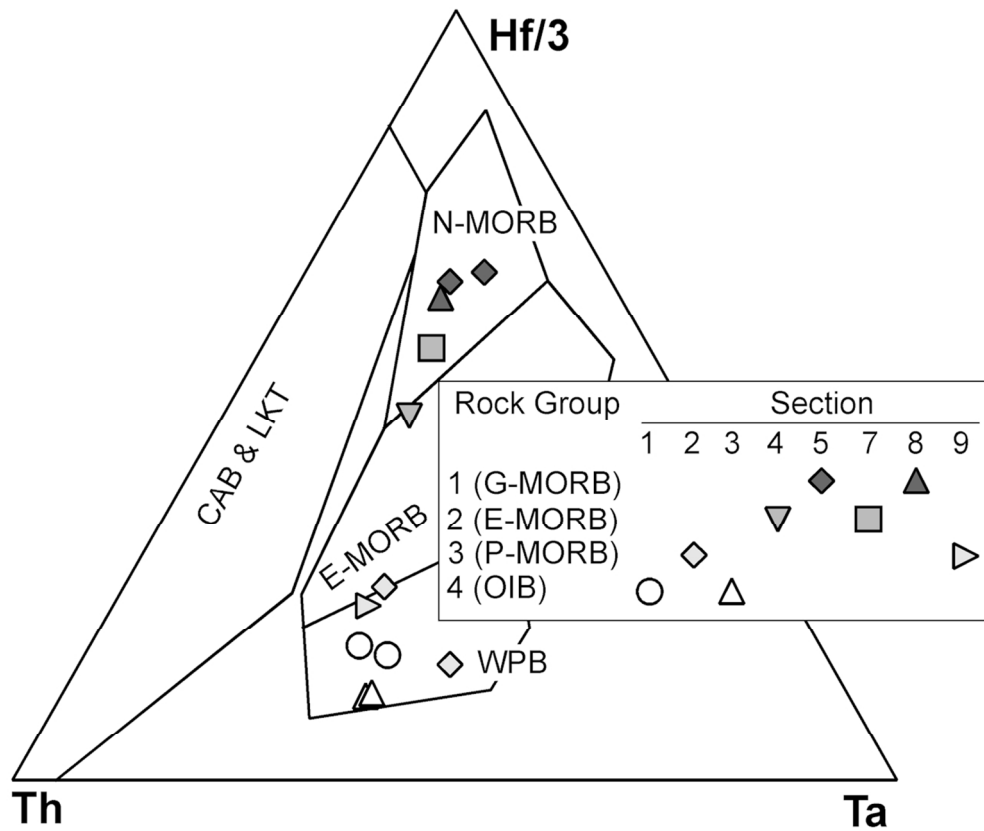


FIGURE 10 black and white

110x92mm (300 x 300 DPI)

view

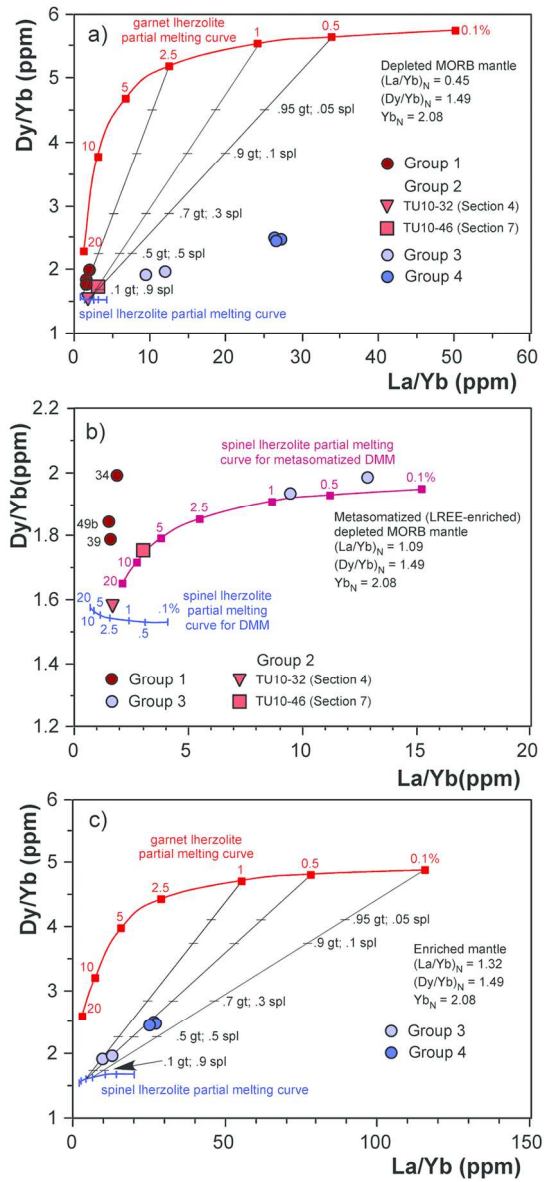


FIGURE 11

80x172mm (300 x 300 DPI)

1
2
3
4
5
6
7
8
9
10
11
12
13
14
15
16
17
18
19
20
21
22
23
24
25
26
27
28
29
30
31
32
33
34
35
36
37
38
39
40
41
42
43
44
45
46
47
48
49
50
51
52
53
54
55
56
57
58
59
60

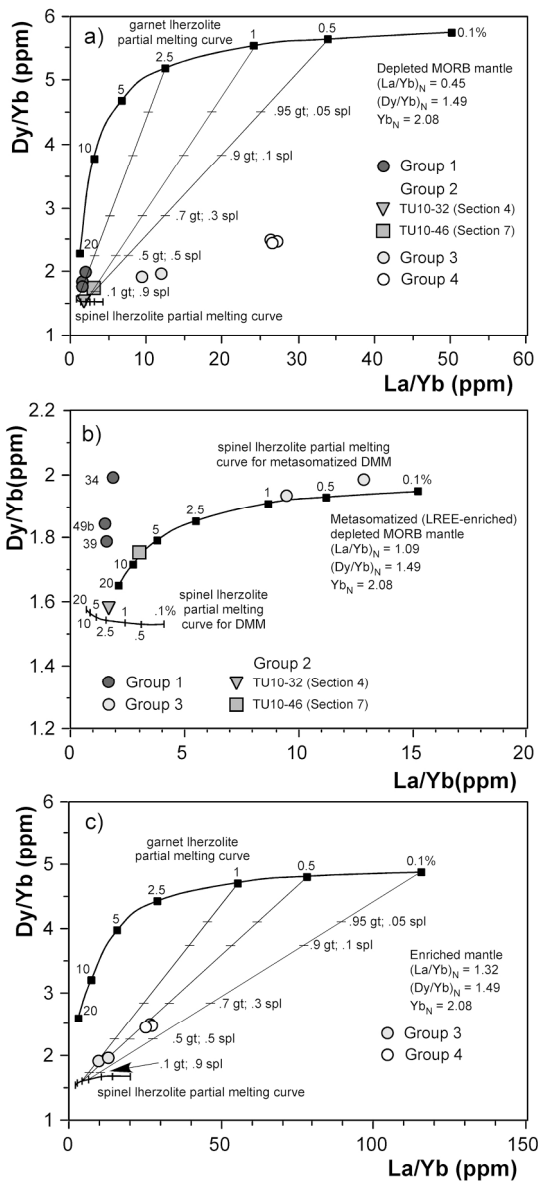


FIGURE 11 black and white

119x257mm (300 x 300 DPI)

1
2
3
4
5
6
7
8
9
10
11
12
13
14
15
16
17
18
19
20
21
22
23
24
25
26
27
28
29
30
31
32
33
34
35
36
37
38
39
40
41
42
43
44
45
46
47
48
49
50
51
52
53
54
55
56
57
58
59
60

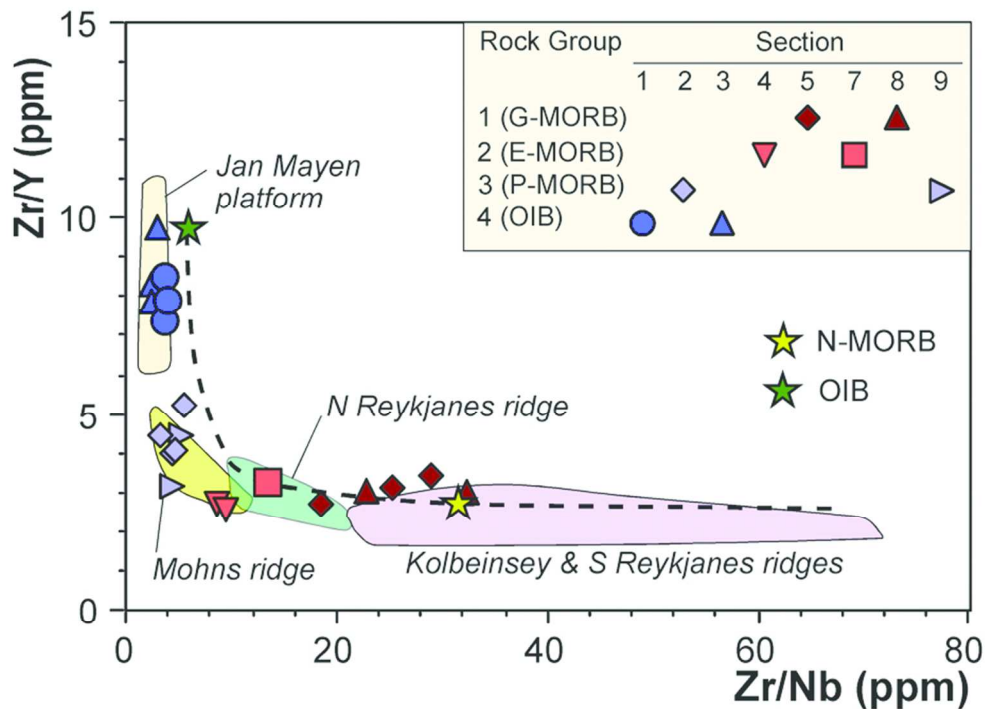


FIGURE 12

80x58mm (300 x 300 DPI)

Review

1
2
3
4
5
6
7
8
9
10
11
12
13
14
15
16
17
18
19
20
21
22
23
24
25
26
27
28
29
30
31
32
33
34
35
36
37
38
39
40
41
42
43
44
45
46
47
48
49
50
51
52
53
54
55
56
57
58
59
60

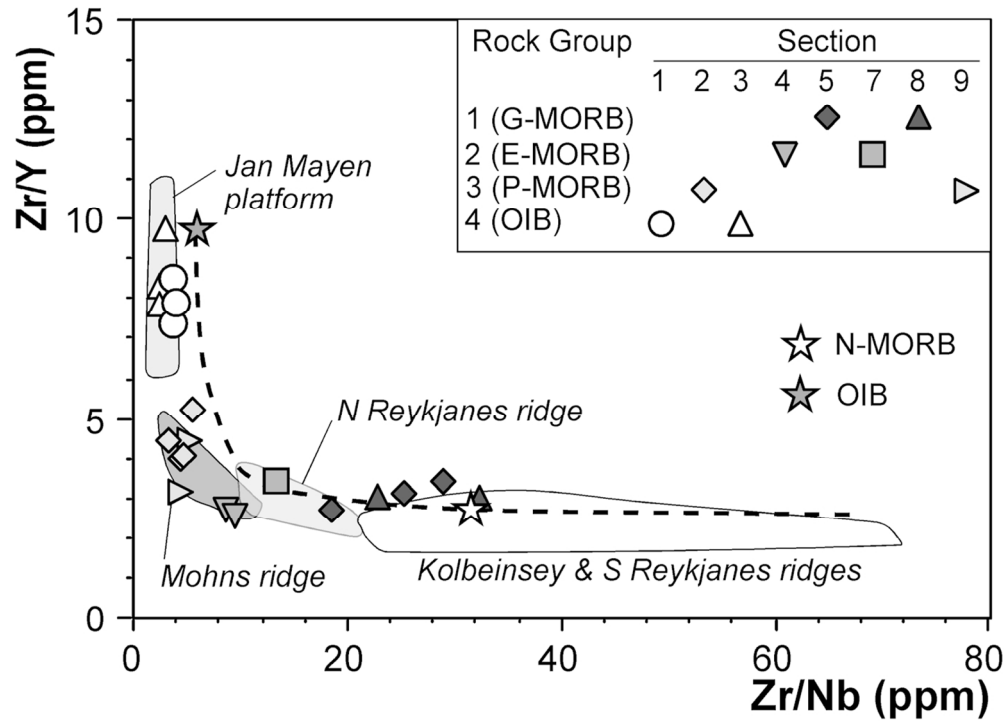


FIGURE 12 black and white

116x84mm (300 x 300 DPI)

Review

1
2
3
4
5
6
7
8
9
10
11
12
13
14
15
16
17
18
19
20
21
22
23
24
25
26
27
28
29
30
31
32
33
34
35
36
37
38
39
40
41
42
43
44
45
46
47
48
49
50
51
52
53
54
55
56
57
58
59
60

1
2
3
4
5
6
7
8
9
10
11
12
13
14
15
16
17
18
19
20
21
22
23
24
25
26
27
28
29
30
31
32
33
34
35
36
37
38
39
40
41
42
43
44
45
46
47
48
49
50
51
52
53
54
55
56
57
58
59
60

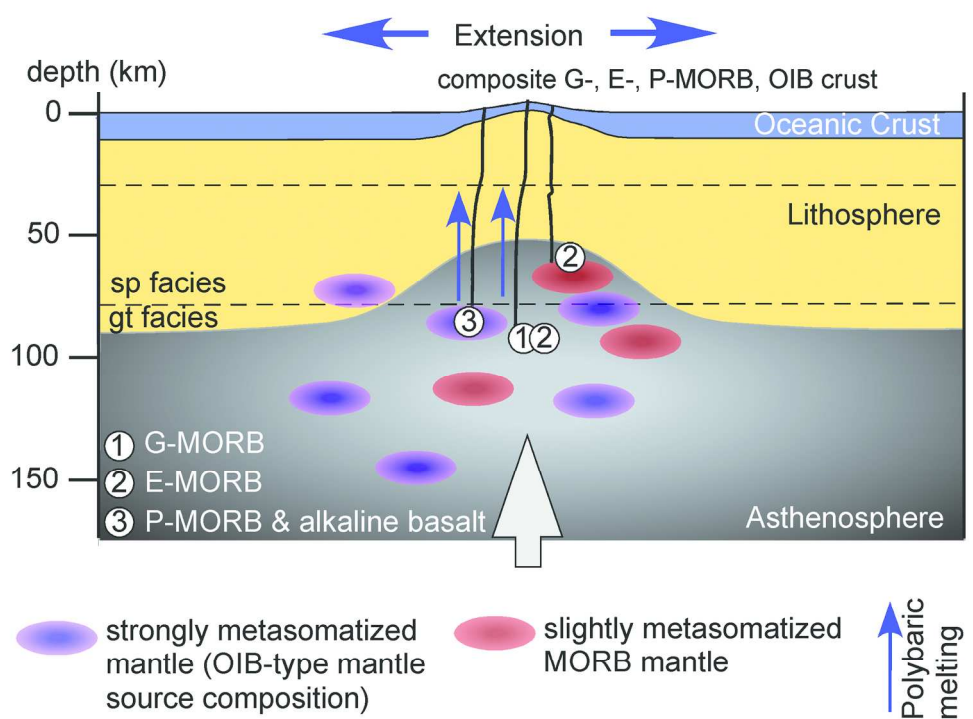


FIGURE 13

168x127mm (300 x 300 DPI)

review

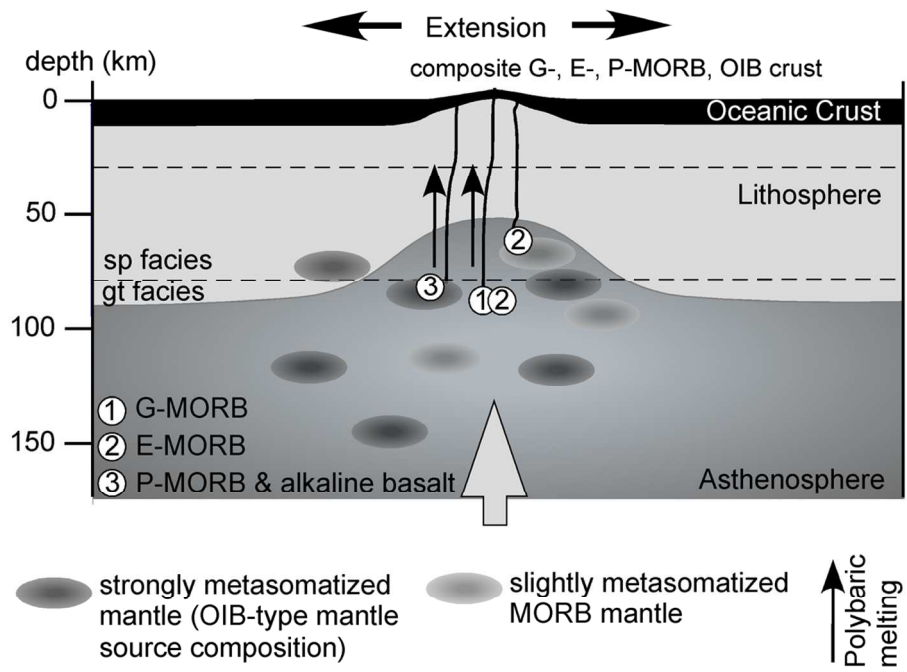


FIGURE 13 black and white

114x84mm (300 x 300 DPI)

review

1
2
3
4
5
6
7
8
9
10
11
12
13
14
15
16
17
18
19
20
21
22
23
24
25
26
27
28
29
30
31
32
33
34
35
36
37
38
39
40
41
42
43
44
45
46
47
48
49
50
51
52
53
54
55
56
57
58
59
60

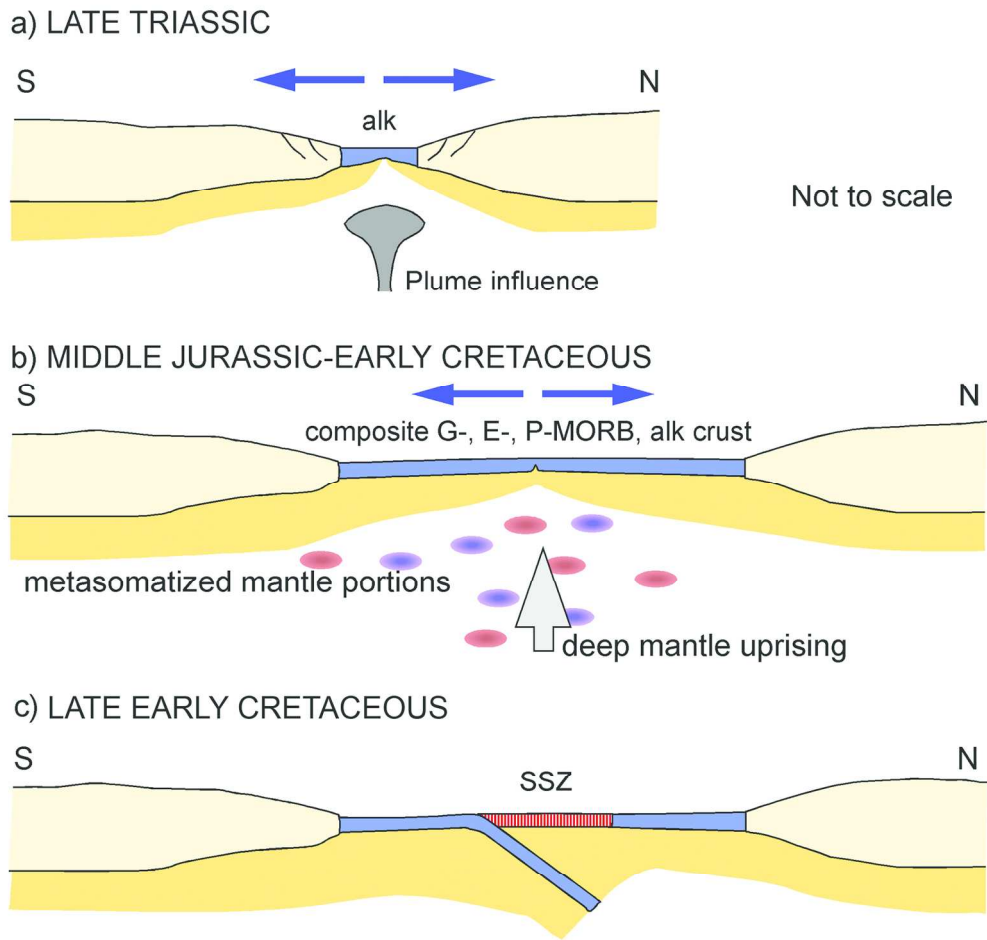


FIGURE 14

168x164mm (300 x 300 DPI)



1
2
3
4
5
6
7
8
9
10
11
12
13
14
15
16
17
18
19
20
21
22
23
24
25
26
27
28
29
30
31
32
33
34
35
36
37
38
39
40
41
42
43
44
45
46
47
48
49
50
51
52
53
54
55
56
57
58
59
60

Appendix A. Comparison of major (wt%) and trace element (ppm) concentrations in reference samples analyzed using X-Ray Fluorescence spectrometry (XRF) and Inductively Coupled Plasma-Mass Spectrometry (ICP-MS), as well as simple volumetric technique for CO₂.

	BE-N			BHVO-1			Detection limit
	Recomm.	Measured	Relative error (%)	Recomm.	Measured	Relative error (%)	
<i>XRF:</i>							
SiO ₂	38.48	38.59	-0.3	49.94	49.57	0.74	0.05
TiO ₂	2.63	2.62	0.3	2.71	2.75	-1.48	0.01
Al ₂ O ₃	10.14	9.79	3.4	13.80	14.02	-1.59	0.05
Fe ₂ O ₃	12.93	12.77	1.3	12.23	12.52	-2.37	0.10
MnO	0.20	0.19	7.4	0.17	0.17	0.00	0.05
MgO	13.25	13.61	-2.8	7.23	6.90	4.56	0.01
CaO	13.97	13.71	1.9	11.40	11.52	-1.05	0.04
Na ₂ O	3.20	3.29	-2.7	2.26	2.36	-4.42	0.01
K ₂ O	1.40	1.35	3.6	0.52	0.50	3.85	0.01
P ₂ O ₅	1.06	0.99	6.4	0.27	0.25	7.41	0.01
Zn	120	116	3.3	105	98	6.67	2
Cu	72	73	-0.8	136	140	-2.94	3
Sc	22	21	4.6	31.8	32	-0.63	3
Ga	17	16	4.4	21	22	-4.76	4
Ni	267	261	2.2	121	124	-2.48	2
Co	60	63	-5.0	45	46	-2.22	2
Cr	360	352	2.2	289	298	-3.11	2
V	235	231	1.7	317	312	1.58	2
Ba	1025	991	3.3	139	145	-4.32	3
Rb	47	47	0.2	11	10	9.09	1
Sr	1370	1362	0.6	403	408	-1.24	2
Y	30	28	5.3	27.6	28	-1.45	2
Zr	260	269	-3.6	179	172	3.91	2
La	82	81	1.6	15.8	17	-7.59	5
Ce	152	161	-6.0	39	42	-7.69	8
Nd	67	65	3.7	25.2	24	4.76	3
Nb	105	105	-0.1	19	18	5.26	1
Th	10.4	11	-2.7	1.08	1	7.41	1
<i>ICP-MS:</i>							
Rb				11	10.8	2.09	0.02
Sr				403	389	3.47	0.02
Y				27.6	28.6	-3.55	0.003
Zr				179	184	-2.79	0.02
La				15.8	16.0	-1.20	0.051
Ce				39	37.7	3.44	0.051
Pr				5.7	5.54	2.81	0.009
Nd				25.2	26.2	-3.89	0.023
Sm				6.2	6.38	-2.90	0.004
Eu				2.06	2.12	-2.91	0.05
Gd				6.4	6.29	1.72	0.007
Tb				0.96	0.93	3.12	0.057
Dy				5.2	5.47	-5.19	0.002
Ho				0.99	1.05	-6.06	0.046
Er				2.4	2.52	-5.00	0.005
Tm				0.33	0.31	6.06	0.017
Yb				2.02	2.12	-4.95	0.01
Lu				0.291	0.31	-6.53	0.012
Nb				19	18.3	3.79	0.01
Hf				4.38	4.31	1.60	0.007
Ta				1.23	1.28	-4.07	0.026
Th				1.08	1.10	-1.85	0.007
U				0.42	0.41	2.38	0.027
CO ₂						0.35	0.25

Recommended (Recomm.) values for international reference materials BE-N and BHVO-1 are from K. Govindaraju (1994) Geostandard Newsletter, Special Issue, v. 118, 158 p. Detection limits for XRF and ICP-MS analyses were determined using 29 international reference standards run as unknowns. Accuracy and detection limits for CO₂ analyses were determined using standard amounts of reagent grade CaCO₃.

Proof For Review

1
2
3
4
5
6
7
8
9
10
11
12
13
14
15
16
17
18
19
20
21
22
23
24
25
26
27
28
29
30
31
32
33
34
35
36
37
38
39
40
41
42
43
44
45
46
47
48
49
50
51
52
53
54
55
56
57
58
59
60